ELSEVIER

Coordination Chemistry Reviews
165 (1997) 1–92

COORDINATION CHEMISTRY REVIEWS

Conformational and UV photoelectron spectroscopy analysis of the chalcogenobispyridines

Simon J. Dunne [1], Lindsay A. Summers, Ellak I. von Nagy-Felsobuki *

Department of Chemistry, The University of Newcastle, Callaghan, NSW 2308, Australia

Received 28 March 1995; received in revised form 13 March 1996

Contents

Abstract

It is now possible to review the conformational and electronic behaviours of the isomers of chalcogenobispyridines and related compounds, so providing information on the link between the geometric and electronic properties, and providing some insight into their observed and anticipated physical and biological activities. Moreover, observations can now be made on the effect of the bridging atoms (O, S, Se, Te) and positional isomerism on conformation and electronic distributions; on the balance between resonance and inductive effects; and on the energetics of conformer interconversion. As a result of the non-rigid nature

* *Corresponding author.*
[1] Present address: Department of Inorganic Chemistry, University of Basel, 4056 Basel, Switzerland.

PII S0010-8545(96)01315-X

of the chalcogenobispyridines and related compounds, it is necessary to determine the preferred geometries to calculate the ionization energies (IEs). For the entire family of the chalcogenobispyridines, the minimum energy structures predict the pyridine ring planes to be nearly perpendicular, allowing maximum overlap of the chalcogen valence orbitals with the π system of only one of the pyridine rings. Rotational barrier height calculations do not support the fully conjugated planar forms on steric grounds, but suggest that a range of near-isoenergetic conformers surround the minimum structure. Ab initio methods (such as restricted Hartree–Fock (HF) methods) were found to assign incorrectly the UV photoelectron spectra of these pyridine-based compounds. While HF methods were shown to be reasonably successful for the prediction of the IEs of the π-type molecular orbitals (MOs), they failed to position the IEs correctly for the lone-pair nitrogen MOs (n_N), so requiring the use of computer-intensive configuration interaction (CI) methods. Bands caused by distinct conformers could not be resolved in the UV photoelectron spectra of the chalcogenobispyridines. Conformational analyses predicted low energy pathways for concerted disrotatory motion, permitting a smooth transition between near isoenergetic rotamers. The calculated IEs of the most populated conformers were found to be within the instrumental resolution, so were difficult to resolve. This was supported by the production of 'synthetic' spectra. Within the composite–molecule model, correlations with the IEs of pyridine and the methylchalcogenopyridines assisted in the spectral assignment of the chalcogenobispyridines. For each congener, the first IE was assigned to ionization from an anti-bonding π–n_X combination in which the contribution of pyridine π character was found to decrease down the group. The spectra recorded with different radiation sources were valuable in identifying bands associated primarily with the chalcogen character. © 1997 Elsevier Science S.A.

1. Introduction

There are six chalcogenobispyridine isomers, which have the following structures: 2,2′- (**1**), 2,3′- (**2**), 2,4′- (**3**), 3,3′- (**4**), 3,4′- (**5**) and 4,4′- (**6**) (see Fig. 1). In 1987, Summers [1] reviewed the chemistry of the chalcogenobispyridines and showed that experimental studies on these compounds have been limited [1]. Surprisingly,

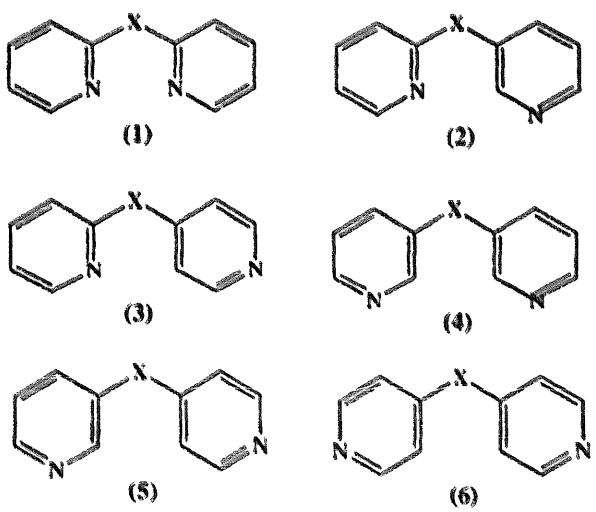

Fig. 1. Structural formuale of the six isomers of the chalcogenobispyridines.

Summers reported [1] that only two complete families of six isomers (the oxy- and thiobispyridines) were synthesized; syntheses of only the 2,2′- and 4,4′-selenobispyridines were recorded, while none of the tellurobispyridines was generated. Recently, Dunne et al. [2,3] have achieved the synthesis of the remaining isomers of the chalcogenobispyridines and, moreover, have reviewed the synthetic bases to all the isomers of the chalcogenobispyridines [4].

The wide range of biological and industrial applications displayed by the oxy- and thiobispyridines warrants thorough and systematic study of these compounds. For example, 2,2′-oxybispyridine is a suitable ligand for a cobalt carbonyl complex catalyst, so is useful in the hydroformulation of olefins [5,6]. 2,3′-Oxybispyridine is claimed to have both psychotropic and bactericidal properties [7], whereas 3,3′-oxybispyridine and its *N*-oxides have been found to affect the learning ability of mice [8]. In the case of the thiobispyridines, the 2,2′- isomer shows pronounced activity against streptococcus infections of rabbits [9], as well as some anti-thyroid [10,11], anti-bacterial, anti-fungal and anti-tumour activity [12]. 2,4′-Thiobispyridines were patented as bactericides, fungicides and herbicides [13], with the 4,4′-thiobispyridines [13] being patented as bactericides, fungicides, herbicides, nematocides and pesticides. 4,4′-Thiobispyridine is also an effective promoter of electron transfer to cytochrome C at a gold electrode [14–16] and is also used as an additive in photosensitive layers for electrophotography [17]. The biological activities of seleno- and tellurobispyridines have not yet been explored.

Conformational analysis of the chalcogenobispyridines is an important precursor to understanding their biological activity. For example, in the associated family of bipyridinium dications (such as paraquat), herbicidal activity was found to arise from the production of a superoxide radical anion in the regeneration of the dication by air [18]. Here, conformational analysis of the dication played an important role in understanding this process, because a planar structure was postulated to be an important prerequisite for the active dication derivatives. Therefore, knowledge of the barrier heights between the fully conjugated conformers and their equilibrium structures may provide a basis for future studies.

While structural studies on molecules that contain oxygen and sulphur are abundant in the chemical literature, experimental data on organo-selenium and organo-tellurium compounds are scarce. This area was recently reviewed by Hargittai and Rozsondai [19], who reported that there was little information on diaryl chalcogenides. Thus, a comprehensive review of recent conformational studies on the chalcogenobispyridines using molecular orbital (MO) methods [20–27] would be timely.

A technique which gives direct information on the IEs and characters of valence MOs is UV photoelectron spectroscopy (UPS). Photoelectron spectra in conjunction with ab initio MO calculations help us to gain further understanding of the electronic structure of molecules. A review by Cauletti and Distefano [28] on the UPS of organo-selenium and organo-tellurium derivatives illustrated that there were few studies on diaryl systems. In fact, the HeI UV photoelectron spectra of only 2,2′-thiobispyridine [29] and three of the dichalcogenobispyridines [30] were covered by this review. Hence, there has been no recent assessment on the effect of positional isomerism on electronic structure.

A number of features of the UPS experiment allow additional information to be gleaned other than just IEs. For example, the IEs of valence MOs—particularly the highest occupied MO (HOMO)– have been linearly related to electrical properties such as the oxidation half-wave potentials and electrophilic substituent constants (σ) of a number of molecules [31]. For example, electrochemical studies have shown that the 1,1′-di-substituted 4,4′-bipyridinium ions possess some of the lowest (most cathodic) redox potentials of any organic system, showing a significant degree of reversibility, making them useful as electron relays, redox indicators in biological studies and potent herbicides [32]. The measurement of the IEs of chalcogenobispyridines provides a valuable resource for molecular design in these areas.

The comparison of UV photoelectron spectra measured using different radiation sources identifies MOs with particular characteristics. The band intensities vary with the energy of the ionizing radiation and this variation is not uniform for all MOs. The band intensities of localized lone-pair orbitals on halogens, for example, show a dramatic reduction in intensity when ionized by high energy photons. This reduction is dependent on the degree of resonance interaction between the lone pair and the σ or π systems of the molecule. The greater the degree of delocalization is, the smaller will be the reduction in band intensity on changing to a higher energy photon source. Studies on the use of more than one radiation source are rare, so a complete summary of the HeI and HeII spectra of chalcogenobispyridines provides valuable information on the receptivity of chalcogen-containing MOs to ionizing radiation.

Conformational information can also be obtained by UPS. The presence of planar conformers is identified using UPS. In the planar form, the chalcogen lone-pair orbital that lies in the molecular plane shows marked reduction on going from HeI to HeII radiation, compared with the lone-pair orbital perpendicular to the ring plane. This perpendicular orbital resonately interacts with the π system, resulting in delocalization and, hence, a lowering of the IEs of the corresponding orbitals. However, if the ring planes are orthogonal, then there will be extensive delocalization of both chalcogen lone pairs over the entire pyridyl framework, minimizing the intensity changes observed when changing the radiation sources. The measurement of these changes allows us to estimate the extent of delocalization and, thus, the degree of planarity.

As an extension of our earlier work [2–4,20–27], we are now able to report a thorough and systematic study of the conformational and electronic behaviours of the isomers of chalcogenobispyridines, so providing information on the link between the geometric and electronic properties, and giving some insight into their observed and anticipated physical and biological activities. The effects of the bridging atoms and positional isomerism on the conformation and electronic distributions; on the balance between resonance and inductive effects; and on the energetics of conformer interconversion of the chalcogenobispyridines can now be discussed. Recent reviews [1,4,19,28] highlight the lack of data in this area, making this review of 34 chalcogenobispyridines and related compounds timely. However, before discussion of the conformational and electronic behaviours of these compounds, it is necessary to outline the principles of UPS and the methods of spectral interpretation which underlie the conformational and electronic analysis.

2. Assignment tools in UPS

2.1. Introduction

Procedures for the interpretation of UPS spectra have been outlined in a number of monographs by Rabalais [33], Carlson [34], Eland [35], Ballard [36] and Berkowitz [37]. For large molecules, such as the bispyridines, not all the techniques are appropriate. For example, the observation of fine structure in spectral bands, such as vibrational progressions, rotational structure, spin–orbit splitting, and Jahn–Teller and Renner–Teller effects, can lead to the positive identification of specific states in only small and highly symmetrical molecules. In large molecular systems, it is reasonable to expect that ionization will simultaneously excite a number of molecular vibrations, resulting in a broad and unstructured band profile within the resolution constraints of most spectrometers.

A number of techniques are available for interpreting the UPS spectra of moderately sized compounds. The intensity of the bands in a photoelectron spectrum is approximately proportional to the probability of the available ionic states. These probabilities of ionization are called relative partial photo-ionization cross-sections (σ). To the first order, the cross-section for a particular orbital is proportional to the number of electrons available for ionization. The photo-ionization cross-section also depends on the nature of the ionized orbital—its degree of delocalization, its atomic composition, the number of nodes, etc. Importantly, σ varies with the energy of the ionizing radiation and this variation is not uniform for MOs of differing atomic character. The variation of σ allows comparative band intensities to be used as an interpretive tool.

Most UPS experiments are performed using two or more ionizing sources; i.e. HeI α and HeII α lines (the α symbol will be assumed hereafter), which have energies of 21.2 and 40.8 eV respectively. The comparison of such data allows the enunciation of a number of general rules. For photo-ionization by HeI radiation, the cross-section of the valence atomic orbital increases on moving down a group of the Periodic Table. When light of a shorter wavelength (such as HeII) is used, this trend is partially reversed. The cross-sections of the np orbitals of chlorine, bromine and sulphur, for example, decrease significantly on changing from HeI to HeII radiation. The σ values of carbon 2p orbitals remain approximately unchanged on switching from HeI to HeII, while the σ values of nitrogen and oxygen 2p orbitals increase.

Few data are available on the photo-ionization cross-sections of the Se 4p and Te 5p atomic orbitals, although a significant decrease is expected relative to the photo-ionization cross-section of the carbon 2p orbitals on changing from HeI to HeII radiation. Theoretical calculations suggest a $\sigma_{HeI}/\sigma_{HeII}$ ratio of about 17 for Se 4p atomic orbitals [38] and a ratio of about 14 for Te 5p orbitals [39]. In contrast, for carbon 2p orbitals, experimental evidence suggests that this ratio is about 1. This phenomenon is a valuable tool for the identification of bands that contain substantial chalcogen character, and for the determination of the degree of chalcogen participation in those orbitals. More tentatively, relative photo-ionization cross-sections are

used to assign the nitrogen lone-pair MOs and for the production of 'synthetic' UPS spectra (such as oxybispyridines [22]).

MOs that are highly localized on specific atoms, such as non-bonding orbitals, usually occur in specific spectral regions determined mainly by the electronegativity of that atom. For example, halogen or chalcogen non-bonding orbitals occur in predictable spectral regions, regardless of the nature of the molecule in which the atom is contained. The IE shifts of MOs formed from bonding and anti-bonding combinations of chalcogen lone-pair orbitals with the π-orbitals of the pyridine system are related to the electronegativity of the bridging atom. The nitrogen 'lone-pair' MO in pyridine is essentially unaffected on substitution.

In complex molecules, such as the chalcogenobispyridines, in which many of the ionization bands overlap and possess no fine structure, the correlation of spectral bands with a series of related compounds provides a useful tool for band analysis. Understanding of the UPS spectra of pyridine and methylchalcogenopyridines (see Sections 3.1 and 3.2) is vital for assigning the more complex spectra of the chalcogenobispyridines.

In the absence of fine structure, it is sometimes still possible to obtain qualitative information from band shapes. Non-bonding orbitals generally produce sharp bands with identical adiabatic and vertical IEs, whereas strongly bonding orbitals are expected to produce broad bands. Band shapes are used to predict the delocalization of the n_N MOs and the changing contributions of the chalcogen atoms to HOMOs down through the group.

Despite this armoury of assignment tools, it is often not feasible to assign spectra without using rigorous MO calculations. With the rapid increase in the efficiency and capacity of computers, the performance of all-electron calculations on moderately sized molecules has become commonplace. Semi-empirical techniques, while still useful, are losing ground to more rigorous methodologies for molecules that contain 200 electrons or less. Despite the sophistication of the ab initio techniques, their use in conjunction with Koopmans' approximation is not foolproof, so should be treated with caution.

Before the assignment tools can be applied in the case of the complex spectra of the chalcogenobispyridines, an overview of the experimental and theoretical considerations will be given in Section 2.2, to rationalize the otherwise incomprehensible wealth of spectroscopic information which can be gleaned from UPS spectra.

2.2. *Principles of measurement*

Photoelectron spectra are a plot of the electron flux vs. the kinetic energy of the photo-ejected electrons (the two observable features in the experiment). Because the electrons are collected at an angle relative to the ionizing photon beam (90° in most cases), conversion of the electron flux is required to obtain the photo-ionization cross-sections. The kinetic energy E_k values of the electrons are converted to IEs using Einstein's equation [33–37]

$$E_{kn} = h\nu - IE_n - E^+_{vib}(p) - E^+_{rot}(q) \quad (1)$$

where $E^{+}_{vib}(p)$ and $E^{+}_{rot}(q)$ are the energies of the pth and qth vibrational and rotational excited states of the nth state of the molecular ion. In UPS, the available photon energy in Eq. (1) arises from a cold cathode discharge in 'ultrapure' helium, yielding predominantly the HeI or HeII radiation line [33–37].

For light molecules, such as H_2 or HF, rotational fine structure is observed in their UPS spectra [33]; however, for larger molecular systems, instrumental resolution for the non-zero kinetic energy electrons is usually not sufficient (20–30 meV) to allow a similar level of detection. In most cases, it is only possible to resolve vibrational structure, such as in large molecular systems with low molecular symmetry (such as the chalcogenobispyridines). Therefore, no discussion will be given here of the various selection rules for vibrational and rotational processes, because they are not applicable to UPS study of the chalcogenobispyridines.

The Franck–Condon principle states that the most probable electronic transitions occur when there is a large overlap between the initial state vibrational wave function of the neutral molecule and the final state vibrational wave function of the molecular ion. It is implicit in this principle that an electronic transition takes place in a shorter time interval than that for one molecular vibration. Consequently, the geometries of the neutral and ionic molecules are unchanged on ionization.

In any UPS spectral assignment, two types of IE are often quoted: adiabatic and vertical IEs. In the absence of rotational fine structure, the adiabatic IE is defined as the difference in energy between the ground electronic vibrational state of the neutral molecule and the energy of the molecular ion. It follows that the energy of the transition is given by

$$M(\chi, v''=0)+h\nu \rightarrow M^{+}(\chi, v'=0)+e^{-} \quad (2)$$

However, the vertical IE is defined as the energy that corresponds to the transition

$$M(\chi, v''=0)+h\nu \rightarrow M^{+}(\chi, v'=n)+e^{-} \quad (3)$$

where n is the vibrational quantum number and v' corresponds to the vibrational level whose wave function gives greatest overlap with the $v'=0$ wave function [33] (because most molecules are in their ground vibrational state at room temperature). The vertical IE is often quoted, because the adiabatic IE may not be discernible. It is the vertical IE that is comparable with Koopmans' approximated IEs; it is this experimental quantity which shall be quoted in the remainder of this paper.

Although the design of photoelectron spectrometers varies significantly [33–37], a number of salient features remain common, because of the nature of the experiment. Photoelectrons are produced when photons are absorbed by molecules of a sample vapour. A fraction of these photoelectrons pass through a narrow slit (100 μm) in the wall of the target chamber and into the electron energy analyzer. (With the earlier spectrometer designs, such as in the case of the Perkin–Elmer PS 16/18, only a small solid angle was sampled). The electrons that pass through the analyzer exit slit strike a channeltron. Responses of the order of 40–40 000 counts per second (cps) are typically processed, although the PS 16/18 spectrometer produced count rates of the order of 1000 cps under HeI conditions and 400 cps for HeII conditions.

In the PS 16/18 spectrometer, a Helectros lamp allows the recording of the HeI and the HeII spectra under a single set of conditions (i.e. discharge voltage and helium pressure) with intensity ratios of the order of about 4: 1. Even under conditions of high voltages and low helium pressures, the HeI line is dominant. The ionization region between 30 and 40.8 eV is then obscured, as a result of the superposition of bands that arises from the ejection of outer electrons by the HeI radiation, with the bands arising from the ejection of inner electrons with HeII radiation. Therefore, unmonochromatized HeII radiation is useful only up to about 30 eV. Because the valence molecular levels of most organic molecules lie in the range 7–30 eV, HeI and HeII radiation lines adequately cover this region. Generally, for these compounds under HeI conditions, the operating resolution of the PS 16/18 spectrometer is between 25 and 35 meV, and each spectrum is usually accumulated for 20 min with a maximum intensity in the region of about 1000 cps. A number of spectra are typically recorded over a duration of about 3 h to ensure that the intensities recorded are reproducible under the existing operating conditions.

In the PS 16/18 spectrometer, the heated probe modification allows the UPS spectra of oils and solid samples to be recorded. The modification consists of a helium lamp surround, which contains a heat exchanger through which air or water coolant may be circulated at a controllable rate to provide fine temperature control. The normal working temperature range using water coolant is 35–100 °C, while the minimum temperature using air as the coolant is about 70 °C—although this may be lowered by inserting a heat sink into the probe. For oils, solids or liquids of very low volatility, the solids inlet probe is usually employed.

To ensure uniform surface potentials in the region of the target chamber exit slit, the probe tips are usually freshly coated with colloidal graphite. The calibration of solid spectra is achieved by bleeding a mixture of calibrant gases (argon–nitrogen and butadiene–acetylene) into the target chamber to give an internal calibration scale. To ensure that the peak intensities observed are reproducible for non-volatile samples, a number of spectra are usually recorded during a period of 2 h.

The energy analyzer used in the PS 16/18 spectrometer discriminates against slow-moving electrons. Hence, for a comparison of band areas, the integrated curves are scaled as $1/E_k$ for use in density-of-states analysis. This scaling removes the dependence of the transmission effects of the HeI cross-section ratios, because, to a first-order approximation, the collection efficiency of the electrostatic 127° deflection analyzer is proportional to the initial kinetic energy of the photo-ejected electron [40].

2.3. *Koopmans' approximation*

Koopmans invoked an MO concept to estimate the vertical IEs [41]. Specifically, he showed that the negatives of the orbital energies, as given by the HF equations, are identical to the differences in the total energies of ion(s) (E_m^+) and the neutral molecule (E_o). Simply put, Koopmans showed that [41]

$$IE_i \sim IE_i^o \equiv -e_i \tag{4}$$

where IE_i^o is the 'best' orbital approximation (in a variational sense) to the experimental vertical IE_i. In Eq. (4), Koopmans' approximation and theorem are identified by the relation symbols "$\sim$" and "$=$" respectively. We shall now designate Koopmans' approximation as the desired relation.

Koopmans made use of HF canonical MOs. In doing so, the Born–Oppenheimer approximation is necessarily assumed to be valid, so the concept of a potential energy surface and an equilibrium geometry is deemed appropriate. Therefore, if the expectation value of the electron–nuclei coupling operator is large (such as Jahn–Teller or Renner–Teller effects), then Koopmans' approximation will incorrectly predict the number of vertical IEs.

Koopmans' approximation can include relativistic effects, provided that orbital–spin and spin–spin angular momentum coupling operators are incorporated into the Fock operator (as was done by Koopmans [41]). However, the non-relativistic Schrödinger equation is generally incorporated in ab initio packages (such as the GAUSSIAN suite of programs [42]); thus, under this additional restriction, Koopmans' approximation will incorrectly predict the number of observed vertical IEs for molecules that exhibit spin–orbital interactions.

Koopmans assumed that the HF canonical MOs for the ground electronic state of the neutral molecule were exactly the same as those of the ion. Therefore, the equilibrium geometry of the neutral molecule must be fixed for the duration of the ionization process (i.e. a vertical transition must occur). Hence, the Franck–Condon principle is incorporated by Koopmans' choice of canonical MOs.

There are two parts to the proof given by Koopmans [41]. In the first part, he showed that Eq. (4) holds; in the second part of the theorem, he showed that the negative of the orbital energy is the 'best' approximation in a variational sense. In constructing the proof, Koopmans also had to assume that the determinants of the molecular ions differed only by a single occupied spin orbital from the determinant that described the neutral ground electronic state. The use of the same determinant ensured that the one-electron process is the dominant process in photo-ionization. For instance, the electronic transition moment is given by

$$[G_{e\to n}]^2 = |\iiint \Psi_o^{2N} \mu_{DIP} \Psi^{Final}\, d\tau|^2 \tag{5}$$

where μ_{DIP} is the dipole moment operator. This integral factors into

$$\left(\iiint \Psi_o^{2N-1} \Psi^{Ion}\, d\tau\right)\left(\iiint \psi_i |\mu_{DIP}| \phi_j\, d\tau\right) \tag{6}$$

where Ψ_o^{2N-1} and Ψ^{Ion} are the wave functions of the neutral molecule (minus the ionized electron) and ion respectively. The terms ψ_i and ϕ_j are the wave functions involved in the electron ejection process. Because the MOs are orthonormal, the determinants of the neutral molecule (minus its electron) and the ion must be identical for the first integral to be non-zero. In other words, all one-electron transitions are allowed. However, for two-electron transitions (such as ejection and excitation), the ion determinant would no longer be the same as that of the neutral molecule (minus the ionized electron); therefore, the first integral of Eq. (6) would be zero. By invoking this assumption, Koopmans significantly simplified the inter-

pretation of a photoelectron spectrum, because two-electron processes, such as shake-up (ionization and simultaneous excitation) and shake-off (double ionization), would be of extremely weak intensity.

Koopmans' approximation cannot apply to open-shell molecules. In open-shell configurations, there may be double- and single-occupied orbitals of the same symmetry, which are determined by different sets of self-consistent field (SCF) equations, whose off-diagonal multipliers λ_{jj} cannot be completely eliminated by a unitary transformation. However, Roothaan restricted SCF equations overcame this situation for many open-shell problems [43]. Nevertheless, the virtual orbitals for the closed- and open-shell sets are no longer the same. In the case of the unrestricted HF (UHF) SCF equations [44], the α and β spin orbitals are no longer degenerate for the doubly occupied MOs, because they are obtained from variational solutions of two different Fock operators. Therefore, the UHF wave function is no longer an eigenfunction of the spin squared S^2 operator. This clearly means that it is impossible to choose the same set of canonical MOs for both the neutral molecule and ion wave functions in either of these open-shell formulations. Hence, Koopmans' approximation cannot hold for open-shell molecules.

Because the same set of canonical MOs is used for the ion and the neutral molecule, the approximation neglects the fact that the electrostatic field of the ion is not the same as that of the neutral molecule. In other words, the MOs of the ion would reorganize (i.e. relax) in energy when compared with the canonical set of MOs for the neutral molecule. Hence, at the HF-SCF level, using the total energies of the ion and the neutral molecule yields

$$IE_i = IE_i^o + \Delta E_{RELAX} \tag{7}$$

Errors caused by relaxation processes at the HF-SCF level may be accounted for by subtracting the total electronic energy of the neutral molecule ground state from the total electronic energy of the ion state. This method is known as the ΔSCF–HF method, because it is reliant on the SCF method to recover the relaxation energy. The vertical IEs calculated using this method are basis set dependent, so a model that utilizes a large basis set should represent a recovery of the relaxation errors expected at the HF limit.

Koopmans' approximation does not take into account that electrons adjust their motions to an instantaneous charge distribution rather than to the average charge distribution (as assumed by the HF-SCF equations). Hence, while Eq. (7) takes into account relaxation, it still does not take into account electron correlation. These limitations are severe for both the ion and the neutral molecule. The vertical IEs at the configuration interaction (CI) level can be written in terms of

$$IE_i = IE_i^o + \Delta E_{CORR} \tag{8}$$

The computational simplest treatment of electron correlation is the second-order Møller–Plesset perturbation (MP2) theory [45]. Although the MP2 theory is non-variational, it still represents a cost-effective alternative to variational CI techniques. The difference between the 'true' molecular Hamiltonian and the SCF Hamiltonian is defined as a perturbation. The set of all configurations constructed from SCF-

determined orbitals is taken to be the zero-order set of state functions. Møller and Plesset [45] have shown that the first-order correction to the SCF energy is zero. With the MP2 theory, it is only necessary to use configurations that involve double substitutions from a single reference HF determinant. Furthermore, higher-order perturbations are described by MP*n* theory ($n=2, 3, 4, ...$), where n is the order of perturbation. The derivation and use of the MPn theory have been well documented [45,46]. Eq. (8) will be labelled as 'ΔSCF–MP', because it takes into consideration the 'full' relaxation and correlation effects caused by inter-electronic repulsions. Koopmans' approximation assumes that ΔE_{CORR} is zero.

Eqs. (4), (7) and (8) clearly give the hierarchy of the approximations used in the calculation of vertical IEs. The Koopmans' approximation (KA)–HF model (Eq. (4)) is the least rigorous of the three, because it uses the MO concept as an 'observable'. Eq. (7) uses the total electronic energies (which are observable quantities) but calculates at the HF level (labelled ΔSCF–HF), whereas Eq. (8) takes into consideration the same energy observables, but with the incorporation of electron correlation. The importance here of the MO concept is that it clearly shows the relationships between these approximations. In subsequent sections, all experimental IEs quoted are the vertical IEs.

2.4. MO calculations

The calculation of accurate vertical IEs requires knowledge of the geometry of the neutral molecule. In the absence of experimental data, the structure can be based on a model compound, or either fully or partially optimized structures using an MO method. The accuracy of the calculated structure depends on the MO method utilized and on the basis set employed.

One of the most widely used basis sets for geometry optimization is the STO-3G minimal basis set developed by Pople and coworkers [47]. This basis set has been formulated for first-row to fourth-row main group elements and for all three rows of the transition metals. The popularity of this basis set rests on its effectiveness in predicting geometries, despite its small size. Pople [48] has reported that, for a large number of molecules that contain C, H, N, O and F, the mean absolute deviation from the experiment for the SCF bond lengths is 0.03 Å (which is in excellent agreement). Therefore, it was found that a large basis set superposition error—which is inherent when employing the STO-3G basis set—helps to correct other defects in the HF model (such as neglecting electron correlation) to produce reasonable structural parameters. This fortuitous cancellation allows the calculation of geometries that are often more accurate than the HF model is capable of yielding. Unfortunately, energy-related properties are not predicted with the same accuracy as geometric parameters. The restriction to a single exponent for both σ and π p-based functions results in π MOs with IEs that are too low relative to their σ counterparts. This deficiency is highlighted below in the calculation of vertical IEs of the chalcogenobispyridines.

To improve the accuracy of IE calculations, basis sets that include increased numbers of primitives devoted to core and valence subspaces, such as the 6-31G set,

need to be used. Adding all six components of a Cartesian d function for first-row atoms yields the 6-31G* basis set, while further addition of p functions to hydrogen defines the 6-31G** basis set [42]. The addition of such polarization functions can make a marked difference to calculated equilibrium structures. While the polarization functions may contribute only slightly to the optimal valence MOs, that contribution is important in terms of orbital flexibility. Such augmentation of the basis set comes at the expense of increased computer times and extended memory requirements. Although the 6-31G** basis set is generally too large to perform routine optimizations, it is a useful tool for the prediction of the vertical IEs of the π MOs of pyridine-based molecules.

Fig. 2 shows the fully optimized geometries of pyridine using STO-3G (Fig. 2(a)), 3-21G (Fig. 2(b)) and 6-21G (Fig. 2(c)) basis sets [49]. All the optimizations were performed using the Fletcher–Powell (FP) routine [50] within the GAUSSIAN 86 suite of programs [42]. The results for the split-valence 3-21G set are almost identical to those of the larger 6-21G set. The bond lengths predicted by the latter 3-21G and 6-21G basic sets are all within 0.001 Å (except for the R_{C-N} bond which is within 0.003 Å). The bond angles are commonly within 0.25°. The similarity between these structures reveals the small contribution that atomic core functions make to chemical bonding.

The STO-3G optimized structure of pyridine found by Dunne [49] is similar to that reported by Del Bene [51] and closely mimics the structure predicted by the spectroscopic results of Sorensen et al. [52] (labelled Fig. 2(d)). Thus, the minimal STO-3G set has fortuitously produced a more acceptable result (when compared with the experimental results) than the larger split-valence sets, so giving credence for its use in the determination of structural parameters in pyridine-based systems [20–27].

2.5. *Photo-ionization cross-sections*

Within the dipole approximation, the angular distribution of photoelectrons ejected from a subshell ϕ_μ of isolated randomly oriented atoms is given by [53]

$$\sigma_\mu^{AO}(\epsilon) = \frac{\sigma_\mu(\epsilon)}{4\pi}\left[\frac{1+\beta_\mu(\epsilon)}{4}\right] \tag{9}$$

where the photoelectrons are collected at 90° to the incident beam.

The terms $\sigma_\mu(\epsilon)$ and $\beta_\mu(\epsilon)$ (the asymmetry parameter) are functions of the ejected photoelectron's kinetic energy. For example, using data calculated by Manson and Msezane [54,55], the least-squares regression fits to σ and β for nitrogen and chlorine atoms are [56]

$$\begin{aligned}
\beta^{N} &= 0.1146 + 0.1283(\epsilon) - 0.0031(\epsilon)^2 \\
\beta^{Cl} &= 0.5098 + 0.2159(\epsilon) - 0.0092(\epsilon)^2 \\
\sigma^{N} &= 11.9860 - 0.2047(\epsilon) - 0.0027(\epsilon)^2 \\
\sigma^{Cl} &= 66.7590 - 6.4744(\epsilon) + 0.1495(\epsilon)^2
\end{aligned} \tag{10}$$

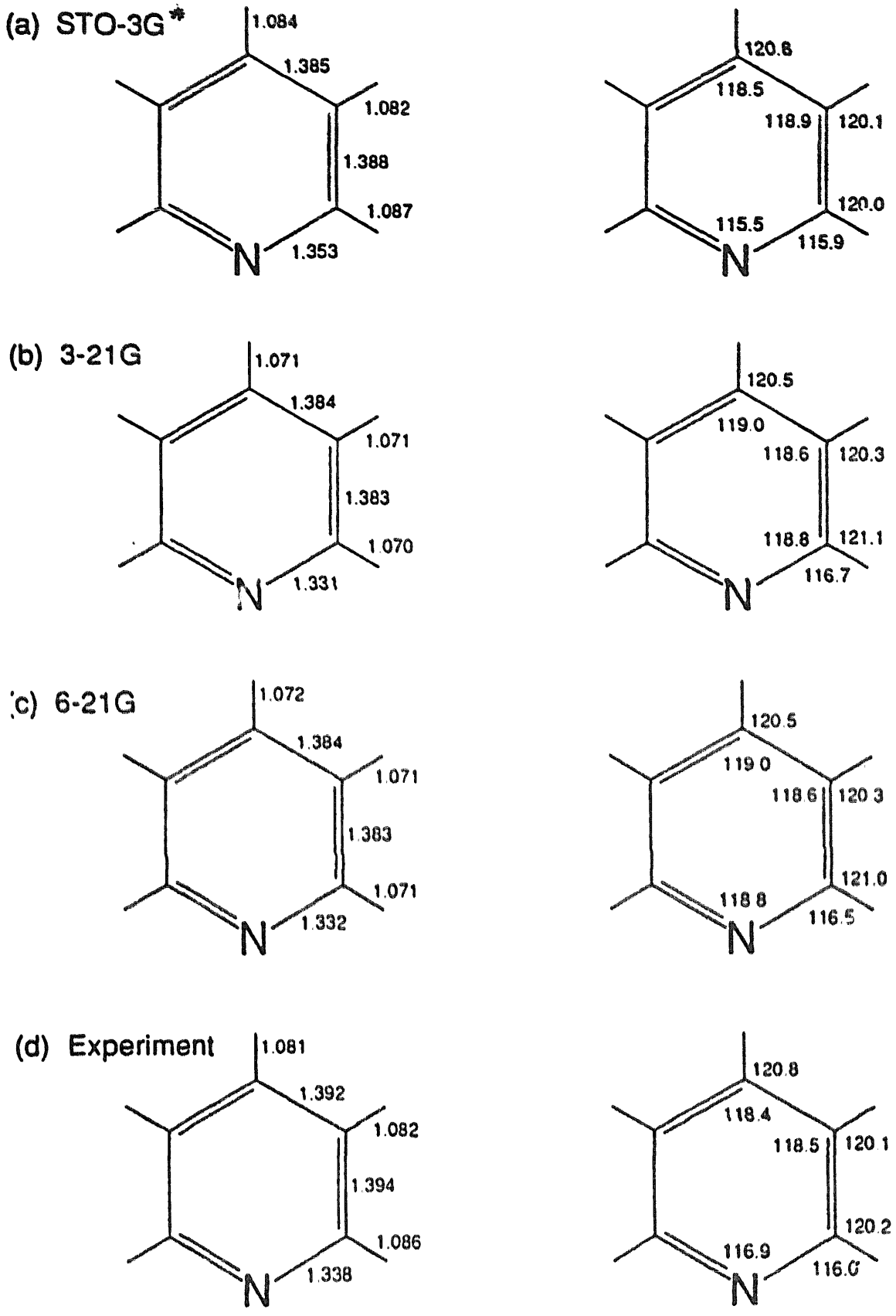

Fig. 2. Pyridine geometry optimized using (a) STO-3G, (b) 3-21G and (c) 6-21G sets, and (d) experimental structure determined by Sorensen et al. [52]. Reproduced with permission from reference [49].

where ϵ is the kinetic energy of the ejected electron, and the superscript designates the atom. From these equations, it is clear that, under HeI conditions, ionization from a valence MO composed primarily of a halogen 3p or 4p atomic orbital would result in a more intense band than would ionization from a valence MO composed primarily from a nitrogen 2p atomic orbital. Thus, the MO coefficients should give a description of the MOs in terms of atomic orbitals, and should also yield information about the variations in the spectral intensities of the UPS bands.

Using a plane wave approximation, the theoretical molecular photo-ionization cross-sections have been derived by Huang and Ellison [57]. The general expression for the molecular photo-ionization cross-section is given by

$$\sigma^{MO}(\epsilon)=\sum_{\mu} C_{i\mu}^2\sigma_{\mu}^{AO}(\epsilon)+2\sum_{\mu>\nu}\sum_{\mu} C_{i\mu}C_{i\nu}[\sigma_{\nu}^{AO}(\epsilon)\sigma_{\mu}^{AO}(\epsilon)]^{1/2}g_{\mu\nu} \quad (11)$$

where the C terms are the MO eigenvectors and $g_{\mu\nu}$ represents the interference factor.

It has been shown by Kaplan and Makin [58] and Schweig and Thiel [59] that the two centre terms $g_{\mu\nu}$ are important when comparing MOs of certain molecules. Moreover, for UPS, the interference factors have a more complicated form than that of spherical Bessel function [60] and are not considered to be negligible.

Because $g_{\mu\nu}$ is generally a function of the internuclear distance and depends on the atomic orbital of the MO, Peel and coworkers [61] have replaced it with the overlap integral $S_{\mu\nu}$, yielding the empirical expression

$$\sigma^{MO}(\epsilon)=\sum_{\mu} C_{i\mu}^2\sigma_{\mu}^{AO}(\epsilon)+2\sum_{\mu>\nu}\sum_{\mu} C_{i\mu}C_{i\nu}[\sigma_{\nu}^{AO}(\epsilon)\sigma_{\mu}^{AO}(\epsilon)]^{1/2}S_{\mu\nu} \quad (12)$$

where the σ_{μ}^{AO} values are now based on accurate theoretical atomic cross-section data discussed above. In a series of ab initio calculations, Peel and coworkers [61] have demonstrated that Eq. (12) is a 'good' approximation to the photo-ionization cross-section of an MO (i.e. σ^{MO} is a 'good' measure of the band intensity).

The analysis of the variation of the photoelectron band intensities with the incident photon energy (especially for HeI and HeII radiation) is a well-established aid in spectral assignment. Photo-ionization cross-section data for MOs (calculated using Eq. (12)) allow us to carry out semi-quantitative analysis of photoelectron band intensities. For example, the atomic cross-section for oxygen 2p atomic orbitals does not change significantly over the energy range of HeI or HeII UPS studies (shown in Fig. 3(a)), so the measurement of HeII spectra is expected to provide little additional information. Likewise, the similarity between the carbon and nitrogen 2p atomic orbital values over the HeI–HeII range makes differentiation between the n_N and ring-based π MOs of the pyridine systems difficult. However, the variation in the photo-ionization cross-section values (σ) for sulphur, selenium and tellurium over this range make HeII studies a very useful assignment tool (as seen in Fig. 3(b)).

The theoretical and experimental HeI photo-ionization cross-sections also form the basis of a density-of-states analysis [56,61]. The density-of-states analysis assumes that the band intensity is a measure of orbital degeneracy, so that, where

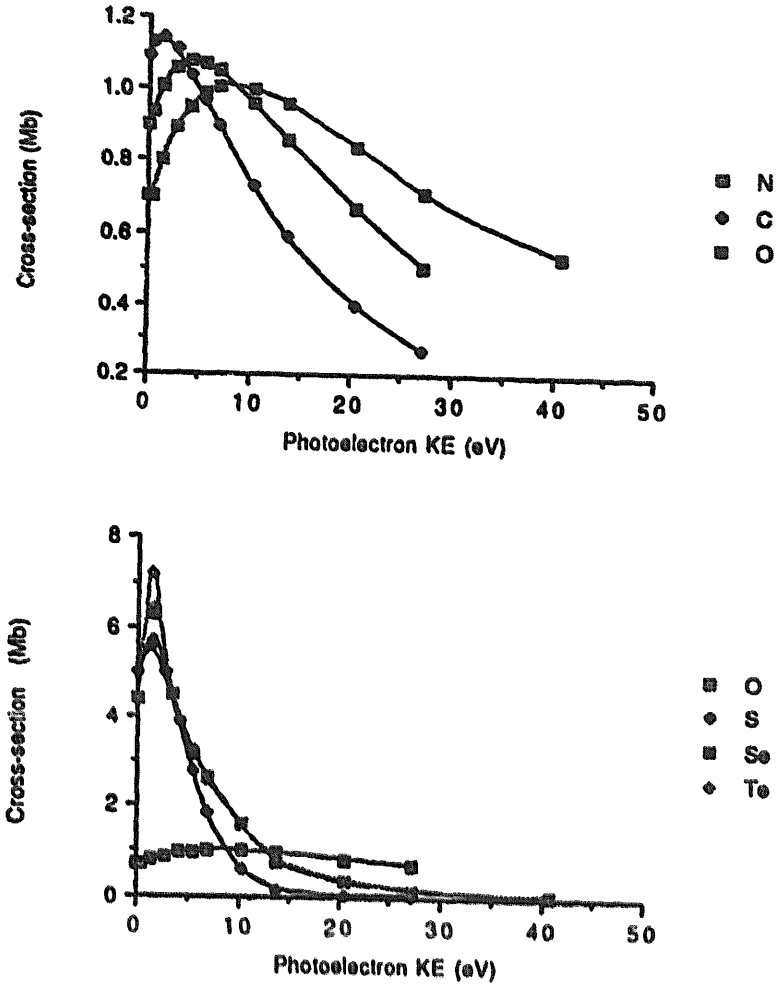

Fig. 3. (a) Total cross-section of the valence p atomic orbitals of C (◆), N (□) and O (■) as a function of the energy of the ejected electron. (b) Total cross-section of the valence p atomic orbitals of O (□), S (◆), Se (■) and Te (◇) as a function of the energy of the ejected electron. Reproduced with permission from reference [49].

bands are overlapped, the total band area in each separable region of the spectrum is related to the number of occupied orbitals. Based on the s–p separation rule, the number of p-based bands below 18 eV is given by

$$N_T = N_C + 0.5N_H + 1.5N_N + 2.0N_X + 2.5N_Y \quad (13)$$

where N_C, N_H, N_N, N_X and N_Y are the numbers of carbon, hydrogen, nitrogen, chalcogen and halogen atoms respectively. Care must be taken when using this rule, because a cross-over of an s-based and a p-based band occurs for pyridyl and aryl groups in the region 15–18 eV. Nevertheless, the s–p separation rule, together with the density-of-states analysis, is valuable in predicting vertical IE distributions.

3. Conformational and UPS analysis of the chalcogenobispyridines and related compounds

3.1. Pyridine

The UPS assignment of pyridine is fundamental in understanding the photoelectron spectra of the chalcogenobispyridines and related compounds. The electronic structure of pyridine has been the subject of numerous theoretical [62–64] and experimental investigations [64–66]. The ordering of the first three ionic states of pyridine corresponds to ionization from the nitrogen lone pair (n_N) and two highest p orbitals. The near-degeneracy of the first two bands in the UPS spectrum makes an unambiguous assignment impossible within the operating resolution of most spectrometers [62–65].

The s–p separation rule [56,61] allows the prediction of the number of p-based bands below 18 eV. For pyridine, Eq. (13) gives nine p-based bands and, allowing for a cross-over of an s-based and a p-based band occurring in the region 15–18 eV [64–67], a total of 10 bands would be predicted below 18 eV. The region between 9.5 and 12.5 eV contains four bands that exhibit π and σ character.

A number of UPS studies on pyridine and substituted pyridines have substantiated the spectral IE sequence as follows: $\pi(^2A_2) \sim n_N(^2A_1) < \pi(^2B_1) < \sigma(^2B_2)$. In the case of the substituted pyridines, the perfluoro effect, which provides greater stabilization for the σ-type MOs when compared with the π MOs, was used by Brundle et al. [65] and Daamen and Oskam [66] to show that the first band was caused by ionization from both a σ- (the n_N MO) and a π MO. The second and third bands were assigned to ionizations from π and σ MOs respectively [64–66].

Quantum mechanical calculations used in conjunction with Koopmans' approximation have been only partially successful in predicting the order of ionized states. Ab initio HF methods have failed to predict the accepted IE sequence [62–65]. This failure does not arise solely from basis set deficiencies, because basis sets of double-zeta quality [62–65] were utilized in some cases . The addition of polarization functions and the use of large extended basis sets have produced changes in the ordering of the inner valence orbitals, but have failed to rectify the relative positioning of the outer orbitals. Table 1 gives the KA–HF assignment calculated by von Nagy-Felsobuki and coworkers [27,67] using the 6-31G** basis set. It yielded the negative MO energy pattern

$$\pi(a_2) < \pi(b_1) < n_N(a_1) < \sigma(b_2)$$

which is in error with the accepted spectral assignment. Moreover, the absolute energy differences between the experimental and calculated IEs are of the order of 0.3 and 1.5 eV for the π and σ MOs respectively. It is clear that there are large variations in the energy differences between the π and σ types of MOs with respect to the IEs, indicating that the fortuitous cancellation may not have occurred, so placing the validity of the KA–HF model in doubt.

The importance of relaxation effects for the prediction of the IEs of pyridine was highlighted by Dobson et al. [63]. For pyridine, the C_{2v} molecular symmetry allows

Table 1
Comparison of experimental and theoretical IEs for pyridine[a]

Ionic state	IE[b] (eV)				
	Experimental	KA–HF/6-31G**	ΔSCF–HF		
			STO-3G*	3-21G*	6-31G**
$^2A_1$	9.7	11.32	6.08	8.19	8.17
$^2A_2$	9.7	9.37	7.04	8.58	8.34
$^2B_1$	10.5	10.26	7.38	9.13	8.77
$^2B_2$	12.5	13.95	12.03	13.09	12.85
	HAM/3[c]	MP2/STO-3G*	MP4/STO-3G*	MP2/3-21G*	MP4/3-21G*
$^2A_1$	9.68	8.08	7.87	9.78	9.48
$^2A_2$	10.03	8.13	8.04	9.74	9.58
$^2B_1$	10.68	9.16	8.96	10.76	10.46
$^2B_2$	12.88	12.85	12.60	13.64	13.30

[a] See references [27,67].
[b] See reference [64].
[c] HAM/3 IE calculation is for the STO-3G optimized geometry (see Fig. 2) and is a transition state calculation—one electron diffusively removed (see references [69–72]).

the calculation of the lowest four IEs, because the cationic states have different symmetries, i.e. $^2A_2$, $^2A_1$, $^2B_1$ and $^2B_2$. Table 1 also shows a series of ΔSCF–HF calculations performed on pyridine using the optimized STO-3G structure (see Fig. 2). It can be seen that, relative to the KA–HF assignments, the IE ordering at the ΔSCF–HF level more closely mirrors the experimental IE sequence, because all three basis sets yield the IE sequence [27,67]

$$n_N(^2A_1) < \pi(^2A_2) < \pi(^2B_1) < \sigma(^2B_2)$$

In comparison with the KA–HF model, the ΔSCF–HF method identifies MOs (such as the n_N MO) in which cancellation between relaxation and correlation error does not occur sufficiently. The ΔSCF–HF method is less successful for MOs, such as the π MOs of pyridine, in which these errors do effectively cancel, because the HF method only takes into consideration orbital relaxation. While an improvement in the ordering of the ionic states is seen at the ΔSCF–HF level, the separations between the calculated IEs are still too large when compared with the experimental findings. This results from basis set limitations and the neglect of correlation energies, because it is assumed in the ΔSCF–HF approach that the correlation error of the ground state (a $2N$-electron system) is identical in magnitude and sign to the correlation error of the cationic states ($2N-1$ electron systems). While correcting some of the errors inherent in the KA–HF approach, the ΔSCF–HF method also requires judicious use as an assignment tool.

von Niessen et al. [62] have used many-body perturbation calculations for the interpretation of the UPS spectra of the azapyridines. Their many-body Green's function calculations accounted for both electron correlation and reorganization.

They proposed that the existence of low-lying virtual orbitals led to non-uniform many-body effects, resulting in strong shifts of the IEs of the n_N electrons relative to the shifts of the π electrons, and rendering the KA–HF models useless for these molecules. Their calculations predicted the IEs of pyridine to within 0.25 eV of the experimentally derived pattern.

The ΔSCF–MP method, which is computationally tractable for pyridine, yields results that are comparable with the more extensive many-body Green's function calculations of von Niessen et al. [62]. Table 1 also compares a series of ΔSCF–MP2 and ΔSCF–MP4 calculations using the STO-3G* and 3-21G* basis sets [27,67]. The results at the 3-21G* level show 'good' agreement with the accepted pattern (a difference of less than 0.2 eV between the first two IEs calculated at the ΔSCF–MP2/3-21G* level and the experimental value). The improvement in the cationic distribution is evident using the ΔSCF–MP4/3-21G* model, with the largest discrepancy between theory and experiment being 0.8 eV for the $\sigma(^2B_2)$ state. It may be possible to achieve greater accuracy using more flexible basis sets. Nevertheless, it is clear that the ΔSCF–MP/3-21G* model is not only tractable but is also useful for the assignment of IEs of pyridine-based molecules.

Of the semi-empirical techniques, only MINDO/3 [68] and HAM/3 [69–72] have correctly predicted the IE sequence in pyridine. The IEs from the MINDO/3 calculation are shifted to energies about 1 eV higher than the accepted experimental pattern given in Table 1. The absence of parameters for third- and fourth-row atoms restricts the use of MINDO/3 for the study of molecules that contain heavy chalcogen atoms. The HAM/3 method of Åsbrink and coworkers [69–72] has been shown to predict reliably the distribution of ionic states for a number of problematic molecules, including pyridine. The success of the HAM/3 method arises from its inclusion of monocentric many-body effects, so that it accounts directly for relaxation and correlation processes in its calculation of IEs. However, the HAM/3 model's conformation analysis is not as reliable as all electron calculations. Table 1 clearly indicates that, for pyridine, the HAM/3 method yields the experimental order to within about 0.3 eV. Hence, combined use of the HAM/3 and STO-3G optimized geometries (denoted by HAM/3–STO-3G) is a useful—but still not a definitive—tool for the interpretation of the chalcogeno- compounds that contain first-row atoms.

It is clear that the use of ΔSCF–HF techniques must be treated with caution for the prediction of IE distributions, because a delicate balance exists between relaxation and correlation errors. However, if used in conjunction with an MO method that incorporates electron correlation, it is a useful aid for the assignment of IEs in simple pyridine-based systems. Despite criticism of the methodology employed in the HAM/3 method for the computation of correlation energies and self-repulsion [72], the HAM/3 method faithfully reproduces the IE distribution of pyridine in a fraction of the computation time needed for the ΔSCF–MP method—fortuitously or otherwise. Unfortunately, the HAM/3 method is currently only programmed for molecules that contain first-row atoms, so that it is of limited use.

3.2. Methylchalcogenopyridines

There have been few UPS studies on substituted pyridines and, of these, fewer still have been supported by theoretical calculations to reinforce spectral assignments.

A series of fluoro-substituted pyridines was studied by King et al. [73] to establish the relative order in pyridine. However, their ordering ($\pi(a_2) < n(a_1) < \pi(b_1)$) was contradicted by a similar study that compared methyl-, tertiary-butyl- and trimethylsilyl-substituted pyridines [74].

Only Cook et al. [75] and Dunne et al. [24,27,49] have studied the UPS spectra of the methylchalcogenopyridines. Cook et al. [75] used UPS to study the prototrophic equilibria between the hydroxy/oxo- and mercapto/thioxo- forms of the hydroxy- and mercaptopyridines respectively. The methoxy- and methylthio- forms of these compounds were used to block potential tautomerism, so simplifying the spectra observed. In contrast, Dunne et al. [24,27,49] studied the HeI and HeII spectra of the isomers of the methylchalcogenopyridines (with the exception of the methyltelluropyridines, which have still not been characterized). They used HeI/HeII cross-section comparisons, theoretical calculations, correlations and a composite–molecule model to substantiate their assignments.

Dunne et al. [24,27,49] optimized the geometries of the hydroxy-, mercapto- and selenopyridines at the STO-3G (for O) and STO-3G* levels (for S and Se) (denoted by STO-3G(*) hereafter) to study the effect of substitution on ring geometry. The fully optimized structures are shown in Fig. 4. In general, the ring bonds adjacent to the site of substitution are most affected with a marked increase in bond length relative to the bond length in pyridine. Bonds that are distant from the site show little variation from the pyridine structure. The degree of elongation of the bonds to the ipso carbons was found not to increase linearly down the group. For example, the bonds to the ipso carbons in the selenopyridines are shorter than those of the mercaptopyridines, although this may be caused by the relief of steric hindrance in the ring plane by the longer C–Se bond. The optimized structures of 2-hydroxypyridine and 2-mercaptopyridine are comparable with the reported 6-31G* and 3-21G* optimized structures of Adamowicz [76] and Nowak et al. [77] respectively. Although no experimental data exist on the hydroxy compound, the STO-3G(*) structure compared favourably with the crystal structure data on the 2-pyridinethiolato ligand in phenylbis[2-pyridylthiolato(1-)] antimony(III) [78] and tris(2-pyridylthiolato) antimony(III) complexes [79] respectively. This gives additional confidence in the STO-3G(*) basis sets for structural analysis of larger pyridine systems.

For the hydroxy-, mercapto- and selenopyridines, the relative stabilities of the (3-, 4-) isomers compared with the 2- isomer are (31 kJ mol^{-1}, 26 kJ mol^{-1}), (7 kJ mol^{-1}, 6 kJ mol^{-1}) and (8 kJ mol^{-1}, 7 kJ mol^{-1}) respectively [49]. They follow the trend

$$\text{ortho}(2-) > \text{para}(4-) > \text{meta}(3-)$$

which agrees with the nature of these substituents being both σ-electron acceptors and π-electron donors [27]. The ring-nitrogen in pyridine acts as a π-electron acceptor. Hence, the π electron densities at C_2, C_4 and C_6 are lower than those in benzene, whereas the densities at C_3 and C_5 are greater. The introduction of a π-electron donor at the 2 or 4 position of pyridine stabilizes the molecule, whereas

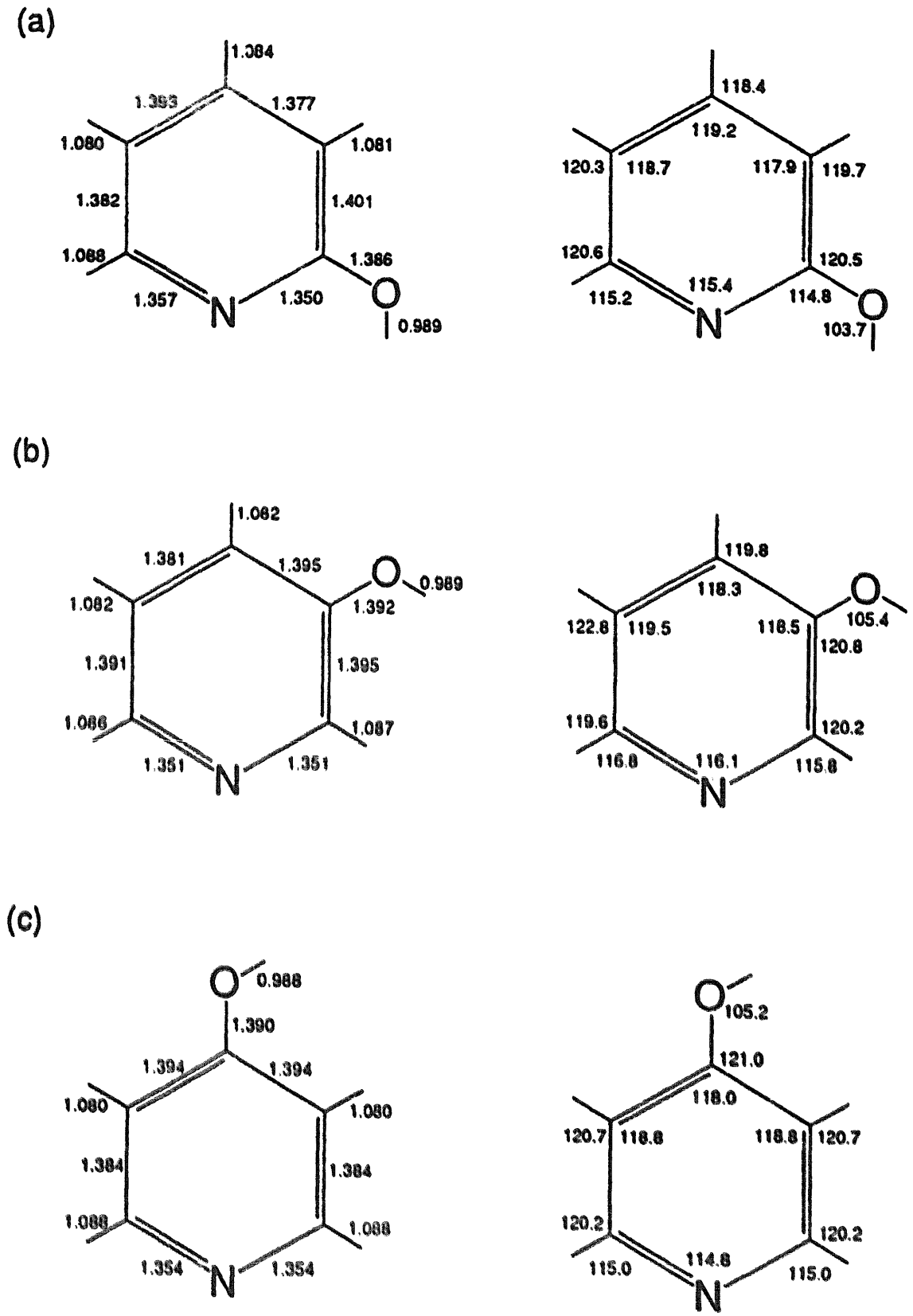

Fig. 4. STO-3G(*) optimized structures of (a) 2-hydroxypyridine; (b) 3- hydroxypyridine; (c) 4-hydroxypyridine; (d) 2-mercaptopyridine; (e) 3-mercaptopyridine; (f) 4-mercaptopyridine; (g) 2-selenopyridine; (h) 3-selenopyridine; (i) 4-selenopyridine. Reproduced with permission from reference [49].

(d)

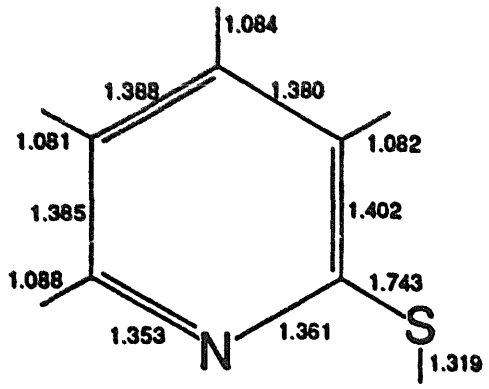
1.084
1.388
1.380
1.081
1.082
1.385
1.402
1.088
1.743
1.353
N
1.361
S
1.319

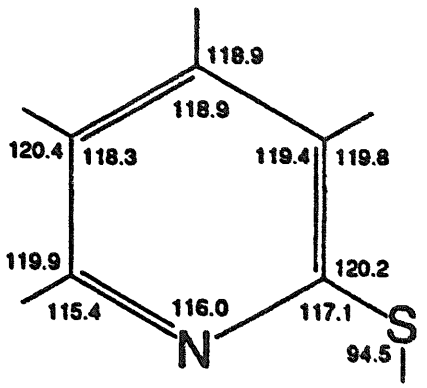
118.9
118.9
120.4
118.3
119.4
119.8
119.9
120.2
115.4
116.0
117.1
S
N
94.5

(e)

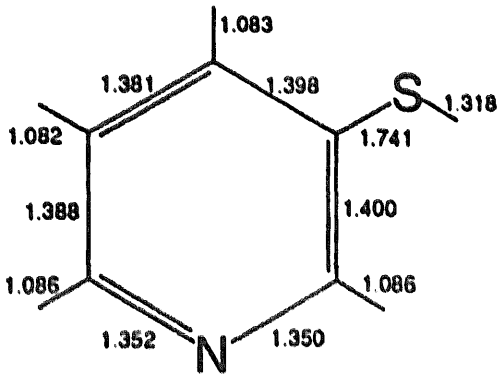
1.083
1.381
1.398
S
1.318
1.082
1.741
1.388
1.400
1.086
1.086
1.352
N
1.350

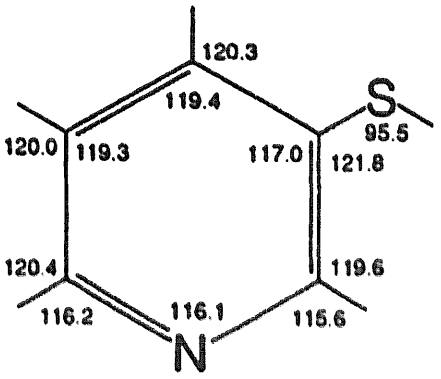
120.3
119.4
S
95.5
120.0
119.3
117.0
121.8
120.4
119.6
116.2
116.1
115.6
N

(f)

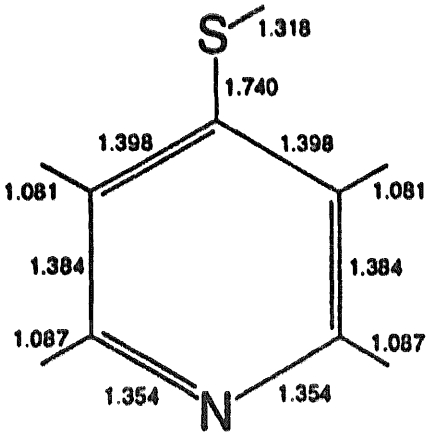
S
1.318
1.740
1.398
1.398
1.081
1.081
1.384
1.384
1.087
1.087
1.354
N
1.354

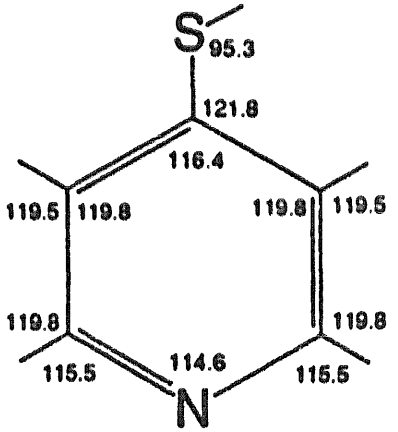
S
95.3
121.8
116.4
119.5
119.8
119.8
119.5
119.8
119.8
115.5
114.6
115.5
N

(g)

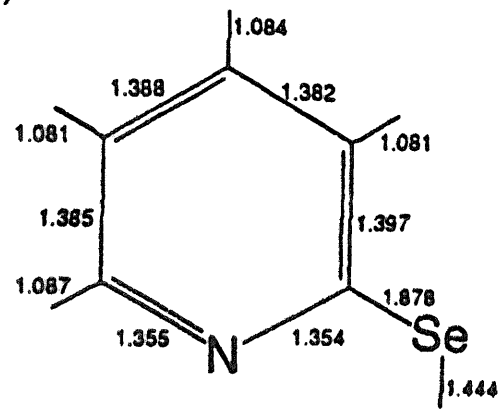
1.084
1.388
1.382
1.081
1.081
1.385
1.397
1.087
1.878
1.355
N
1.354
Se
1.444

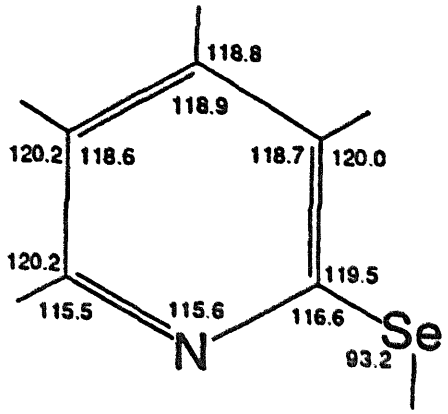
118.8
118.9
120.2
118.6
118.7
120.0
120.2
119.5
115.5
115.6
116.6
Se
93.2
N

(h)

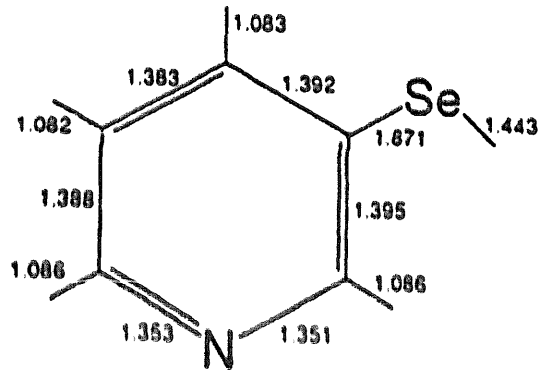
1.083
1.383
1.392
Se
1.443
1.082
1.871
1.388
1.395
1.086
1.086
1.353
N
1.351

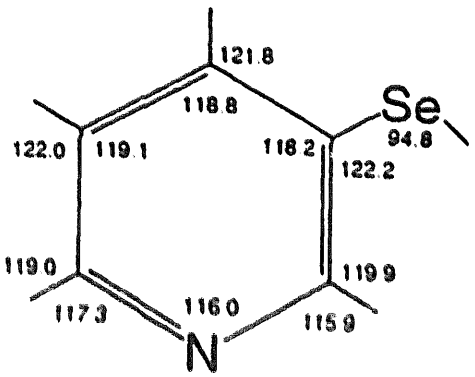
121.8
118.8
Se
94.8
122.0
119.1
118.2
122.2
119.0
119.9
117.3
116.0
115.9
N

(i)

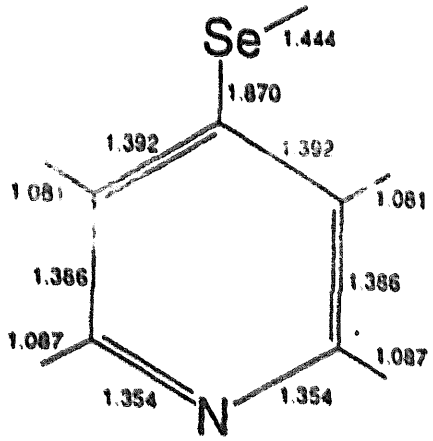
Se
1.444
1.870
1.392
1.392
1.081
1.081
1.386
1.386
1.087
1.087
1.354
N
1.354

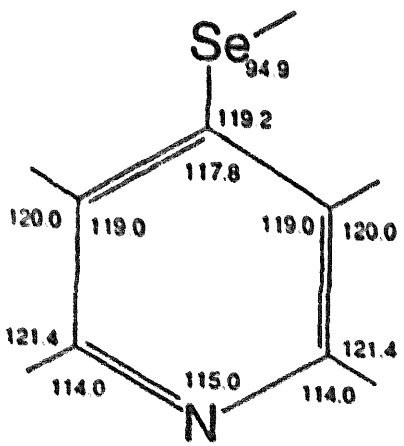
Se
94.9
119.2
117.8
120.0
119.0
119.0
120.0
121.4
121.4
114.0
115.0
114.0
N

substitution in the 3 position has a destabilizing effect. It was found that, for mono-substituted benzenes, the presence of a π-electron-donating group increases the π electron density at the ortho position more than at the para position [80], so it may be expected that the substitution of a π-electron-donating group at the 2 position in pyridine should be more favoured than substitution at the 4 position, because the nitrogen atom can better accommodate the increased π electron density. Another contributing factor to the greater stability of the 2-substituted systems is the hydrogen-bonding interaction between the pyridine nitrogen and the in-plane hydrogen of the XH group.

A complication in the analysis of the UPS spectra of large organic molecules is the possible presence of rotamers. For example, there have been several reports of the presence of rotational isomers in the UPS spectrum of thioanisole [81]. It was postulated that the two dominant conformers are a planar form (in which the methyl carbon lies in the plane of the phenyl ring with maximum p–π interaction) and a non-planar form (in which the methyl carbon–sulphur bond lies perpendicular to the plane of the ring). To model the ratio of these two conformers in the pyridine analogues, a series of geometry optimizations was performed by Dunne et al. [24] on all the isomers of the methylchalcogenopyridines (X = O, S, Se). The ring geometry was fixed at the optimized alcohol form and the ether bridge parameters (i.e. the $R_{\text{Ring-X}}$ and $R_{\text{X-methyl}}$ bond lengths and the bridge angle) were optimized at torsional angles of 30° using the routine of Fletcher and Powell [50]. The optimized variables and calculated rotational barrier heights are given in Table 2.

The bridge bond lengths were found to be shortest for the planar form, in which the maximization of p–π overlap competes with the relief of steric interaction by elongation of these bonds [24]. The relief of the strain energies in the planar form (Ø = 0°) is achieved by the opening of the bridge angle. The opposite trend is observed for the non-planar forms (Ø = 90°), i.e. longer bonds but a more acute bridge angle. The longer $R_{\text{Ring-X}}$ bond results from electron repulsions between the chalcogen lone pair and the σ system of the pyridine ring, while the contraction of the bridge angle may enhance the participation of the X–Me group in a hyperconjugative interaction with the π system of the pyridine ring.

The rotational barrier heights between the planar and non-planar forms show a number of interesting trends [24]. In the 2-methylchalcogenopyridine series, the barriers are 23.8 (O), 21.4 (S) and 16.2 kJ mol^{-1} (Se) in favour of the planar conformer. Of all the congeners, these barriers are the largest, highlighting the stabilization that results from the presence of the ortho ring-nitrogen. Assuming that only the planar and non-planar conformers exist, a Boltzmann distribution can be used to predict their relative populations in an equilibrium mixture. For example, at 300 K (the ambient temperature of the general UPS experiment), the proportions of the non-planar form would be 0.00 (O), 0.01 (S) and 0.11% (Se) and, therefore, would be undetectable.

A similar analysis for the 3- series gave barrier heights between the planar and non-planar forms of 6.1 (O), 8.1 (S) and −0.2 kJ mol^{-1} (Se), with the corresponding populations of 6.9% (O), 3.2% (S) and 51.7% (Se). However, in the case of the 3-methylselenylpyridine, the predicted minimum was a gauche form (Ø = 60.0°) [24].

Table 2
STO-3G(*) optimized parameters for the methylchalcogenopyridines[a]

Ø (deg)	ΔE (kJ mol^{-1})	R_{Ring-X} (Å)	R_{Me-X} (Å)	A_{C-X-C} (deg)
(a) *2-Methoxypyridine*				
0	0.0	1.390	1.438	113.7
30	6.9	1.396	1.440	113.1
60	16.6	1.406	1.443	110.8
90	23.8	1.410	1.444	109.8
120	30.3	1.409	1.442	112.2
150	36.8	1.402	1.436	116.8
180	33.2	1.397	1.432	117.4
(b) *2-Methylthiopyridine*				
0	0.0	1.745	1.785	100.5
30	5.8	1.752	1.788	99.9
60	15.6	1.763	1.791	98.3
90	21.4	1.768	1.792	97.6
120	21.0	1.766	1.793	99.0
150	21.6	1.761	1.791	103.0
180	18.6	1.756	1.787	104.0
(c) *2-Methylselenylpyridine*				
0	0.0	1.878	1.899	98.5
30	3.8	1.882	1.902	98.1
60	11.1	1.886	1.904	96.9
90	16.2	1.888	1.905	96.6
120	17.0	1.888	1.906	97.7
150	18.8	1.888	1.902	101.2
180	17.9	1.887	1.900	102.2
(d) *3-Methoxypyridine*				
0	0.0	1.396	1.436	115.7
30	4.9	1.401	1.439	115.2
60	5.4	1.408	1.444	111.6
90	6.1	1.411	1.445	109.8
120	11.4	1.410	1.443	112.0
150	19.8	1.404	1.436	116.8
180	16.9	1.400	1.432	117.5
(e) *3-Methylthiopyridine*				
0	0.0	1.746	1.786	103.1
30	3.7	1.752	1.789	102.3
60	6.1	1.759	1.794	99.4
90	8.1	1.762	1.794	98.1
120	8.4	1.761	1.794	99.3
150	12.1	1.757	1.789	103.1
180	10.6	1.754	1.785	104.1

Table 2 (*continued*)

Ø (deg)	ΔE (kJ mol^{-1})	R_{Ring-X} (Å)	R_{Me-X} (Å)	A_{C-X-C} (deg)
(f) *3-Methylselenylpyridine*				
0	0.5	1.875	1.900	102.0
30	1.3	1.876	1.903	101.1
60	0.0	1.876	1.906	98.1
90	0.3	1.876	1.906	97.1
120	1.2	1.877	1.905	97.9
150	5.7	1.879	1.903	101.4
180	6.2	1.878	1.899	102.3
(g) *4-Methoxypyridine*				
0	0.0	1.393	1.435	116.4
30	2.5	1.399	1.439	109.6
60	4.5	1.407	1.446	104.0
90	4.9	1.409	1.446	103.6
(h) *4-Methylthiopyridine*				
0	0.0	1.746	1.786	103.4
30	2.6	1.751	1.789	101.8
60	7.6	1.761	1.794	98.6
90	10.6	1.765	1.795	98.1
(i) *4-Methylselenylpyridine*				
0	0.0	1.873	1.900	101.4
30	1.2	1.875	1.903	101.0
60	3.8	1.879	1.906	98.2
90	5.5	1.881	1.907	97.0

[a] Reproduced with permission from reference [24].

For the 4- series, the barrier heights were 4.9 (O), 10.6 (S) and 5.5 kJ mol^{-1} (Se), which correspond to non-planar populations of 11.0% (O), 1.1% (S) and 8.8% (Se) [24]. In general, these results show an increase in the population of the non-planar conformer down the group and reflect experimental results on similar molecules [81–83].

A series of single-point calculations were performed with the STO-3G(*) optimized planar and non-planar geometries using the 6-31G** basis set (denoted by 6-31G**//STO-3G(*), even though the LWD [84] basis set was employed for the Se and Te compounds) to predict more accurately the population balance between these two conformers [27]. The 6-31G**//STO-3G(*) model reveals a somewhat different picture of the expected distribution of conformers in some cases. Although the barrier heights to the non-planar forms of the 2-methylchalcogenopyridines have all been reduced compared with the case for the STO-3G(*)//STO-3G(*) model,

this conformer would still be difficult to detect in UPS spectra, because of its low abundance (less than 1%).

The situation is different, however, for the 3-methylchalcogenopyridines. While the barrier to the non-planar form of 3-methoxypyridine is reduced to only 4.47 kJ mol^{-1}, the non-planar conformers of the sulphur and selenium analogues are predicted to be dominant, in contrast to the predictions of the STO-3G(*)//STO-3G(*) model [27]. For the 4-methylchalcogenopyridines, the 6-31G**//STO-3G(*) model shows a greater proportion of the non-planar conformer down the group compared with the STO-3G*//STO-3G* results; for example, 86% in the case of 4-methylselenopyridine [27]. Hence, it is anticipated that the UPS spectra of these compounds may contain a significant presence of rotational contamination. The accuracy of the 6-31G**//STO-3G(*) and STO-3G(*)//STO-3G(*) models [27] can be directly tested by observation of their UPS spectra.

The interpretation of the UPS spectra of pyridine-based molecules is complicated by the inability of ab initio KA–HF models to predict the correct IE ordering. In a study on 4,4′-di-substituted 2,2′-bipyridines, Dobson et al. [63] used a ΔSCF–HF approach for the assignment of the pyridine spectrum (see Section 3.1). Using 3-21G calculations, they showed that the orbital relaxation associated with ionization from the localized a_1 MO was significantly greater than that of the delocalized π orbitals. However, while the inclusion of relaxation effects changed the relative orbital ordering, the energy distribution was still poor. In view of the inability of calculations—both at the KA–HF and ΔSCF–HF levels of theory—to predict accurately the IEs of pyridine (see Section 3.1), it was shown that a method that incorporated both relaxation and correlation effects is needed to obtain an accurate assignment of the methylchalcogenopyridines [24,27].

The four lowest experimental IEs are listed in Table 3, together with the composite-molecule model assignments for the planar conformers based on the eigenvalues and eigenvectors obtained from the HAM/3 model (in the case of the methoxypyridines) [24,27], and from the STO-3G* and 6-31G** methods [24]. Table 3 also shows the 6-31G** MO energies and assignments (in parentheses) for the non-planar conformers.

The HeI UPS spectra of 2-methoxypyridine and all three of the methylthiopyridines have been reported by both Cook et al. [75] and Dunne et al. [24,27]. The vertical IEs quoted in both studies are in reasonable agreement with each other, although Dunne et al. made use of butadiene as a calibration gas to achieve greater accuracy for the lower IEs. The assignments of Cook et al. [75] were based on simple correlations and match those presented in Table 3.

The HeI spectra were digitized for use in the density-of-states analysis [24,27]. In the case of the methylchalcogenopyridines, Eq. (13) would predict 13 p-based bands and, with the corresponding cross-over, a total of 14 bands would be expected below 18 eV. As a result of the large number of overlapping cationic states at higher energies, the assignments of the UPS spectra of the methylchalcogenopyridines (given in Table 3) are restricted to the four lowest valence IEs. The assignments given are in terms of a composite-molecule model, which assumes that the MOs are

Table 3
Comparison of experimental vertical IEs with HAM/3 and KA–HF IEs for the planar conformers of the methylchalcogenopyridines[a]

	IE (eV)	Assign. MO	Koopmans' approximation			
			HAM/3	STO-3G*	3-21G*	6-31G**
(a) *2-Methoxypyridine*						
IE_1	8.59	$p\text{-}n_O(\pi(a_2))$	9.07	7.14	9.02	8.82 (9.25)
IE_2	9.66	$n_N(n_N)$	9.69	9.34	11.42	11.56 (11.52)
IE_3	10.16	$\pi\text{-}\delta n_O(\pi(b_1))$	10.30	8.79	10.62	10.42 (10.42)
IE_4	11.41	$\pi + n_O(n_O)$	11.25	10.89	12.71	12.76 (12.32)
(b) *3-Methoxypyridine*						
IE_1	8.98	$\pi\text{-}n_O(\pi(a_2))$	9.04	7.22	9.06	8.85 (9.23)
IE_2	9.75	$n_N(n_N)$	9.49	9.10	11.15	11.34 (11.30)
IE_3	10.24	$\pi\text{-}\delta n_O(\pi(b_1))$	10.14	8.67	10.36	10.16 (10.32)
IE_4	11.88	$\pi + n_O(n_O)$	11.56	11.28	13.23	13.23 (12.60)
(c) *4-Methoxypyridine*						
IE_1	9.15	$\pi\text{-}n_O(\pi(a_2))$	9.42	7.50	9.59	9.46 (9.56)
IE_2	9.82	$n_N(n_N)$	9.50	9.19	11.20	11.38 (11.51)
IE_3	9.82	$\pi\text{-}\delta n_O(\pi(b_1))$	9.71	8.30	9.61	9.86 (10.04)
IE_4	11.97	$\pi + n_O(n_O)$	11.67	10.98	13.19	13.36 (12.42)
(d) *2-Methylthiopyridine*						
IE_1	8.16	$\pi\text{-}n_S(n_S)$	—	5.91	8.34	8.24 (9.31)
IE_2	9.52	$n_N(n_N)$	—	8.88	11.28	11.44 (11.37)
IE_3	10.25	$\pi\text{-}\delta n_S(\pi(a_2))$	—	8.52	10.52	10.34 (9.42)
IE_4	11.40	$\pi + n_S(\pi(b_1))$	—	9.14	11.16	10.98 (10.44)
(e) *3-Methylthiopyridine*						
IE_1	8.47	$\pi\text{-}n_S(\pi(a_2))$	—	6.03	8.41	8.27 (9.43)
IE_2	10.04	$n_N(n_N)$	—	8.81	11.10	11.25 (11.49)

Table 3 (*continued*)

	IE (eV)	Assign. MO	Koopmans' approximation			
			HAM/3	STO-3G*	3-21G*	6-31G**
IE_3	10.89	$\pi-\delta n_S(n_S)$	—	8.45	10.31	10.09 (9.56)
IE_4	11.72	$\pi+n_S(\pi(b_1))$	—	9.42	11.61	11.47 (10.40)
(f) *4-Methylthiopyridine*						
IE_1	8.46	$\pi-n_S(\pi(a_2))$	—	6.27	8.81	8.77 (9.54)
IE_2	9.58	$n_N(n_N)$	—	8.92	11.18	11.35 (11.50)
IE_3	9.58	$\pi-\delta n_S(n_S)$	—	8.10	9.85	9.54 (9.70)
IE_4	11.03	$\pi+n_S(\pi(b_1))$	—	9.60	11.82	11.70 (10.20)
(g) *2-Methylselenylpyridine*						
IE_1	8.22	$\pi-n_{Se}(n_{Se})$	—	6.72	8.12	8.07 (8.78)
IE_2	9.53	$n_N(n_N)$	—	9.28	11.12	11.25 (11.19)
IE_3	10.12	$\pi-\delta n_{Se}(\pi(a_2))$	—	8.79	10.46	10.27 (9.44)
IE_4	11.15	$\pi+n_{Se}(\pi(b_1))$	—	9.46	10.93	10.74 (10.45)
(h) *3-Methylselenylpyridine*						
IE_1	8.52	$\pi-n_{Se}(n_{Se})$	—	6.83	8.20	8.11 (9.06)
IE_2	9.89	$n_N(n_N)$	—	9.18	11.02	11.13 (11.37)
IE_3	10.67	$\pi-\delta n_{Se}(\pi(a_2))$	—	8.72	10.29	10.07 (9.46)
IE_4	11.43	$\pi+n_{Se}(\pi(b_1))$	—	9.74	11.30	11.16 (10.40)
(i) *4-Methylselenylpyridine*						
IE_1	8.57	$\pi-n_{Se}(n_{Se})$	—	7.07	8.54	8.53 (9.15)
IE_2	9.83	$n_N(n_N)$	—	9.24	11.11	11.27 (11.39)
IE_3	9.83	$\pi-\delta n_{Se}(\pi(a_2))$	—	8.36	9.84	9.55 (9.57)
IE_4	10.81	$\pi+n_{Se}(\pi(b_1))$	—	9.93	11.53	11.40 (10.20)

[a] Values in parentheses are the calculated IEs for the non-planar conformer. Reproduced with permission from references [24,27].

linear combinations of orbitals from the pyridine ring and those of the methylchalcogen group.

The UPS spectra of the 2- series show low intensity bands attributable to the presence of minor conformer(s), which are not predicted by either of the models. The UPS spectra of 3-methylthiopyridines and 3-methylselenylpyridines show an even mixture of two conformers (assuming that the photo-ionization cross-sections for the MOs of each conformer are the same). These results do not agree with the 6-31G**//STO-3G(*) model barrier heights, which predict domination by the non-planar form for the S and Se analogues (more than 90%) [27]. The STO-3G(*)//STO-3G(*) results are generally in better agreement with the spectra. Furthermore, the STO-3G(*)//STO-3G(*) results are consistent with the UPS spectra of thioanisole [81,82], which give a presence of 10%–30% of the non-planar form. The UPS spectra of the 4- series show no evidence of the presence of minor conformers, which is again supported by the STO-3G(*)//STO-3G(*) calculations.

For the non-planar electron-dense methylchalcogens (i.e. S and Se analogues), both the STO-3G(*)//STO-3G(*) and 6-31G**//STO-3G(*) models predict ionization from an MO with significant chalcogen p- atomic orbital character. Hence, reductions of the order of 60%–70% should be exhibited on changing from HeI to HeII radiation. The peaks that are attributed to the presence of conformer(s) other than the dominant planar conformer show no such reduction, indicating that the conformer(s) present may be non-planar, but not at $\emptyset = 90^{\circ}$ [24]. For example, a gauche structure was predicted by the STO-3G(*)//STO-3G(*) model as the lowest energy conformer for 3-methylselenylpyridine. Thus, the accurate determination of the equilibrium distribution between the non-planar and planar conformers requires the use of extended basis sets with polarization functions, in conjunction with extensive geometry optimization.

The HeI/HeII ratios are useful (to a first-order approximation) for identifying those MOs that contain atoms with atomic cross-sections, that are markedly reduced under HeII conditions. The ratio of these cross-sections ($\sigma_{HeII}/\sigma_{HeI}$) represents the extent of band reduction expected on HeII irradiation. Normalized $\sigma_{HeII}/\sigma_{HeI}$ values for the elements which comprise the methylchalcogenopyridines are as follows: 0.62, C; 0.80, N; 1.00, O; 0.32, S; 0.29, Se; 0.24, Te. Delocalization and extensive mixing alter the σ values for the MOs of these compounds. However, these atomic values provide a basis for qualitative predictions of the MO character of molecules that contain S, Se and Te atoms, for which the effects are most marked.

While the HeII UPS spectra of the methoxypyridines show little variation relative to those recorded under HeI conditions, the thio- and seleno- analogues exhibit useful differences (as predicted by the $\sigma_{HeII}/\sigma_{HeI}$ values). Those bands that show significant reduction under HeII conditions must contain a significant contribution of S (or Se) p atomic orbitals. The greater the reduction is, the larger will be the contribution. Table 4 gives the band intensities and the percentage change in those bands on changing the radiation source.

The methylthiopyridines exhibit significant variation in the first and fourth bands, i.e. those assigned to the anti-bonding and bonding S π MOs of the planar conformer. The degree of reduction is approximately the same, suggesting that the contributions of ring and S electrons are about the same in both cases. The predicted IE distribu-

Table 4
Relative HeI and HeII band intensities and percentage change for the methylchalcogenopyridines[a]

Band	IE range (eV)	Band intensity[b]		Percentage change[c] (%)
		HeI	HeII	
(a) *2-Methoxypyridine*				
1	8.0–9.1	0.88	0.84	−4.6
2	9.1–10.0	1.08	1.03	−4.1
3	10.0–11.0	1.02	1.17	15.1
4	11.0–11.9	1.02	1.35	32.7
5	11.9–18.0	10.05	9.60	−4.5
(b) *3-Methoxypyridine*				
1	8.0–9.4	0.91	0.94	3.3
2	9.4–10.2	1.10	1.38	25.5
3	10.2–11.5	1.11	0.95	−14.4
4	11.5–12.3	0.99	1.00	1.0
5	12.3–18.0	9.90	9.73	−1.7
(c) *4-Methoxypyridine*				
1	8.0–11.0	3.52	3.64	3.4
2	11.0–12.3	1.47	1.43	−2.7
3	12.3–18.0	9.01	8.92	−1.0
(d) *2-Methylthiopyridine*				
1	8.0–9.0	0.98	0.60	−38.8
2	9.0–10.1	1.04	1.59	52.9
3	10.1–10.9	1.49	1.61	8.1
4	10.9–11.9	1.32	0.99	−25.0
5	11.9–18.0	9.17	8.94	−2.5
(e) *3-Methylthiopyridine*				
1	8.0–9.1	1.09	0.91	−16.5
2	9.1–10.2	1.56	1.86	19.2
3	10.2–11.2	1.19	1.58	32.8
4	11.2–12.2	1.19	0.79	−33.6
5	12.2–18.0	8.86	8.63	−2.6
(f) *4-Methylthiopyridine*				
1	8.0–8.9	1.40	0.92	−34.3
2	8.9–10.1	1.80	2.40	33.3
3	10.1–11.3	0.98	1.01	3.1
4	11.3–12.0	1.04	0.80	−23.1
5	12.0–18.0	8.62	8.68	0.7
(g) *2-Methylselenylpyridine*				
1	8.0–8.9	1.31	0.69	−47.3
2	8.9–9.8	0.89	1.07	20.2
3	9.8–10.8	1.55	1.83	18.1
4	10.8–11.6	0.95	0.83	−12.6
5	11.6–12.5	1.20	0.90	−25.0
6	12.5–18.0	8.11	8.68	7.0

Table 4 (*continued*)

Band	IE range (eV)	Band intensity[b]		Percentage change[c] (%)
		HeI	HeII	
(h) *3-Methylselenylpyridine*				
1	8.0–9.0	1.08	0.63	−41.7
2	9.0–10.2	1.98	2.78	40.4
3	10.0–11.2	1.33	1.86	39.8
4	11.2–12.0	0.96	0.62	−35.4
5	12.0–18.0	8.92	8.11	−9.1
(i) *4-Methylselenylpyridine*				
1	8.0–9.0	1.29	0.70	−45.7
2	9.0–10.4	1.86	2.53	36.0
3	10.4–11.3	0.88	0.82	−6.8
4	11.3–11.9	0.99	0.62	−37.4
5	11.9–18.0	8.95	9.29	3.80

[a] Reproduced with permission from references [24,27].
[b] Normalized to 14 bands.
[c] [(HeII/HeI) − 1] × 100.

tions for the non-planar conformers suggest that only one valence band has significant S character, so giving weight to the planar model. The methylselenylpyridines exhibit a greater decrease in the HOMO and a decreased reduction of the bonding Se–π MO under HeII conditions, suggesting a greater contribution of Se 4p electrons to the HOMO.

The ionization from primarily pyridine π-based MOs should exhibit a relative intensity enhancement under HeII conditions, as a result of the intensity reduction of S- or Se-containing MOs. Delocalization of lone-pair MOs should decrease the extent of reduction on changing the radiation source. The band assigned to the n_N MO exhibits various changes (see Table 4), highlighting its delocalized nature. The delocalization of this MO over the σ framework of the pyridine moiety has been reported previously by Del Bene [51] and Dunne et al. [24,27].

The HeI/HeII ratios suggest that the STO-3G(*)//STO-3G(*) model yields relative barrier heights that are more consistent with the spectra than does the 6-31G**//STO-3G(*) model. This is consistent with the proton affinities investigation by von Nagy-Felsobuki and Kimura [85], in which it was concluded that hybrid theories performed poorly in predicting properties associated with energy differences, where the optimized structures are extremely sensitive to the basis set employed. However, it should be noted that this does not suggest that the Koopmans approximation IEs calculated also follow this trend, because, for this property, the fortuitous cancellation of relaxation with correlation error is of paramount importance.

For the non-planar forms of the methylchalcogenopyridines, the KA//6-31G** model predicts an IE distribution that is a composite of the IEs of pyridine and those of chalcogen lone-pair atomic orbitals. The IEs of the π and n_N MOs for the non-planar forms are within 0.2 eV of the pyridine IEs calculated using the same

model. The highest π MO of the non-planar form is similar to the equivalent MO in pyridine (which would be anticipated on symmetry grounds, because the chalcogen lone-pair atomic orbital is orthogonal to the pyridine π-based MO). Unlike the planar conformers, the π MOs of the non-planar forms do not show a 'rotation', as a result of substitution. The experimental valence IEs are in poor agreement with those predicted for the non-planar form. Hence, the assignment focused on the planar conformer, which was considered to be the most dominant conformer in the spectra. This is consistent with the ab initio calculations (STO-3G*//STO-3G* model) and HeI/HeII ratios [24,27].

Substitution of a π-electron-donating substituent into the pyridine moiety results in a number of perturbations to the electronic structure of the ring system. In a composite–molecule model, the valence p atomic orbitals of the chalcogen atom will form bonding and anti-bonding combinations with the b_1 π MO of the pyridine system. Depending on the point of substitution, this will entail a 'rotation' of the pyridine π MOs. The b_1 MO in the parent pyridine molecule has maximum electron density on the N and C_4 atoms. However, on interaction with a substituent in the 2 or 3 position, this electron density shifts. Similarly, the a_2 MO of pyridine, which has minimal electron density in the parent molecule on the N atom, can shift on substitution to form an MO with substantial N character. The change in character of these MOs can produce predictable shifts in their IEs, so permitting reliable assignments.

The n_N MO (a_1) of pyridine cannot be significantly altered in character on substitution, although its IE is shifted by the presence of electronegative substituents. Strong σ-electron acceptors withdraw electron density from the N atom, so raising the IE of this σ-type MO. Similarly, with π-electron donors (acceptors), the addition (depletion) of electron density to the ring system results in lower (higher) π IEs. The balance between these factors is often difficult to assess, especially for flexible systems, but the observation of this series of compounds allows correlations to be made.

As in the case of pyridine, the HAM/3 method provides a better IE distribution of the methoxypyridines than do the KA–HF models (see Table 4). The KA–HF models position the n_N orbital as the third IE, in contradiction to the HAM/3 model and the experimental correlations for 2-methoxypyridine [27], which assign it as the second IE.

While the HAM/3 method provides the 'best' IE distribution, the larger basis set (6-31G**) calculations provide a more accurate description of the three π IEs—failing only to predict properly the position of the n_N IE. To correct this, a series of calculations at the ΔSCF–MP2/3-21G* level were performed on the methylchalcogenopyridines [27] and the results are presented in Table 5. The first π IEs (A″ symmetry) predicted by this method differ from their Koopmans' approximation equivalents by 0.143, 0.002 and 0.007 eV for 2-, 3- and 4-methoxypyridine, respectively, while those of a′ symmetry (i.e. the n_N IEs) have shifted to lower energies by 1.624, 1.476 and 1.939 eV respectively. Applying the ΔSCF–HF approach to the same systems results in differences of 1.239, 1.206 and 1.526 eV for the respective A″ states (with respect to the Koopmans' approximation IEs), and differences of 2.878, 2.945 and 3.048 eV for the A′ states. The difference between the two ΔSCF models is the inclusion of correlation effects in the first model, which are of the order of 1.2 eV.

Table 5
Comparison of experimental IEs with ΔSCF–MP2/3-21G* and KA/3-21G* IEs for the methylchalcogenopyridines[a]

Compound	Ionic state	IE (eV)		
		Experimental	ΔSCF–MP2/3-21G*	KA/3-21G*
2-OMe	$^2A''$	8.64	9.16	9.02
	$^2A'$	9.66	9.79	11.42
3-OMe	$^2A''$	8.98	9.06	9.06
	$^2A'$	9.75	9.67	11.15
4-OMe	$^2A''$	9.15	9.58	9.59
	$^2A'$	9.82	9.26	11.20
2-SMe	$^2A''$	8.16	8.67	8.34
	$^2A'$	9.52	9.68	11.28
3-SMe	$^2A''$	8.47	8.75	8.41
	$^2A'$	10.04	9.74	11.10
4-SMe	$^2A''$	8.46	9.12	8.81
	$^2A'$	9.58	9.35	11.18
2-SeMe	$^2A''$	8.22	8.55	8.12
	$^2A'$	9.53	9.71	11.12
3-SeMe	$^2A''$	8.38	8.66	8.20
	$^2A'$	9.89	9.75	11.02
4-SeMe	$^2A''$	8.57	8.98	8.54
	$^2A'$	9.83	9.37	11.11

[a] Only the IEs of the HOMO and the n_N MOs for the planar conformer are included. Reproduced with permission from reference [27].

Because the HAM/3 model was not programmed for sulphur or selenium, it was necessary to use a combination of models to assign the UPS spectra of the methylthio- and methylselenopyridines. Using pyridine as a basis (see Section 3.1), it was found that the KA–HF models gave a reasonable prediction of the IEs of the π-type MOs, but failed to position the n_N MOs correctly. However, the ΔSCF–MP2 model was found to give a better description of the n_N IE and a comparable description for the lowest π-type IE. Therefore, the KA/6-31G** model was used primarily to assign the π IEs (as shown in Table 3), whereas the ΔSCF/MP2–3-21G* model was used to assign the n_N IEs (as shown in Table 5) [27].

The first band in each spectrum is assigned to an anti-bonding combination of the valence p atomic orbitals of the chalcogen atom and the b_1 MO of pyridine. In the 2- and 4- series, this band becomes sharper down the group. The change in band shape is a reflection of the changing band character—becoming more 'lone pair' in character, as a result of the reduction in overlap of the pyridine π orbitals and the chalcogen valence atomic orbitals. For example, the b_1 MO in pyridine has an IE of about 10.5 eV, while the first IEs of the dimethylchalcogenides are 10.04 eV (O), 8.71 eV (S) and 8.40 eV (Se) [86]. Thus, the HOMO in the case of oxygen will have substantial ring character, leading to a broader band shape. The shift to lower IEs stems from the lower first IEs of the more electron-dense chalcogens.

The second and third bands seen in the UPS spectra arise from the a_1- and

a_2-based MOs of pyridine. There is much conjecture over the relative ordering of these two bands. There is little difference in their band shapes, and their behaviour under HeII conditions does not give conclusive resolution of their nature. The fourth band is assigned to the bonding combination of the p atomic orbitals of the chalcogen and the pyridine b_1 MO, while the fifth can be assigned, in some cases, as having substantial chalcogen p character. Similar to the HOMO, the bonding MO also shifts to lower IEs with atomic number in a predictable manner.

Of the KA–HF models used, only the 3-21G*//STO-3G(*) and 6-31G**//STO-3G(*) models produced reasonable IEs for the π MOs [24,27]. The STO-3G results are typically shifted by several electronvolts to lower IE values. The 3-21G* values are comparable with—and, in some cases, better than—the more extensive 6-31G** results. This suggests that the KA–HF model may not be capable of producing 'better' results, even when employing more extensive basis sets.

As shown for pyridine (see Section 3.1), the effect of electronic relaxation can have a dramatic effect on specific IEs (shifts of up to 2 5 eV), rendering the KA–HF models useless. However, the ΔSCF process is limited in its use, by symmetry constraints. The ΔSCF–MP2 method has been used to calculate the IEs for the HOMO and the n_N MOs. The results show 'good' correspondence with the experimental values. The IEs of the n_N MOs show vast improvement, while the HOMO IEs are comparable with the KA/6-31G** results, revealing the difference in the effect of relaxation on these two MOs. The success of the ΔSCF–MP2 model decreases down the group, suggesting that the interplay between correlation and relaxation is changing for molecules that contain second- and third-row atoms.

The σ-type n_N MO is directly affected by the electronegativity of the substituent. Substituents in the 2 position exert the greatest effect. The methoxy group (OMe) is assigned a group electronegativity value of 3.53, whereas the value for the methylthio- group (SMe) is 2.65 [87]. It is anticipated that the methylseleno- (SeMe) group shares the group electronegativity value of its thio- analogue, as a result of the similar atomic electronegativities of S and Se [88,89]. The OMe group will inductively draw electrons from the n_N MO, resulting in a stabilization of that MO. The similarity between the electronegativities of the pyridine ring and the SMe and SeMe groups may lead to the donation of electron density into the ring σ system, and a resultant destabilization of the n_N MO (i.e. a shift to a lower IE). The methylthiopyridine a_2 MO is stabilized by 0.40–0.65 eV in the 2- series. This can be directly related to an increase in the π electron density on the ring-nitrogen (a strong π acceptor), and results in a lower IE for the second π band. These trends are applicable to all the systems in this study, although overlapping of peaks and rotational contamination can make unambiguous assignment difficult.

The preferred sequence for all isomers of the dominant planar methylchalcogenopyridines, which is consistent with spectral and ab initio MO analyses, is given by [24,27]

$$\pi - n_X < n_N \sim \pi < \pi + n_X \tag{14}$$

where X represents the chalcogen element.

3.3. Oxybispyridines

The study on the methylchalcogenopyridines showed the importance of a theoretical conformational study for the interpretation of UPS spectra. The presence of a number of rotamers, while complicating the interpretation, can give valuable information on the energetics of the system. The oxybispyridine system represents a more complex system in terms of the number of degrees of freedom, but steric crowding acts to limit rotational motion. Four different models have been proposed for the oxybispyridine structures, based on the conformational study of diphenyl ether [90] and oxybispyridines [20,22].

The four basic structures are shown in Fig. 5 for 3,3'-oxybispyridine: a planar structure (**A**); the 'Morino' structure (**B**), which is based on electron diffraction [91], dielectric relaxation [92] and IR spectroscopy [93,94] studies; a structure (**C**) in which both rings are rotated at various angles relative to the C–O–C plane, which is based on investigations of molar Kerr constants [95,96], optical anisotropy [97], dielectric relaxation [98], UV spectroscopy [98] and vibrational spectroscopy [99]; the 'butterfly' structure (**D**) with both phenyl rings orthogonal to the C–O–C plane. While some of the isomers of oxybispyridine do closely mimic the conformational behaviour of diphenyl ether, the presence of ortho ring-nitrogens in isomers that contain a 2-pyridyl group results in structural relaxation, as a result of the removal of neighbouring ortho-hydrogen interactions.

A number of approaches have been used to study the conformational behaviour of moderately sized molecules. The most popular approach is the concept of the multi-dimensional potential energy surface. The central approximation in this model lies in the number and type of variables. For example, variation in only a single dimension produces a potential energy curve. The number of degrees of freedom in the oxybispyridines is 57. Such a potential energy surface is conceptually difficult and is difficult to compute, so a reduction is usually achieved by using a rigid-rotor model.

In the case of the oxybispyridines, the pyridine ring geometries were fixed at the STO-3G optimized structure [20]. The variable set was reduced to the two ring twist angles ($\emptyset_1$ and $\emptyset_2$), the inter-ring angle A_{C-O-C}, and the two ring–oxygen bond lengths (R_{C-O}), making a five-dimensional model. To reduce the variable set further,

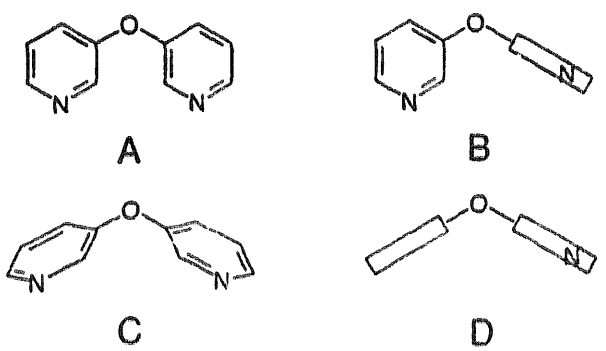

Fig. 5. A–D conformers for 3,3'-oxybispyridine.

the inter-ring angle (denoted by ω) was fixed at 120° and the two R_{C-O} values equated for all the calculations. The algorithm of Fletcher and Powell [50] was then used to optimize the R_{C-O} values for the **B**(0, 90) conformer of each isomer (because this conformer was thought to resemble most closely the minimum energy conformer). These R_{C-O} values were then held fixed for each torsional rotation by 30° of the twist angles. Therefore, the rigid-rotor model used consisted of only two variables ($\emptyset_1$ and $\emptyset_2$), so it could be plotted as a two-dimensional energy contour map.

To establish contour maps for each isomer of the oxybispyridines, the internal STO-3G(s=p) basis set was used within the LCAO MO SCF restricted HF method of the GAUSSIAN 86 suite of programs [42]. Taking the planar (N-inside, N′-inside) conformer as the **A**(0, 0) torsional position, the torsional angles of the oxybispyridine structures given by **A**–**D** (as shown in Fig. 5) were denoted by **A**(0, 0), **B**(0, 90), **C**($\emptyset_1$, $\emptyset_2$) and **D**(90, 90) respectively [20]. Here, a clockwise rotation of each pyridine moiety (as viewed along the respective inter-ring C–O bond) was considered as being a positive rotation. Hence, disrotatory twisting modes were characterized from (+$\emptyset_1$, +$\emptyset_2$) or (−$\emptyset_1$, −$\emptyset_2$) torsional combinations, whereas conrotatory modes are identified from (+$\emptyset_1$, −$\emptyset_2$) or (−$\emptyset_1$, +$\emptyset_2$) combinations [20].

The energy differences using the rigid-rotor model (ΔE_{RR}) between all the rotational isomers of the **A**–**D** structures are listed in Table 6. It is only for 2,4′-oxybispyridine that the 'Morino' structure (**B**) is also the minimum energy conformer. Nevertheless, from the contour energy maps, it is clear that the Morino structure is accessible to all isomers, because of the broad potential energy minima in the region of **C**. For example, the differences in energy between the structures **C** and **B**(0, 90) for 2,2′-, 2,3′-, 3,3′-, 3,4′- and 4,4′-oxybispyridine are 2.2, 0.2, 1.3, 0.8 and 1.8 kJ mol^{-1}, respectively [20]—all within the 2.5 kJ mol^{-1} available from the ambient surroundings.

From the **A**(0, 0) position, the **D**(90, 90) conformers are obtained via a conrotatory twisting mode. The energy differences between the **C** and the 'butterfly' (**D**) conformers for 2,2′-, 2,3′-, 3,3′-, 2,4′-, 3,4′- and 4,4′-oxybispyridine are 19, 19, 14, 20, 14 and 13 kJ mol^{-1} respectively [20]. The disrotatory twisting mode yields the cisoid conformer (i.e. **D**(−90, 90)). For three of the isomers, these two conformers are distinct. For 2,2′-, 2,3′- and 3,3′-oxybispyridine, the transoid conformer is found to be more stable by 9.7, 1.6 and 0.7 kJ mol^{-1} respectively [20]. In the case of the 2,2′- isomer, the stabilization results from the removal of the steric interaction between ortho-hydrogens in the transoid conformer and the stabilizing effect of non-bonded interactions between the nitrogen lone pair and the ortho-hydrogens.

For all the isomers, the planar **A** structure is the least favourable conformer. The energy differences between the minimum energy conformer and the **A**(0, 180) structure for the 2,2′-, 2,3′-, 3,3′-, 2,4′-, 3,4′- and 4,4′-oxybispyridines are 72, 116, 658, 111, 616 and 845 kJ mol^{-1} respectively [20]. Again, the reduction in the barrier heights for the isomers that contain a 2-pyridyl group shows the dramatic effect that the presence of the ring-nitrogen has on stabilization. For 2,2′-, 2,3′- and 3,3′-oxybispyridine, the **A**(0, 0) conformers are energetically distinct from the **A**(0, 180) and **A**(180, 180) structures. For the 2,3′- and 3,3′-oxybispyridines, the **A**(0, 0) struc-

Table 6
Optimized parameters and a comparison of barrier heights for the A–D conformers of the oxybispyridines[a]

Conformer	R_{C-O} (Å)	A_{C-O-C} (deg)	ΔE_{OPT} (kJ mol^{-1})	ΔE_{RR} (kJ mol^{-1})
(a) *2,2'-Oxybispyridine*				
A(0, 0)	1.390	130.4	56	84
A(180, 180)	1.377	142.3	115	368
A(0, 180)	1.389	131.7	49	72
B(0, 90)	1.404	113.9	4	2
B(180, 90)	1.404	116.6	25	16
C(42, 42)	1.403	114.0	0	0
D(90, 270)	1.415	111.4	32	29
D(90, 90)	1.414	110.8	20	19
E(0, 0)	1.327	180.0	207	—
E(0, 180)	1.326	180.0	199	—
(b) *3,3'-Oxybispyridine*				
A(0, 0)	1.383	141.5	93	475
A(180, 180)	1.381	142.1	101	963
A(0, 180)	1.382	141.8	96	658
B(0, 90)	1.406	116.8	4	1
B(180, 90)	1.407	116.8	7	6
C(47, 47)	1.408	114.7	0	0
D(90, 270)	1.418	111.2	9	15
D(90, 90)	1.418	111.1	8	14
E(0, 0)	1.334	180.0	195	—
E(0, 180)	1.334	180.0	194	—
(c) *4,4'-Oxybispyridine*				
A(0, 0)	1.381	141.3	89	846
B(0, 90)	1.405	116.6	4	2
C(45, 45)	1.406	115.1	0	0
D(90, 90)	1.417	111.0	10	13
E(0, 0)	1.335	180.0	218	—
(d) *2,3'-Oxybispyridine*				
A(0, 0)	1.392	131.5	45	84
A(180, 180)	1.379	142.2	111	583
A(0, 180)	1.391	131.6	46	116
A(180, 0)	1.380	141.9	105	419
B(0, 90)	1.405	114.4	0.1	0.2
B(180, 90)	1.405	116.9	19	14
B(90, 0)	1.405	116.7	16	9
B(90, 180)	1.405	116.7	19	14
C(6, 82)	1.405	114.5	0	0
D(90, 270)	1.416	111.0	20	21
D(90, 90)	1.416	111.0	18	19
E(0, 0)	1.330	180.0	202	—
E(0, 180)	1.331	180.0	201	—
(e) *2,4'-Oxybispyridine*				
A(0, 0)	1.390	131.5	41	111
A(0, 180)	1.379	141.8	103	545

Table 6 (*continued*)

Conformer	R_{C-O} (Å)	A_{C-O-C} (deg)	ΔE_{OPT} (kJ mol^{-1})	ΔE_{RR} (kJ mol^{-1})
B(0, 90)	1.405	114.4	0	0
B(180, 90)	1.405	116.9	19	13
B(90, 0)	1.403	116.7	13	11
C(6, 80)	1.404	114.5	0	0
D(90, 90)	1.416	110.9	18	20
E(0, 0)	1.330	180.0	211	—
(f) *3,4'-Oxybispyridine*				
A(0, 0)	1.382	141.4	90	616
A(180, 0)	1.381	141.7	95	889
B(0, 90)	1.406	116.8	5	1
B(180, 90)	1.406	116.8	8	5
B(90, 0)	1.405	116.8	3	3
C(51, 39)	1.407	115.3	0	0
D(90, 90)	1.418	111.1	9	14
E(0, 0)	1.334	180.0	206	—

[a] Reproduced with permission from reference [20].

tures are more stable by 32 and 183 kJ mol^{-1}, respectively, whereas, for 2,2'-oxybispyridine, the A(0, 180) structure is the more stable conformation by 12 kJ mol^{-1} [20]—allowing a comparison of the forces involved in the lone-pair–lone-pair repulsions, ortho-hydrogen steric interactions and the non-bonded interactions of a nitrogen lone pair with an ortho-hydrogen. For 2,2'-oxybispyridine, the destabilizing effect of the nitrogen 'through-space' steric interaction may be evidence for a hydrogen-bonding interaction in the A(0, 180) case, because the A(0, 0) conformer is not the preferred conformer. The A(180, 180) conformer for 2,2'-, 2,3'- and 3,3'-oxybispyridine is 296, 467 and 305 kJ mol^{-1} above the A(0, 180) energy. From this analysis, Dunne et al. [20] concluded that it is evident that there are no apparent low energy pathways to the planar **A** structures.

To analyze the effectiveness of the rigid-rotor model, a series of optimizations of the ether bridge parameters were performed for all the rotational-distinct **A**–**D** conformers of the oxybispyridines. For each conformer, the inter-ring bond lengths (R_{C-O}) and bond angle (A_{C-O-C}) were optimized at the STO-3G level [20]. For the **C** structures, the two ring twist angles ($\emptyset_1$ and $\emptyset_2$) were also optimized. The optimized parameters (R_{C-O} and A_{C-O-C}) and barrier heights (ΔE_{OPT}) calculated using the STO-3G–STO-3G model are presented in Table 6.

Table 6 also gives results for the 'fully conjugated' linear conformers (**E**). As expected, the calculations for all the **E** conformers yield optimized R_{C-O} bond lengths that are significantly shorter (by about 0.07 Å) than those of the **C** structures. Remarkably, the energy differences between the **C** and **E** structures are about 200 kJ mol^{-1} for all the isomers. For the 2,2'-, 2,3'- and 3,3'- isomers, the difference in energy between the **E**(0, 0) and **E**(0, 180) conformers is less than 8 kJ mol^{-1}. From these barrier heights, it is clear that, at ambient temperature, the p electrons of the

oxygen atom do not fully conjugate with the π systems of both pyridine rings, because both the A and E structures are well removed from the energy minima.

Gust and Mislow [100] have suggested that there are three possible rotational mechanisms for conformer interconversion about the C–O bond in diphenyl ethers. In the case of the oxybispyridines, interconversion from one C structure to another may occur via the following mechanisms: a conrotatory rotation of both rings through structure A(0, 0), involving zero-ring flip; a disrotatory rotation via structure B(0, 90), involving a one-ring flip; or a conrotatory rotation through structure D(90, 90), involving a two-ring flip. Because the A(0, 0) structures are between 41 and 93 kJ mol^{-1} above the minimum, the first mechanism is unlikely. Dunne et al. [20] concluded from the barrier heights shown in Table 6 that the second mechanism is the most viable, because the B(0, 90) structure is within 2.5 kJ mol^{-1} of the minimum for all the isomers. The third mechanism may be possible at elevated temperatures, because of the moderate barrier heights (8–18 kJ mol^{-1}), although it also is unlikely at room temperature.

The optimized variables in Table 6 reveal a number of interesting trends. The R_{C-O}(opt) values for all the B and C structures lie in a very narrow range, i.e. 1.404 ± 0.003 Å, which is in good agreement with the rigid-rotor values. As expected, the A structures possess the shortest optimized bond lengths (1.377–1.391 Å). The shortening of the bond length maximizes the overlap between the oxygen p electrons with the π orbitals of the ring. The A structures were found to have A_{C-O-C}(opt) values in two ranges: the first range (130.3°–131.7°) belongs to those conformers that contain a 2-pyridyl group in the N-inside position, while the second range (141.2°–142.3°) is for all the other A structures, i.e. those that possess H–H′ interactions in the C–O–C plane. The hydrogen-bonding interaction between ortho-nitrogens and ortho-hydrogens (on adjacent rings) allows a contraction of about 10° and a conformational stabilization of about 60 kJ mol^{-1}. In contrast, the D conformers have the longest bonds (1.414–1.418 Å) and the most acute A_{C-O-C}(opt) values. The lengthening of the R_{C-O} bonds for these conformers is necessary to avoid 'through-space' ortho-hydrogen interaction.

The optimized parameters of the B and C conformers were very similar, with the inter-ring angles contracted slightly from their contour model values. The optimized values of the two twist angles maintained an almost perpendicular attitude between the ring planes (again reinforcing the similarity of the B and C structures). These optimized values of $Ø_1$ and $Ø_2$ for 2,2′-, 3,3′-, 3,4′- and 4,4′-oxybispyridine are in 'good' agreement with the experimental and theoretical values determined for diphenyl ether: (37°, 37°) from molar Kerr constants [95], (50°, 50°) proposed by Nagakura from UV spectra analysis [98] and (52°, 52°) proposed by Galasso et al. [90] using extended Huckel MO theory. The C structures for the 2,3′- and 2,4′-isomers are very similar to their corresponding B structures. The B structure is essentially a composite of the planar and perpendicular conformers of the methoxypyridines. The small energy barriers between these forms reflects the energetic suitability of such a composite structure.

In general, the barrier heights for the B–D conformers (calculated using the STO-3G//STO-3G model) are similar to those calculated using the STO-3G//rigid-

rotor model. The **A** structures, however, exhibit a marked reduction in barrier heights on optimization (up to an order of magnitude), which highlights the necessity of optimizing key structural parameters for the accurate determination of global barrier heights. Thus, the rigid-rotor model, as used for the determination of the energy contour maps, was shown to be quite effective for the prediction of barrier heights of conformers that are well removed from the planar states [20]. Both approaches predict that, at ambient temperature, there will be a range of **B**- and **C**-type conformers in the equilibrium population (as a result of the shallow potential energy minima), so that the UPS spectra of these compounds may be complicated by such a distribution.

To date, the only UPS study performed on the oxybispyridines is that by Dunne et al. [22], although a single HeI study has been reported on the related diphenyl ether [101], which was not assigned. The HeI and HeII photoelectron spectra of the six isomers of oxybispyridine are shown in Figs. 6 and 7 respectively.

The above conformational analysis shows that the minimum energy conformers were centred on a Morino structure, in which the ring planes were essentially perpendicular to each other. It is anticipated that concerted disrotatory movement will allow an interconversion from one **B** structure to another, passing through a continuum of **C**-like structures. The energetic similarity between the **B** and **C** forms suggests that they may be very difficult to resolve and, as a result, that the spectral features may be broad. Hence, the lowest lying vertical IEs were calculated using the STO-3G optimized Morino structure (**B**) [22]. The lowest seven vertical IEs are listed in Table 7, together with the composite-molecule model assignments based on the MO energies and coefficients obtained from the HAM/3, STO-3G(s=p) and 6-31G** MO methods. Table 7 also gives the molecular photo-ionization cross-sections for the seven uppermost MOs, using the **B** geometry and the HAM/3//STO-3G methodology.

From Table 7, it is evident that the HAM/3//STO-3G calculations predict that, for all the oxybispyridines, there are between six and seven ionic states expected between 7.0 and 11.6 eV. The calculations assign two non-bonding orbitals that originate from the two nitrogen lone pairs and five π_{pyr}/n_O combinations that originate from the pyridine π orbitals mixing with the oxygen atomic orbitals. In a strict sense, the non-planarity of the oxybispyridines invalidates σ and π labelling, although such labelling is appropriate within the composite-molecule model.

As a result of the orthogonal nature of the pyridine rings in the **B** geometry, the HAM/3//STO-3G model yields MOs that are highly localized on a single ring system (denoted by primed and unprimed orbitals in Table 7). Furthermore, the valence MOs with IEs greater than about 12.2 eV become highly mixed, so invalidating a composite-molecule model; thus, they are not detailed here. For five of the six oxybispyridines, the HAM/3//STO-3G model assigns the first two IEs from an MO strongly localized on the nitrogen atoms of each pyridine ring (labelled n_N and $n_{N'}$), with the third IE originating from an anti-symmetric combination of $\pi_{6'}$–n_O. For 2,4'-oxybispyridine, a cross-over occurs between the $n_{N'}$ and the π orbital. The next four IEs arise from π–n_O combinations.

The STO-3G//STO-3G and 6-31G**//STO-3G Koopmans' approximation assign-

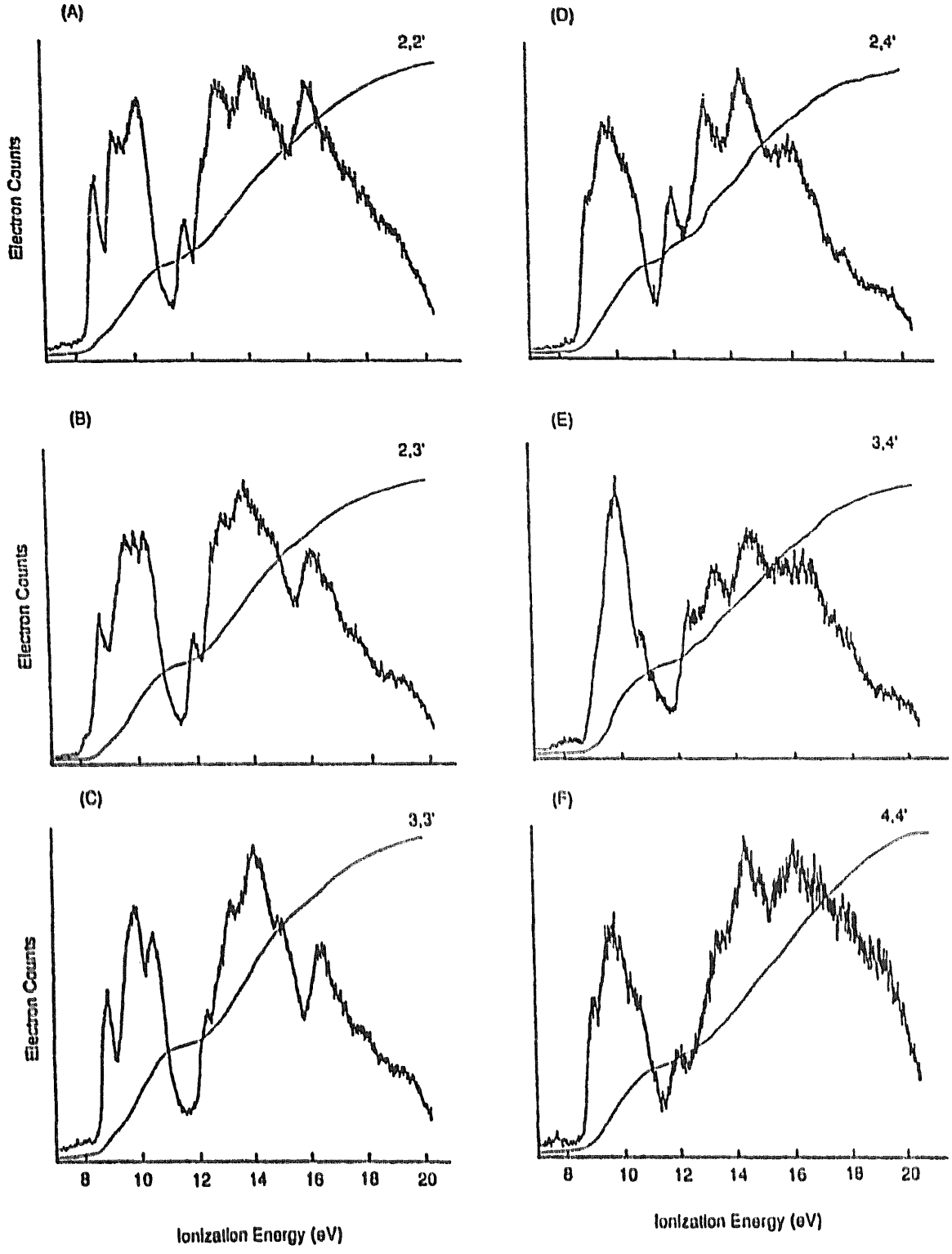

Fig. 6. HeI spectra of (a) 2,2′-oxybispyridine; (b) 2,3′-oxybispyridine; (c) 3,3′-oxybispyridine; (d) 2,4′-oxybispyridine; (e) 3,4′-oxybispyridine; (f) 4,4′-oxybispyridine. Reproduced with permission from reference [22].

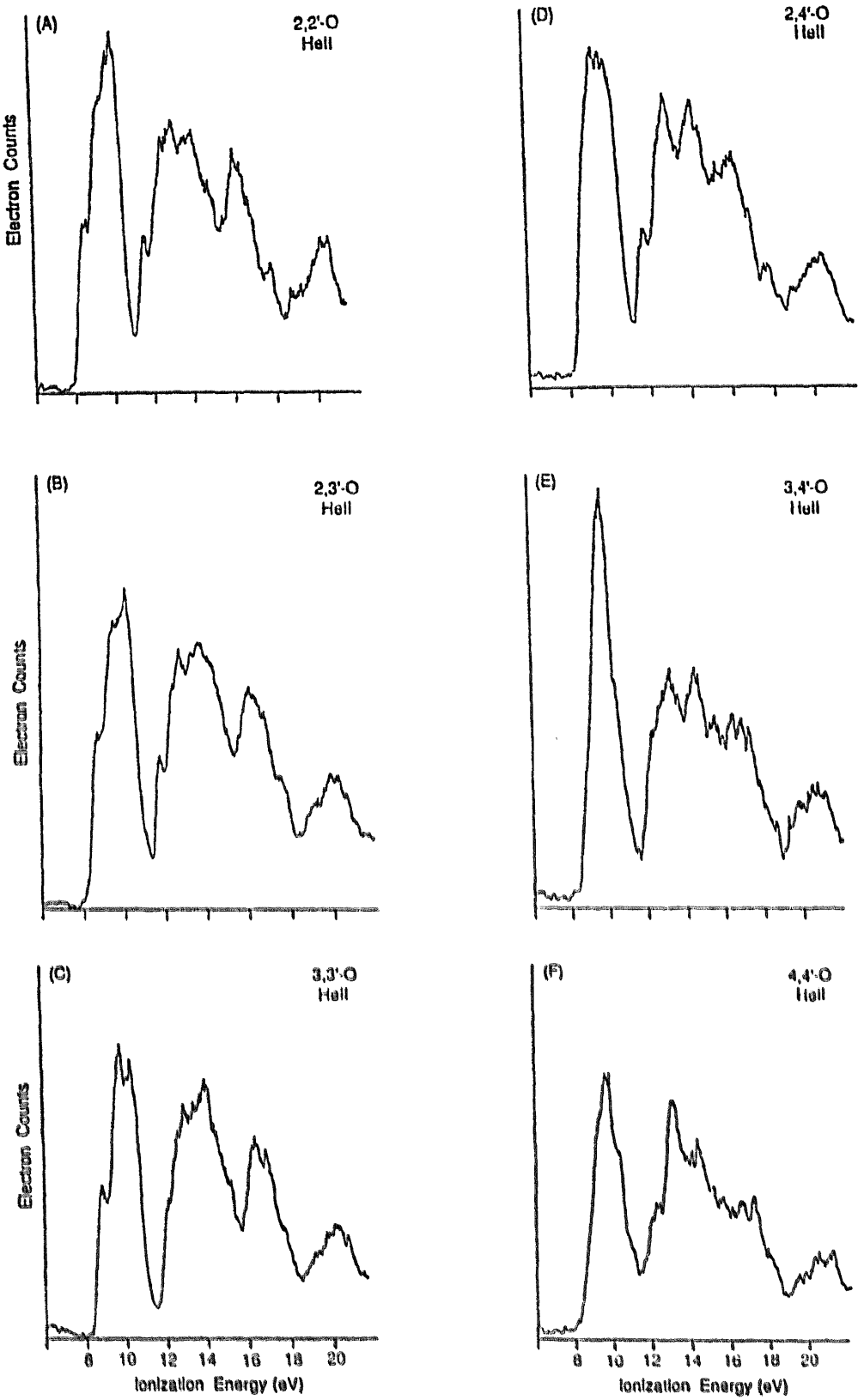

Fig. 7. HeII spectra of (a) 2,2'-oxybispyridine; (b) 2,3'-oxybispyridine; (c) 3,3'-oxybispyridine; (d) 2,4'-oxybispyridine; (e) 3,4'-oxybispyridine; (f) 4,4'-oxybispyridine. Reproduced with permission from reference [22].

Table 7
Comparison of experimental vertical IEs with HAM/3 and KA–HF IEs and preferred orbital assignments for the oxybispyridines[a]

IE	Experimental IE (eV)	MO Assignment	σ^{MO} (Mb)	Calculated IE (eV)		
				HAM/3	STO-3G	6-31G**
(a) *2,2'-Oxybispyridine*						
1	8.74	π_6–n_O	0.794	9.10	7.30	9.01
2	9.42	n_N	0.787	8.78	8.84	11.79
3	9.65	$n_{N'}$	0.836	8.94	9.08	11.42
4	10.26	$\pi_{5'}$–δn_O	0.709	9.31	7.80	9.08
5	10.26	$\pi_{4'}$	0.792	9.88	8.57	10.14
6	10.87	π_3	0.793	9.97	8.70	10.52
7	11.78	π_2+n_O	0.860	11.40	11.36	13.53
(b) *2,3'-Oxybispyridine*						
1	8.82	π_6–n_O	0.767	9.13	7.37	9.19
2	9.73	n_N	0.806	8.74	8.85	11.98
3	9.73	$n_{N'}$	0.823	9.03	9.16	11.31
4	10.11	$\pi_{5'}$–dn_O	0.716	9.34	8.79	9.04
5	10.41	$\pi_{4'}$	0.789	9.95	7.82	10.08
6	11.10	π_3	0.794	9.98	8.54	10.65
7	12.01	π_2+n_O	0.857	11.46	11.43	13.66
(c) *3,3'-Oxybispyridine*						
1	8.85	π_6–n_O	0.790	8.83	7.44	9.12
2	9.77	n_N	0.823	8.87	9.13	11.63
3	9.77	$n_{N'}$	0.790	9.22	9.11	11.73
4	9.77	$\pi_{5'}$–δn_O	0.713	9.55	8.84	9.53
5	10.47	π_4	0.775	9.90	8.71	10.37
6	10.47	$\pi_{4'}$	0.795	10.16	8.02	10.57
7	12.33	π_2+n_O	0.887	11.69	11.69	14.20
(d) *2,4'-Oxybispyridine*						
1	9.00	$\pi_{6+6'}$–n_O	0.850	9.02	7.45	9.19
2	9.46	n_N	0.841	8.72	8.64	12.02
3	9.46	$n_{N'}$	0.735	9.10	9.16	11.29
4	9.85	$\pi_{5+5'}$–n_O	0.688	9.43	8.23	9.35
5	9.85	$\pi_{4'}$	0.798	9.77	8.06	9.82
6	10.24	π_3	0.796	10.01	8.84	10.70
7	11.87	$\pi_{2'}+n_O$	0.843	11.39	11.23	13.33
(e) *3,4'-Oxybispyridine*						
1	9.31	$\pi_{6'}$–n_O	0.737	9.01	7.50	9.87
2	9.77	n_N	0.840	8.90	8.92	11.83
3	9.77	$n_{N'}$	0.840	8.94	9.16	11.51
4	9.77	$\pi_{5'}$	0.697	9.64	8.55	9.60
5	9.77	π_4	0.773	9.93	8.76	9.68
6	11.17	π_3	0.804	9.98	8.21	10.70
7	12.33	$\pi_{2'}+n_O$	0.878	11.64	11.50	13.90

Table 7 (*continued*)

IE	Experimental IE (eV)	MO Assignment	σ^{MO} (Mb)	Calculated IE (eV)		
				HAM/3	STO-3G	6-31G**
(f) *4,4'-Oxybispyridine*						
1	9.00	$\pi_{6+6'}-n_O$	0.815	9.37	7.68	9.63
2	9.70	n_N	0.847	8.77	8.71	11.56
3	9.70	$n_{N'}$	0.815	8.99	8.98	11.80
4	9.70	$\pi_{5+5'}-n_O$	0.701	9.72	8.63	9.80
5	10.32	$\pi_{4+4'}-n_O$	0.695	9.50	8.45	10.07
6	11.17	$\pi_{3+3'}-n_O$	0.803	9.99	8.41	10.46
7	11.94	$\pi_{2'}+n_O$	0.879	11.71	11.57	13.81

[a] Reproduced with permission from reference [22].

ments are also given in Table 7. At the STO-3G level of theory, the lowest IE is assigned to ionization from a $\pi_{6'}-n_O$ MO, which typically gives a Koopmans approximation IE of about 7.5 eV for the oxybispyridines. The STO-3G//STO-3G assignment for the first IE is consistent with the STO-3G//STO-3G assignment of pyridine. The first IE in the 6-31G** model is not consistently assigned. In some cases, an MO with considerable oxygen character is assigned to the HOMO, while other cases have that a ring-based π orbital has a lower IE. The similarity between the IEs of the b_1 pyridine MO and the oxygen functionality has resulted in considerable mixing on MO formation. However, in line with the assignments of the methoxypyridines, the first IE is assigned to a $\pi-n_O$ MO.

The electronegativity of the oxygen atom can be used to ascertain the nature of the HOMO. Oxygen will act as a σ acceptor and a π donor when bound to the pyridine ring. Electron withdrawal from the σ system of the ring will stabilize the n_N MOs, resulting in higher IEs. The oxygen 2p atomic orbitals will interact with the pyridine b_1 MO to form bonding and anti-bonding combinations, whereas there will be little interaction with the pyridine a_2 MO (resulting in little shift from its pyridine IE value). The first experimental IEs of the oxybispyridines range from 8.74 to 9.31 eV, and these IEs can only be rationalized for the $\pi-n_O$ combination, because shifts of 0.5–1.0 eV to lower energies for the n_N and pyridine a_2-based MOs are not expected, on electronegativity grounds.

A comparison of the first band of the oxybispyridines with that observed in the HeI spectra of the methoxypyridines [27,75], diphenyl ether [101], diphenyl sulphide [29], 2-pyridylphenyl sulphide [29] and 2,2'-thiobispyridine [29] reinforces the above assignment of the HOMO. The IEs for the HOMOs in 2-, 3- and 4-methoxypyridine are 8.59, 8.98 and 9.15 eV respectively [22]. These values differ by only about 0.15 eV from the corresponding first IEs of the symmetrical oxybispyridines (8.74, 8.85 and 9.00 eV). The similarity between these results suggests that extensive delocalization over the entire molecular framework is unlikely, because this would result in a substantial lowering of the IEs. For the diphenyl compounds, the first IE can only be associated with ionization from the benzene π MO. Therefore, Colonna et al.

[29] assigned the first IE of the mono- and di-2-pyridyl analogues to a π ionization. Hence, for the oxybispyridines, the preferred assignment is $\pi - n_O < n_N \sim n_{N'}$, which differs from the HAM/3//STO-3G assignment; although it is consistent with the band profiles, shifts of the first IE with respect to electronegativity, and comparison of the differences between the first experimental IEs for 2,2′-oxy- and 2,2′-thiobispyridine and diphenyl ether and diphenyl sulphide (0.57 and 0.47 eV respectively). Nevertheless, Dunne et al. [22] preferred the IE_4–IE_7 HAM/3//STO-3G assignment rather than the corresponding KA–HF assignments.

For most of the oxybispyridines, the KA–HF models place four of the π MOs at lower IE values than the lowest n_N MO. Thus, the $\pi_{6'}$–n_O orbital is consistently lower than the n_N MO by 1.03–1.54 eV, which is in poor agreement with the possible differences in experimental IEs (as gleaned from the HeI spectra) [22]. The poor placement of the n_N MOs by the KA–HF models has been previously highlighted for pyridine and the methylchalcogenopyridines (see Sections 3.1 and 3.2). Models that incorporate orbital relaxation and electron correlation have been shown to predict more accurately the IEs for the σ-type n_N MOs. Thus, the KA–HF models cannot be used as assignment tools without the correction of the n_N IEs.

A ΔSCF–CI model was used for the accurate determination of the n_N IEs in the methylchalcogenopyridines (see Section 3.2). The greater molecular size and often lower symmetry of the oxybispyridines makes the use of this model unsuitable for these systems. The n_N MOs are localized on a specific pyridine ring, so should correlate well with the corresponding values calculated for the methoxypyridines. The IEs for the n_N MOs of the 2-, 3- and 4-methoxypyridines calculated using the ΔSCF–CI model were 9.79, 9.67 and 9.26 eV respectively [24]. The trend in these figures reflects the distance between the oxygen and nitrogen atoms (based on the inductive effect of the oxygen atom), as well as the extent of the delocalization of the n_N MO. Substitution of these values into the 6-31G**//STO-3G model produces a far better IE distribution when compared with the experimental findings.

The predicted HAM/3//STO-3G sequences are not as an effective assignment tool as are the predicted IE distributions. Based on the s–p separation rule, the number of p-based bands below 18 eV, according to Eq. (13), is 19. However, the HAM/3 calculation on pyridine assigns a cross-over of an s-based and a p-based band in the region 15–18 eV, giving the order $3b_2(s) < 3a_1(p)$ (see Section 3.1). Thus, including the corresponding cross-overs in the oxybispyridines, it would be anticipated that there would be a total of 21 bands below 18 eV.

The experimental HeI band intensities can be used for the density-of-states analysis within two specified regions, i.e. 8.0–11.5 eV and 11.5–18.0 eV [22]. The HAM/3//STO-3G IE distribution is in reasonable agreement with the experiments, with the higher IEs being generally underestimated for the oxybispyridines [22]. Furthermore, the experimental and the calculated HeI intensities (normalized to a total of 21 bands) are in 'good' agreement—both indicating that the first region (from about 8.0 to 12.5 eV) contains seven bands, whereas the second region (from about 12.5 to 18 eV) contains the remaining 14 bands. The 6-31G**//STO-3G distribution is distorted by the poor placement of the n_N IEs by the KA–HF model.

The HeII spectra of the oxybispyridines are presented in Fig. 7. Similar to the

methoxypyridines, little variation is seen in the relative intensities of the valence bands, so limiting their usefulness as an interpretative tool. The similarity between the band intensities in the HeI and HeII spectra is in agreement with the predicted $\sigma_{HeI}/\sigma_{HeII}$ ratios of Manson [54]. The overlapping of bands in the UPS spectra of the oxybispyridines makes it difficult to ascertain the presence of distinct conformers, although the separable bands appear free of rotational contamination.

To study the superposition of spectra from isoenergetic conformers, a series of 'synthetic' spectra were produced, based on the photo-ionization cross-section model given in Section 2.5. Fig. 8 shows the HAM/3//STO-3G synthesized HeI photoelectron spectra of 2,3′-oxybispyridine. Fig. 8(a)–8(c) show the spectra of the **B**, **C** and composite (**B**+**C**) compositions respectively. The calculated cross-sections were convoluted with Gaussian functions with a full width at half-maximum (FWHM) of 200 meV. The FWHM was based on the FWHM of the lowest IE n_N and π bands in pyridine. The lowest energy conformations clearly produce spectra that are almost indistinguishable from the composite spectrum; this is consistent with the experimental observation of the relative intensities over a range of 30 K. The HAM/3//STO-3G calculations suggest that the populations, IE distributions and relative cross-sections of these two conformations are similar. These observations apply equally to all the isomers.

Fig. 9 shows the HAM/3//STO-3G synthesized HeI spectra for all the isomers of oxybispyridine. The calculated spectra reproduce the salient features exhibited in the experimental spectra in the region 8–18 eV (notwithstanding the assumptions made about the FWHM). For example, the calculated spectra clearly identify the two separated regions of the outer and inner valence MOs. However, the calculated spectra do not resolve the first band (with a comparatively low cross-section) from the other valence MOs, because the band positions are dependent on the HAM/3 eigenvalues. As can be seen in Table 7, the first band is not always correctly assigned within the HAM/3//STO-3G model. It should be noted that the relative intensity of the first IE was found to be invariant with temperature, so is not attributable to another conformer. While the HAM/3//STO-3G calculations generally reproduced the broad features of the HeI spectra of the oxybispyridines, it is evident that a more sophisticated theory is required if better agreement with the experimental findings is to be achieved.

The experimental and the synthetic HeI spectra of the oxybispyridines give no indication of the presence of rotamers other than the minimum energy conformer. However, within the expected range of conformers, the IEs of the isoenergetic conformers are expected to be almost degenerate, so that overlapping of their spectra masks their presence. Bands that arise from the planar **A** and **E** structures are unlikely, because of the magnitude of the rotational barriers to these conformers.

Thus, the IE distribution of the top seven valence MOs for the oxybispyridines was assigned as [22]

$$\pi_6 - n_O < n_N \sim n_{N'} < \pi_5 - \delta n_O < \pi_4 - \delta n_O < \pi_3 - \delta n_O < \pi_2 + n_O \qquad (15)$$

This is based on correlations with the corresponding pyridine and methoxypyridine

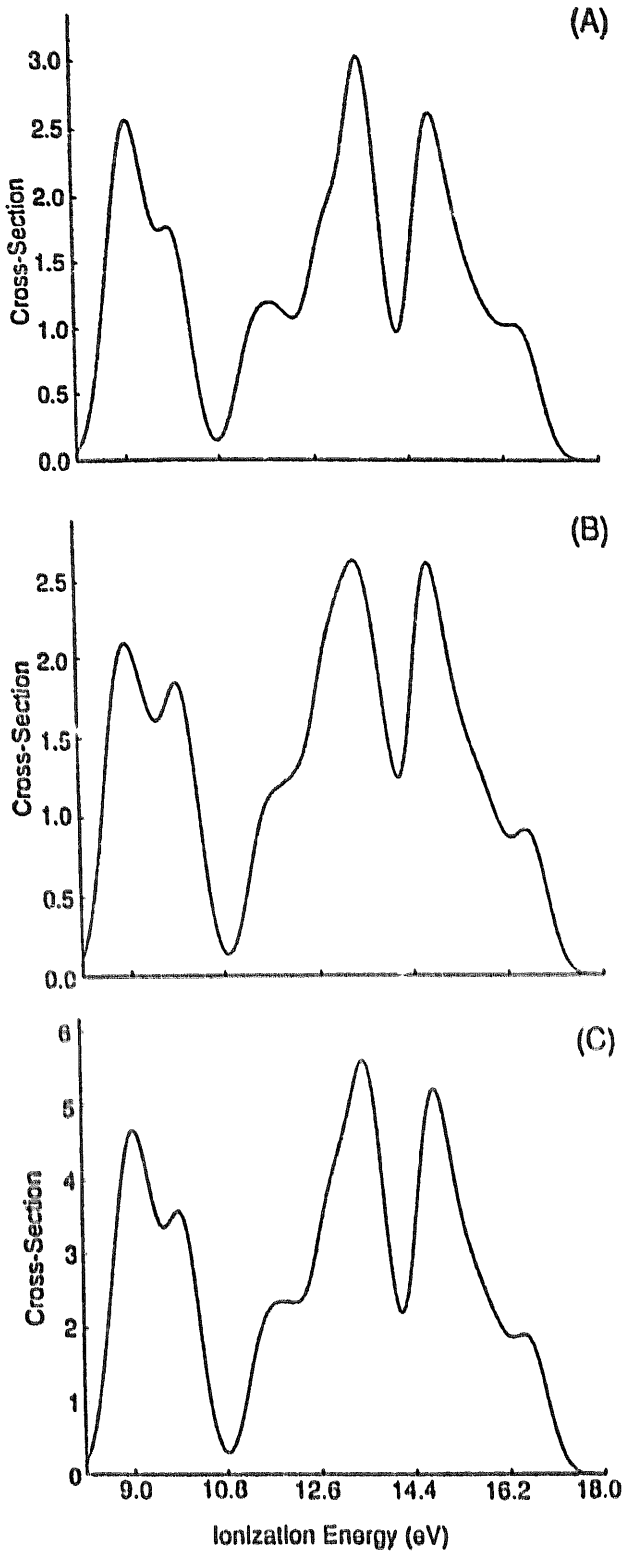

Fig. 8. HAM/3–STO-3G synthesized HeI spectra of 2,3′-oxybispyridine (a) with only conformer C being present; (b) with only conformer B being present; and (c) with both conformers C and B being present in equal proportions. Reproduced with permission from reference [22].

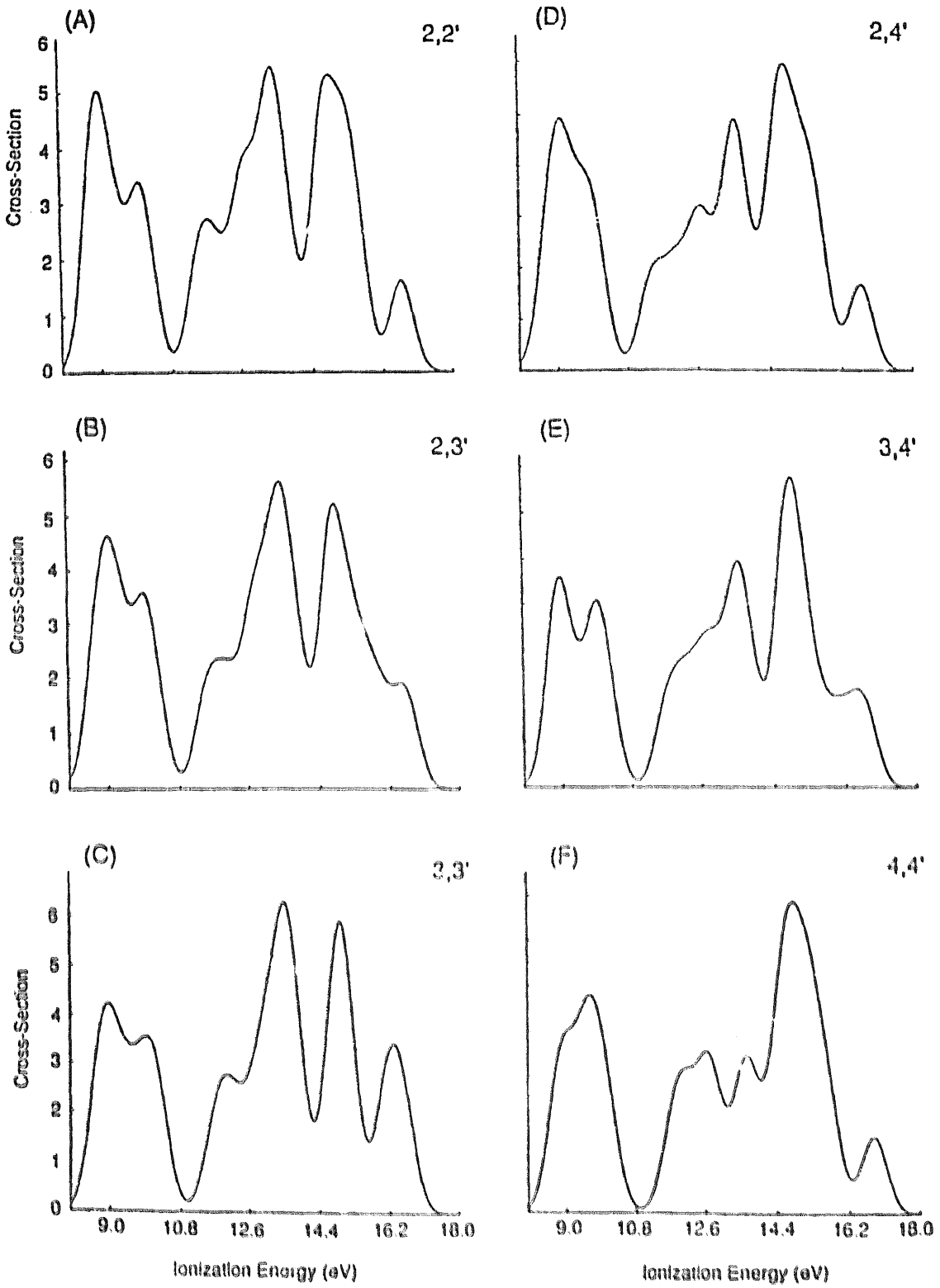

Fig. 9. HAM/3–STO-3G synthesized HeI spectra with both B and C conformers present in equal proportions for (a) 2,2'-oxybispyridine; (b) 2,3'-oxybispyridine; (c) 3,3'-oxybispyridine; (d) 2,4'-oxybispyridine; (e) 3,4'-oxybispyridine; (f) 4,4'-oxybispyridine. Reproduced with permission from reference [22].

spectra, HAM/3//STO-3G eigenvalues and the combined use of the 6-31G**//STO-3G (for the π MOs) and ΔSCF–CI (for the n_N MOs) models.

3.4. Thiobispyridines

2,2′-Thiobispyridine and its nitro- and dinitro- derivatives have been the subject of a number of theoretical and structural studies. The gas-phase electron diffraction study on 2,2′-thiobispyridine by Rozsondai and coworkers [102,103] concluded that the S–C bond distance and the C–S–C bond angle were 1.786 ± 0.004 Å and $104.4 \pm 1.7°$ respectively. The bond lengths of the pyridine ring were found to be similar to those in the free pyridine molecule, and the conformational properties of this molecule were consistent with the notion of the rings performing either large-amplitude torsional motion or a rapid interconversion between conformers.

Chachaty et al. [104] combined a dipole moment study with semi-empirical MO calculations and ^{1}H nuclear magnetic resonance (NMR) techniques to determine the conformation of 2,2′-thiobispyridine. Their complete neglect of differential overlap (CNDO) calculations revealed that activation energies of the order of 0–15 kJ mol^{-1} are required for the conversion of one conformer into another conformer along paths that lie in the minimum energy area. In particular, it was calculated that an energy of about 9 kJ mol^{-1} is required for the complete rotation from 0° to 180° of a pyridine ring, while keeping the other ring coplanar with the C–S–C plane. An unequivocal determination of the conformation of 2,2′-thiobispyridine could not be made on the basis of their dipole moment data, because there were numerous combinations of the ring twist angles ($Ø_1$ and $Ø_2$) for which the calculated dipole moment agreed with the experimental value.

The energetic suitability of a single fixed conformation was thought improbable when considering the shallowness of the potential energy surface in the region of the minimum [21]. The alternative of 'free rotation' about the C–S bonds was excluded on the basis of the barrier heights calculated, especially the sterically restricted conformation (i.e. $Ø_1 = Ø_2 = 180°$). Consequently, the only possibility remaining was the existence of a mixture of equiprobable rotational conformers. The conformers that best fitted their dipole moment data were the 'propeller' forms in which the pyridine ring planes were twisted by about 36° with respect to the C–S–C plane. The ^{1}H NMR studies showed that there was magnetic equivalence between chemically equivalent protons of the two pyridine rings arising from rapid interconversion (on the NMR time-scale) among the populated conformers. The observed pattern did not decoalesce in the temperature range from +50 to −80°, indicating that, even at low temperatures, averaging of the proton signals occurs as a result of the rapid rotation of the pyridine rings.

In a further study on 5-nitro-2,2′-thiobispyridine and 5,5′-dinitro-2,2′-thiobispyridine, Galasso et al. [105] proposed that the mono-nitro-substituted derivative adopts a 'skew' or 'Morino' structure (0, 90), caused by the interaction of the π electrons of the aryl group with the lone-pair electrons of the S atom, which results in the C_{pyr}–S bond on the side of the molecule that contains the nitro-group attaining double-bond character. This view was consistent with UV spectroscopic studies on

the analogous di-(*p*-nitrophenyl) sulfide [106] and implies that a comparatively high energy barrier exists about the S–Cpyr–NO_2 bond. The dinitro-substituted compound, however, was found to adopt a similar minimum conformation to that of its parent compound, i.e. the 'propeller' structure, as did 2-pyridyl phenyl sulfide [105].

The variation in the electronic distribution that occurs with the substitution of sulfur's functionality into the pyridine moiety and the effect of the relative ring-nitrogen position in isomeric compounds have been largely unexplored, although such sulfur-bridged compounds are extremely important in many biological processes. Hence, in the case of the thiobispyridines, information on IEs and the extent of delocalization of sulfur lone pairs and/or π electrons is of paramount importance for developing mechanisms that rationalize their biological activity.

A rigid-rotor model was shown to be reasonably successful for predicting the relative energies of conformers that are well removed from the planar states, while a second model that involves the optimization of critical structural parameters was shown to be more reliable for the determination of global minima (see Section 3.3). The longer R_{C-S} bonds in the thiobispyridines alleviate some of the steric interactions that limit the number of accessible conformations in the corresponding oxybispyridines. This effect was studied by Dunne et al. [21] using both the rigid-rotor and optimized Fletcher–Powell (FP(opt)) models.

In the case of the thiobispyridines, all electron energies were computed using the restricted HF method within the GAUSSIAN 86 suite of programs, and using the internal STO-3G* and 6-31G** basis sets [42]. A rigid-rotor model, in which the inter-ring bond lengths and angle were fixed at 1.74 Å and 120°, respectively, was used to generate the contour energy maps [21]. These parameters were chosen to model reasonable barrier heights, despite the rigidity forced on the structure. The geometry of the pyridine ring was the STO-3G optimized structure shown in Fig. 2.

To study the effect of structural relaxation on the rotational barrier heights, the inter-ring angles and bond lengths of a select group of conformers [21] were optimized using the FP algorithm [50]. All possible rotational isomers of the structures **A**, **B** and **D** (see Fig. 5) were optimized and the results are given in Table 8. In the case of the **C** structures, the two twist angles ($Ø_1$ and $Ø_2$) were included in the optimized variable set. A comparison of the barrier heights generated by the three models (STO-3G*//rigid-rotor, STO-3G*//STO-3G* and 6-31G**//STO-3G*) is presented in Table 8.

The contour energy maps predict that the minimum energy conformers have either planar or near-planar structures. In the case of the 2,2'- and 2,4'- isomers, the **A**(0, 0) conformer is the most stable, while the 2,3'- isomer exhibits a local minimum for this structure. It was shown for the oxybispyridines [22] that the **A** structures lay 70–850 kJ mol^{-1} above the minimum, so it is unlikely that the **A** conformers of the thiobispyridines represent 'true' global minima. The contour maps [21] reveal that very few conformations are accessible to the thiobispyridines at ambient temperature (i.e. those structures within 2.5 kJ mol^{-1}).

A comparison between the barrier heights from the STO-3G*//rigid-rotor model and those optimized within the STO-3G*//STO-3G* model reveals that, in all cases,

Table 8
STO-3G* optimized bridge parameters and rotational barrier heights of thiobispyridines[a]

Conformer	$R_{C\text{-}S}$ (Å)	$A_{C\text{-}S\text{-}C}$ (deg)	Barrier height (kJ mol^{-1})		
			Rigid rotor	STO-3G*(opt)	6-31G**
(a) *2,2'-Thiobispyridine*					
A(0, 0)	1.768	114.14	19.46	47.93	52.01
A(180, 180)	1.783	123.91	86.43	99.65	81.52
A(0, 180)	1.770	115.15	0.00	29.93	28.76
B(0, 90)	1.763	100.23	15.51	0.73	0.00
B(180, 90)	1.766	102.96	15.70	7.21	1.51
C(343, 123)	1.762	101.90	0.00	0.00	1.66
D(90, 270)	1.776	97.72	39.94	21.00	10.83
D(90, 90)	1.775	97.26	34.19	13.50	0.16
(b) *2,3'-Thiobispyridine*					
A(0, 0)	1.767	115.46	0.67	36.79	46.62
A(180, 180)	1.782	124.08	88.54	105.86	100.30
A(0, 180)	1.768	115.36	1.19	36.82	46.81
A(180, 0)	1.781	124.01	82.00	100.54	93.19
B(0, 90)	1.761	100.94	7.76	0.01	0.08
B(180, 90)	1.763	103.36	8.15	5.64	1.40
B(90, 0)	1.764	103.21	12.85	11.10	19.29
B(90, 180)	1.765	103.09	15.95	12.91	20.88
C(2, 90)	1.762	100.88	0.00	0.00	0.00
D(90, 270)	1.772	97.88	28.99	15.41	6.81
D(90, 90)	1.773	97.80	27.70	13.84	4.60
(c) *3,3'-Thiobispyridine*					
A(0, 0)	1.778	124.21	80.00	97.74	98.59
A(180, 180)	1.780	124.25	90.61	106.16	109.86
A(0, 180)	1.779	124.21	84.28	101.08	103.14
B(0, 90)	1.761	103.58	5.03	3.71	9.45
B(180, 90)	1.762	103.42	7.86	4.98	10.36
C(46, 314)	1.761	101.67	0.00	0.00	6.53
D(90, 270)	1.770	98.47	21.05	8.48	1.04
D(90, 90)	1.770	98.40	20.48	7.66	0.00
(d) *2,4'-Thiobispyridine*					
A(0, 0)	1.767	115.27	0.00	31.50	34.03
A(0, 180)	1.780	123.88	80.64	97.01	82.00
B(0, 90)	1.763	100.68	13.26	0.51	0.00
B(180, 90)	1.765	103.13	13.59	6.18	0.88
B(90, 0)	1.763	103.04	13.01	6.56	5.20
C(342, 121)	1.762	101.59	0.00	0.00	1.95
D(90, 90)	1.774	97.52	33.52	14.50	4.00
(e) *3,4'-Thiobispyridine*					
A(0, 0)	1.777	124.01	75.92	95.63	90.18
A(180, 0)	1.779	123.98	80.67	99.79	97.94
B(0, 90)	1.763	103.46	9.36	8.62	14.16
B(180, 90)	1.764	103.36	12.15	10.73	15.69

Table 8 (*continued*)

Conformer	R_{C-S} (Å)	A_{C-S-C} (deg)	Barrier height (kJ mol^{-1})		
			Rigid rotor	STO-3G*(opt)	6-31G**
B(90, 0)	1.761	103.43	3.81	3.12	0.00
C(306, 147)	1.760	102.04	0.00	0.00	3.08
D(90, 90)	1.772	98.05	24.85	12.40	3.52
(f) *4,4'-Thiobispyridine*					
A(0, 0)	1.777	123.83	72.61	93.57	80.71
B(0, 90)	1.762	103.26	7.67	3.97	1.33
C(317, 138)	1.761	102.03	0.00	0.00	0.00
D(90, 90)	1.773	97.74	28.53	12.76	3.38

[a] Reproduced with permission from reference [21].

the **A** structures have destabilized on optimization. The rigid-rotor value of the inter-ring angle (120°) better represents the inter-ring angle of the optimized planar **A** structures than those of the **B**–**D** conformers. The relative energies of the **B**, **C** and **D** structures are lowered more substantially on optimization than is the case for the **A** structures (up to 50 kJ mol^{-1} in some cases). The trend in the energy differences is sensitive to the changes in the inter-ring angle on optimization. The energies of the **D** structures are lowered to the greatest degree, because their optimized angles lie furthest from the value of 120° from the STO-3G*//rigid-rotor model.

Within the STO-3G*//STO-3G* model, the minimum energy structures are no longer the **A** structures but, instead, have become pseudo-**B** in character. Hence, the observed stability of the **A** structures within the STO-3G*//rigid-rotor model arises from the artificial constraints embedded in that model. The range of conformations within 2.5 kJ mol^{-1} of the STO-3G*//STO-3G* minima is still quite small but, importantly, some **B** structures are now accessible, opening a low-energy pathway to concerted disrotatory rotation. The non-uniformity of the energy differences between the STO-3G*//rigid-rotor and the STO-3G*//STO-3G* models highlights the importance of optimizing the critical structure parameters.

Table 8 shows that, for all the isomers, the planar **A**(180, 180) structures have the longest R_{C-S} bond lengths and the largest A_{C-S-C} bond angles. The trans 'butterfly' structure (i.e. **D**(90, 90)) possesses the most acute A_{C-S-C} angle. In the **D** structures, the π systems of the pyridine rings overlap 'through space', resulting in a reduction in the A_{C-S-C} angle. The minimum energy **C** structures have the shortest R_{C-S} bond lengths, reflecting the minimization of steric interaction. For 2,2'-thiobispyridine, the STO-3G*//STO-3G* model gives an R_{C-S} bond length and A_{C-S-C} inter-ring angle of 1.762 Å and 102°, respectively, and these values are in reasonable agreement with the corresponding experimental values of 1.786 Å and 104° [102,103]. The optimized ring twist angles ($Ø_1$ and $Ø_2$) maintain an almost orthogonal attitude between the ring planes, although only for 2,3'-thiobispyridine is the **C** structure of the Morino form.

All the barrier heights calculated at the 6-31G**//STO-3G* level are reduced for the **B**, **C** and **D** structures, while those of the **A** structures remain similar to the corresponding STO-3G*//STO-3G* values. The number of conformations accessible at ambient temperature is now more numerous and, in particular, the **B** structures have become more stable. The 6-31G**//STO-3G* model clearly indicates that the minimum energy conformers are not planar and that energy barriers between 30 and 100 kJ mol^{-1} restrict interconversion to planar structures.

For the oxybispyridines (see Section 3.3), three possible rotational mechanisms for conformer interconversion about the inter-ring bond have been outlined: a conrotatory rotation of both pyridine rings through the **A**(0, 0) structure, involving a zero-ring flip; a disrotatory rotation via the **B**(0, 90) or **B**(90, 0) structure, involving a one-ring flip; and a conrotatory rotation through the **D**(90,90) structure involving a two-ring flip. For all the isomers of thiobispyridine, the second and third mechanisms are possible, because the 6-31G**//STO-3G* model predicts that the barrier heights to some **B** and **D** structures are of the same order of magnitude as the energy available from the ambient surroundings. The first mechanism must be considered highly unlikely, because of the large barrier heights to the **A**(0, 0) structure.

Experimental studies on the thiobispyridines have focused on their dipole moments [104–106]. The range of accessible conformations will have a distinct effect on the measured dipole moments. Table 8 indicates that a range of conformations are available for these molecules at ambient temperature (i.e. all conformations along the low-energy pathways between **C** and the **B** and **D** structures), whereas Table 9 lists the dipole moments for the **A**–**D** structures calculated using the three models. The STO-3G*//rigid-rotor and the STO-3G*//STO-3G* models yield similar results, whereas the 6-31G**//STO-3G* model predicts values that differ by up to 2 Debye (D) from the STO-3G* results. Green [107] has concluded that, at the HF limit, the error associated with the dipole moment of a neutral diatomic molecule with a single sigma bond is of the order of 0.1–0.2 D, provided that a double-zeta basis set (augmented with polarization functions) is employed. The 6-31G** basis set is closer to this criterion, although it is deficient with respect to producing a reliable HF limit. Furthermore, these molecules are not just sigma-bonded. Nevertheless, the 6-31G**//STO-3G* dipole moments are the most accurate calculated to date.

The variation in the dipole moments between the accessible conformers for this model is quite marked, suggesting that attempts to interpret experimental dipole moments in terms of a limited set of conformers may provide a non-unique solution. In the study of 2,2′-thiobispyridine, Chachaty et al. [104] interpreted the experimental dipole moments in terms of a superposition of three 'propeller-type' conformers determined from CNDO calculations. The 6-31G**//STO-3G* model for the **C** and **D**(90, 90) structures yields dipole moments of 3.9 and 3.7 D, respectively, and these values are in good agreement with the experimental value of 3.5 D. However, the equally probable **B** structures **B**(0, 90) and **B**(180, 90) have dipole moments of 2.9 and 5.5 D, respectively, which are both well removed from the experimental result. Hence, the agreement between the CNDO calculations and the experimental findings seems to be fortuitous.

Table 9
Calculated dipole moments of thiobispyridines[a]

Conformer	Dipole moment (D)		
	Rigid rotor	STO-3G*	6-31G**
(a) *2,2'-Thiobispyridine*			
A(0, 0)	1.259	1.151	0.143
A(180, 180)	4.062	4.161	6.064
A(0, 180)	2.464	2.799	4.142
B(0, 90)	1.681	1.719	2.868
B(180, 90)	3.799	3.677	5.521
C(343, 123)	2.464	2.407	3.868
D(90, 270)	3.699	3.638	5.131
D(90, 90)	1.824	1.729	3.658
(b) *2,3'-Thiobispyridine*			
A(0, 0)	3.211	3.293	3.052
A(180, 180)	3.776	3.941	5.622
A(0, 180)	3.948	4.242	5.335
A(180, 0)	0.206	0.380	1.464
B(0, 90)	2.632	2.884	3.487
B(180, 90)	2.658	2.379	3.989
B(90, 0)	2.717	2.400	2.394
B(90, 180)	4.564	4.281	5.707
C(2, 90)	2.966	2.864	3.443
D(90, 270)	3.938	3.733	4.807
D(90, 90)	2.070	2.107	2.917
(c) *3,3'-Thiobispyridine*			
A(0, 0)	3.706	3.643	3.186
A(180, 180)	2.458	2.740	4.229
A(0, 180)	1.923	1.759	2.100
B(0, 90)	2.668	2.941	2.481
B(180, 90)	2.791	2.627	3.637
C(46, 314)	3.217	2.883	1.780
D(90, 270)	3.546	3.618	4.217
D(90, 90)	0.117	0.778	0.666
(d) *2,4'-Thiobispyridine*			
A(0, 0)	4.275	4.471	5.124
A(0, 180)	2.341	2.526	3.753
B(0, 90)	3.092	3.419	3.896
B(180, 90)	1.827	1.220	2.853
B(90, 0)	4.147	3.755	4.460
C(342, 121)	4.275	3.590	4.105
D(90, 90)	3.321	3.064	3.772
(e) *3,4'-Thiobispyridine*			
A(0, 0)	3.348	3.216	3.079
A(180, 0)	0.372	0.589	1.761
B(0, 90)	2.717	3.211	2.603
B(180, 90)	0.969	0.948	1.589

Table 9 (*continued*)

Conformer	Dipole moment (D)		
	Rigid rotor	STO-3G*	6-31G**
B(90, 0)	2.801	2.909	2.845
C(306, 147)	3.163	3.389	3.042
D(90, 90)	2.154	2.497	2.360
(f) *4,4'-Thiobispyridine*			
A(0, 0)	1.759	1.627	0.743
B(0, 90)	1.758	2.382	1.369
C(317, 138)	1.652	2.361	1.224
D(90, 90)	1.217	2.223	1.037

[a] Reproduced with permission from reference [21].

The more accurate hypersurfaces presented here suggest that the inclusion of further conformers in the analysis would be appropriate, in conjunction with geometry optimization of each conformer at the 6-31G**//6-31G** level. The similarity between the dipole moments of some **C** structures with those of **A** structures shows that dipole moments are not diagnostic for the molecular conformations of the thiobispyridines.

Only a small temperature dependence was noted in the dipole moment measurement of 2,2'-thiobispyridine, suggesting very little difference in the distribution of conformers over an interval of 20 K [104]. Assuming a simple Boltzmann distribution between two conformations, then a conformer 10 kJ mol^{-1} from the minimum would represent only 1.2% of the population at 0 °C, and 3.4% at 85 °C. States within 1 kJ mol^{-1} are more highly populated: 39.2% at 0 °C and 41.7% at 85 °C. 85 °C is the average probe temperature at which the UPS spectra of the thiobispyridines were recorded. It can be assumed that, over a range of 100 K, the population of a particular conformer will not change by more than 4%. In the UPS experiment, temperature fluctuations are kept below 3 K, so that populations must be stationary to within 1%. Conformations with barrier heights of 20 kJ mol^{-1} will contribute less than 0.15% to the observed spectra, so that bands that arise from planar conformers are unlikely to be detected.

In summary, it was found that the predicted minimum structure was dependent on the basis set and on the degree of geometric optimization [21]. Partial geometry optimization produced a more sterically acceptable result, while the use of the 6-31G** basis set suggested that the potential energy surface was shallow in the region of the non-planar states. Therefore, it is expected that the thiobispyridines will adopt a wide range of conformations around a minimum point at ambient temperature, with the planar states still inaccessible. It would also be predicted, as was the case for the oxybispyridines, that bands that arise from different conformations in the UPS spectra will be indistinguishable.

Colonna et al. [29] assigned the HeI spectrum of 2,2'-thiobispyridine using correlations with thiophenol, thioanisole and diphenyl sulphide. The first band was assigned

to ionization from an anti-bonding π orbital, which has maximum electron density on the S atom. The second and third IEs were assigned as ionizations from the n_N lone pairs (which are split by a 'through-bond' interaction), while the fourth, fifth and sixth IEs were correlated with phenyl/pyridyl π orbitals of b_1, b_1 and a_1 symmetry respectively. The seventh band was assigned to a π-type MO with marked S character, while the eighth band was associated with ionization from a σ-type S MO.

HeI/HeII cross-section ratios are an effective assignment tool for the location of sulphur lone-pair orbitals [108]. The photo-ionization cross-section of a sulphur 3p atomic orbital has been shown both experimentally [108] and theoretically [54] to be substantially reduced when compared with ionization from a carbon or nitrogen 2p atomic orbital on going from HeI to HeII radiation. HeI/HeII studies can distinguish between ionizations from an MO localized on the sulphur atom compared with ionizations from an orbital composed mainly of carbon or nitrogen p character.

As a result of the low volatility of these compounds, the spectra were recorded by Dunne et al. [23] using the solid inlet probe in the temperature range 330–355 K [23], and the results were digitized for use in the density-of-states analysis and the determination of the HeI/HeII cross-section ratios. Table 10 gives the relative HeI and HeII band intensities. The s–p separation rule [56,61] is used to predict the number of p-based bands below 18 eV; in the case of the thiobispyridines, Eq. (13) would predict 19 p-based bands and, with the corresponding s- and p-based cross-overs, a total of 21 bands would be expected below 18 eV.

The seven lowest vertical IEs are listed in Table 11, together with the composite-molecule model assignments based on the eigenvalues and eigenvectors obtained using the HF SCF STO-3G* and 6-31G** MO methods [23]. The geometry of the thiobispyridines used in the calculations given in Table 11 was the partially optimized Morino structure, in which the ring planes are orthogonal and one ring lies in the plane of the C–S–C bond angle. The conformational analysis presented above revealed that, at ambient temperature, an array of conformers would be present, so that assigning the spectra to the KA–HF IEs of only one conformer represents an approximation. However, the Morino structure was shown earlier to lie within 4 kJ mol^{-1} of the STO-3G* optimized minimum geometry, and the differences between the KA–HF IEs of the Morino structure and those of the minimum energy structure were found to be within the resolution of the spectrometer.

As can be seen from Table 11, agreement is poor between the experimental vertical IEs and the absolute values of the KA–HF IEs at the STO-3G*//STO-3G* level (as shown for oxybispyridines in Section 3.3). At this level, the calculated HOMOs were about 2 eV lower in energy than the negative of the first experimental IE. As anticipated, the 6-31G**//STO-3G* model gives a far better description of the lower energy MOs and, for this reason, only the MO characters for this model are listed in Table 11.

The interpretation of the UPS spectra of the thiobispyridines is complicated by the large number of overlapping cationic states and the possible presence of a range of conformers. However, as shown above, the conformational analysis on the isomers of thiobispyridines suggests that, within the thermal regime of the UPS experiments,

Table 10
Relative HeI and HeII band intensities and percentage change of thiobispyridines[a]

Band	IE range (eV)	Band intensity[b]		Percentage change[c] (%)
		HeI	HeII	
(a) *2,2'-Thiobispyridine*				
1	7.8–8.8	0.838	0.767	−8.5
2	8.8–10.0	2.515	3.457	37.5
3	10.0–11.2	2.204	3.073	39.4
4	11.2–11.9	0.973	0.792	−18.6
5	11.9–12.6	1.166	1.135	−2.7
6	12.6–18.0	13.300	11.776	−11.5
(b) *2,3'-Thiobispyridine*				
1	7.9–8.9	1.018	0.895	−12.1
2	8.9–10.0	2.379	3.250	36.6
3	10.0–11.3	2.713	3.361	23.9
4	11.3–12.0	1.024	0.684	−33.2
5	12.0–12.6	1.371	1.203	−12.3
6	12.6–18.0	12.495	11.607	−7.1
(c) *3,3'-Thiobispyridine*				
1	7.9–9.1	1.029	0.914	−11.2
2	9.1–10.5	3.372	4.481	32.9
3	10.5–11.5	1.837	2.071	12.7
4	11.5–12.3	1.063	0.782	−26.4
5	12.3–12.8	1.120	1.095	−2.2
6	12.8–18.0	12.579	11.656	−7.3
(d) *2,4'-Thiobispyridine*				
1	7.9–8.9	1.076	0.920	−14.5
2	8.9–10.3	3.444	4.432	28.7
3	10.3–11.5	1.787	2.011	12.5
4	11.5–12.2	1.182	1.022	−13.5
5	12.2–18.0	13.511	12.614	−6.6
(e) *3,4'-Thiobispyridine*				
1	7.9–9.1	1.037	0.994	−4.1
2	9.1–10.4	3.228	4.672	44.7
3	10.4–11.1	1.010	1.660	64.4
4	11.1–11.7	0.807	0.686	−15.0
5	11.7–12.4	1.101	0.960	−12.8
6	12.4–18.0	13.817	12.028	−12.9
(f) *4,4'-Thiobispyridine*				
1	7.8–9.2	1.066	0.866	−18.8
2	9.2–10.3	2.915	4.031	38.3
3	10.3–10.9	0.958	1.230	28.4
4	10.9–11.7	1.017	0.926	−8.9
5	11.7–12.4	1.062	0.967	−8.9
6	12.4–18.0	13.981	12.980	−7.2

[a] Reproduced with permission from reference [23].
[b] Normalized to 21 bands.
[c] [(HeII/HeI) − 1] × 100.

Table 11
Comparison of experimental vertical IEs with calculated Koopmans' approximation IEs of thiobispyridines[a]

Band	Experimental IE (eV)	Calculated Koopmans approximation IE (eV)		MO character 6-31G**
		STO-3G*	6-31G**	
(a) *2,2'-Thiobispyridine*				
IE_1	8.17	6.07	8.37	π_6–n_S
IE_2	9.45	7.83	9.27	$\pi_{5'}$
IE_3	9.73	8.49	10.16	π_4
IE_4	10.22	8.56	10.36	π_3–n_S
IE_5	10.52	9.25	11.13	$\pi_2 + n_S$
IE_6	11.47	8.98	11.33	$n_{N'}$
IE_7	12.28	8.90	11.38	n_N
(b) *2,3'-Thiobispyridine*				
IE_1	8.39	6.25	8.56	π_6–n_S
IE_2	9.42	7.83	9.30	$\pi_{5'}$
IE_3	9.71	8.49	10.17	π_4
IE_4	10.23	8.67	10.46	π_3–n_S
IE_5	10.52	9.50	11.13	$\pi_2 + n_S + n_{N'}$
IE_6	10.70	8.96	11.52	$n_N + n_{N'}$
IE_7	11.65	9.06	11.55	$n_N + n_{N'}$
(c) *3,3'-Thiobispyridine*				
IE_1	8.46	6.32	8.51	π_6–n_S
IE_2	9.49	8.12	9.72	$\pi_{5'}$–n_S
IE_3	9.89	8.56	10.18	π_4–n_S
IE_4	10.15	8.83	10.62	$\pi_{3'}$
IE_5	10.63	9.22	11.48	n_N
IE_6	10.99	9.32	11.57	$n_{N'}$
IE_7	12.10	9.76	11.94	$\pi_2 + n_S$
(d) *2,4'-Thiobispyridine*				
IE_1	8.35	6.32	8.63	π_6–n_S
IE_2	9.31	8.02	9.31	$\pi_{5'}$
IE_3	9.60	8.24	10.06	π_4–n_S
IE_4	9.99	8.71	10.51	π_3
IE_5	10.45	9.01	11.29	$n_{N'} + n_S$
IE_6	10.74	9.43	11.38	$\pi_2 + n_S$
IE_7	11.91	9.11	11.61	n_N
(e) *3,4'-Thiobispyridine*				
IE_1	8.65	6.55	9.04	π_6–n_S
IE_2	9.61	8.21	9.55	$\pi_{5'}$
IE_3	9.78	8.30	9.89	π_4–n_S
IE_4	9.93	8.95	10.77	$\pi_3 + n_S$
IE_5	10.67	9.07	11.37	$n_{N'}$
IE_6	11.25	9.39	11.70	n_N
IE_7	12.09	9.93	12.10	$\pi_2 + n_S$

Table 11 (*continued*)

Band	Experimental IE (eV)	Calculated Koopmans approximation IE (eV)		MO character 6-31G**
		STO-3G*	6-31G**	
(f) *4,4'-Thiobispyridine*				
IE_1	8.71	6.61	9.10	π_6–n_S
IE_2	9.57	8.25	9.59	π_5
IE_3	9.79	8.52	9.92	π'_4
IE_4	10.08	8.65	10.66	$\pi_{3'}$–n_S
IE_5	10.55	9.12	11.43	n_N
IE_6	11.21	9.45	11.79	$n_{N'}$
IE_7	12.13	9.88	12.03	$\pi_2 + n_S$

[a] Reproduced with permission from reference [23].

the distribution of rotamers would not change by more than 4%; moreover, no significant broadening of the bands would be expected as a result of the presence of approximately isoenergetic conformers. Hence, the use of a composite-molecule model based on the Morino structure for the thiobispyridines is appropriate for UPS interpretation.

The STO-3G*//STO-3G* model yields poor IE distributions below 18 eV when compared with the density-of-states analysis. Typically, eight bands are predicted above about 11.5 eV (with one IE below about 7.8 eV), which contrasts with the six bands obtained using the density-of-states analysis. In contrast, the 6-31G**//STO-3G* model yields 5–6 IEs below about 11.5 eV, which is in better agreement with the experimental findings. Nevertheless, the variation of this model from the experimental findings can be ascribed to the poor positioning of n_N MOs, and to two cross-over s-based and two p-based MOs (these four MOs being predicted above 18 eV). The overlapping bands centred around 10 eV are not well reproduced by the calculations; instead, the 6-31G**//STO-3G* model places the n_N orbitals at about 11.5 eV.

A more accurate positioning of the n_N orbitals can be achieved by correlation with the ΔSCF–CI calculations on methylthiopyridines. As a result of the localized nature of the MOs in the thiobispyridines, it would be expected that the valence MOs of the methylthiopyridines would mirror those of the larger molecules. The ΔSCF–CI method at the MP2/3-21G* level placed the n_N orbitals at 9.68, 9.74 and 9.35 eV for 2-, 3- and 4-methylthiopyridines, respectively, while a similar calculation on pyridine yields an IE of 9.78 eV for the n_N orbital. Thus, the n_N orbitals for the thiobispyridines should be at IE values much lower than the approximate value of 11.5 eV predicted by the 6-31G** model.

The 6-31G**//STO-3G* model predicts that, for all the thiobispyridines, there are seven ionic states between 8.0 and 12.5 eV (as shown in Table 11). The calculations assign ionizations from an anti-bonding orbital with considerable electron density on the S atom; a group of three π orbitals with little S character; a bonding S π orbital; and two delocalized n_N orbitals. The ordering of these last three orbitals is isomer specific. The non-planarity of the thiobispyridines invalidates σ and π

labelling; however, within the composite–molecule model, such labelling is appropriate. The STO-3G*//STO-3G* model predicts a similar IE sequence. The predicted IEs for this model are shifted to lower energy levels, so the more extensive 6-31G**//STO-3G* model was used for the MO analysis.

It would be anticipated that bands that correspond to ionization from the primarily pyridyl π-based MOs should exhibit a relative enhancement of intensity, whereas ionizations from predominantly localized in-plane N and S lone pairs should exhibit a reduction on changing from HeI to HeII radiation. Extensive mixing of lone pairs with π or σ systems of the pyridyl rings reduces the overall percentage change.

All the isomers between 8 and 9 eV exhibit a single IE, and Table 10 indicates a general reduction of 4%–23% on changing from HeI to HeII radiation. However, relative to the 'pure' π orbitals, these reductions are of the order of 40%–60%. Typically, localized S lone pairs exhibit relative percentage changes of 60%–70% [108]. Hence, the intensity variation is consistent with the 6-31G**//STO-3G* description of ionization from a π_6–n_S MO and suggests that the sulphur lone pair is substantially delocalized with the π system of the pyridyl ring.

The region 9–10.5 eV contains three bands that exhibit marked intensity enhancement of greater than 30%, which typifies ionization from delocalized n_N and π-based MOs. The MOs calculated at the 6-31G** level predict that the n_N orbitals are quite delocalized (which is consistent with the calculations of Del Bene [51] and Dunne et al. [21]), so will undergo only a moderate change under HeII conditions.

Examination of the 6-31G** MO coefficients reveals that π bonding with the S atom is dominated by the pyridine ring coplanar with the C–S–C angle, while the other ring exhibits localized, almost unperturbed 'pyridine' MOs. Therefore, it is reasonable to assign the n_N IEs of pyridine and the methylthiopyridines to the appropriate thiobispyridine orbitals. The differences between the experimental n_N and $n_{N'}$ orbitals and those determined at the ΔSCF–CI level are shown in Table 12.

Table 12
Differences between the experimental n_N and $n_{N'}$ assignments and the ΔSCF–CI predictions of thiobispyridines[a]

Isomer	Experimental IE (eV)		Exp. n_N-ΔSCF[b]	Exp. $n_{N'}$-ΔSCF[c]
	n_N	$n_{N'}$		
2,2'-S	9.45	9.73	0.23	0.05
2,3'-S	9.42	9.71	0.26	0.07
3,3'-S	9.49	9.89	0.25	0.11
2,4'-S	9.31	9.60	0.37	0.18
3,4'-S	9.61	9.78	0.26	0.09
4,4'-S	9.57	9.79	0.22	0.01

[a] Reproduced with permission from reference [23].
[b] The difference between the experimental n_N MO assignment for the coplanar ring and that predicted by the ΔSCF–CI model for the corresponding methylthiopyridine.
[c] The difference between the experimental $n_{N'}$ MO assignment for the non-coplanar ring and that predicted by the ΔSCF–CI model for pyridine.

The fit of these ΔSCF–CI IEs to the experimental IEs is quite good, with average errors of 0.25 eV and 0.08 eV for the n_N and $n_{N'}$ MOs respectively.

The preferred IE sequence for the thiobispyridines in the region 9–10.5 eV is

$$n_N \sim n_{N'} < \pi_5 - \delta n_S$$

where δ indicates a smaller contribution. This IE sequence is consistent with the HeI and HeII analyses of the methylchalcogenopyridines (see Section 3.2) and the oxybispyridines (see Section 3.3), and with the Colonna et al. [29] assignment of 2,2′-thiobispyridine. However, it should be stressed that an unambiguous assignment in this region is difficult, as a result of the mixing exhibited by these composite orbitals.

In the region 10.5–11.5 eV, there are two bands that exhibit significant intensity enhancement for all the isomers. The 6-31G** model gives a small n_S contribution to these orbitals via the p and d polarization functions, which is consistent with the intensity variations for π-based MOs, in which the n_S contribution is indeed small. Hence, the preferred IE sequence in this region is

$$\pi_4 - \delta n_S < \pi_3 - \delta n_S$$

which also correlates with the corresponding oxybispyridine analysis.

The IE_7 band shows significant intensity reduction on changing from HeI to HeII radiation, suggesting a greater n_S contribution than for IE_{2-6}. Hence, the preferred IE sequence for all the isomers of thiobispyridine is [23]

$$\pi_6 - n_S < n_N \sim n_{N'} < \pi_5 - \delta n_S < \pi_4 - \delta n_S < \pi_3 - \delta n_S < \pi_2 + n_S \quad (16)$$

The restriction of inter-ring conjugation in these molecules is also demonstrated in their UV absorption. Comparison of the spectra of the methylthiopyridines with those of the bispyridines reveals no evidence of greater conjugation in the bispyridine spectra. The UV spectra of the thiobispyridines resemble a superposition of the UV spectra of the corresponding methylthiopyridine and pyridine itself. Hence, the symmetrical thiobispyridines (i.e. the 2,2′-, 3,3′- and 4,4′- isomers) should mirror the pyridines and/or methylthiopyridines in their UPS assignment, because the π_{CH_3} IEs are typically positioned above 13 eV [64]. Fig. 10 shows a correlation diagram of the experimental vertical IEs of 3,3′-thiobispyridine, using the assignment given above, with the assignments for pyridine [109] and 3-methylthiopyridine, and MOs extracted from the 6-31G**//STO-3G* models for pyridine, 3-methylthiopyridine and 3,3′-thiobispyridine. Similar correlation diagrams can be drawn for the 2,2′- and 4,4′-thiobispyridines, giving weight to the IE sequence mentioned above.

The correlation of the UPS spectra of the asymmetrical isomers of thiobispyridine with the appropriate methylthiopyridines is more complex. The position of the ring-nitrogen must be reflected in electronic redistribution when compared with the pyridine moiety. The 6-31G**//STO-3G* model suggests that conjugation with the sulfur atom is dominated by only one of the rings, so that the S π MOs of that thiobispyridine have their origins with those of the dominant methylthiopyridine. Hence, correlation with respective monomers is appropriate. Fig. 11 shows a correla-

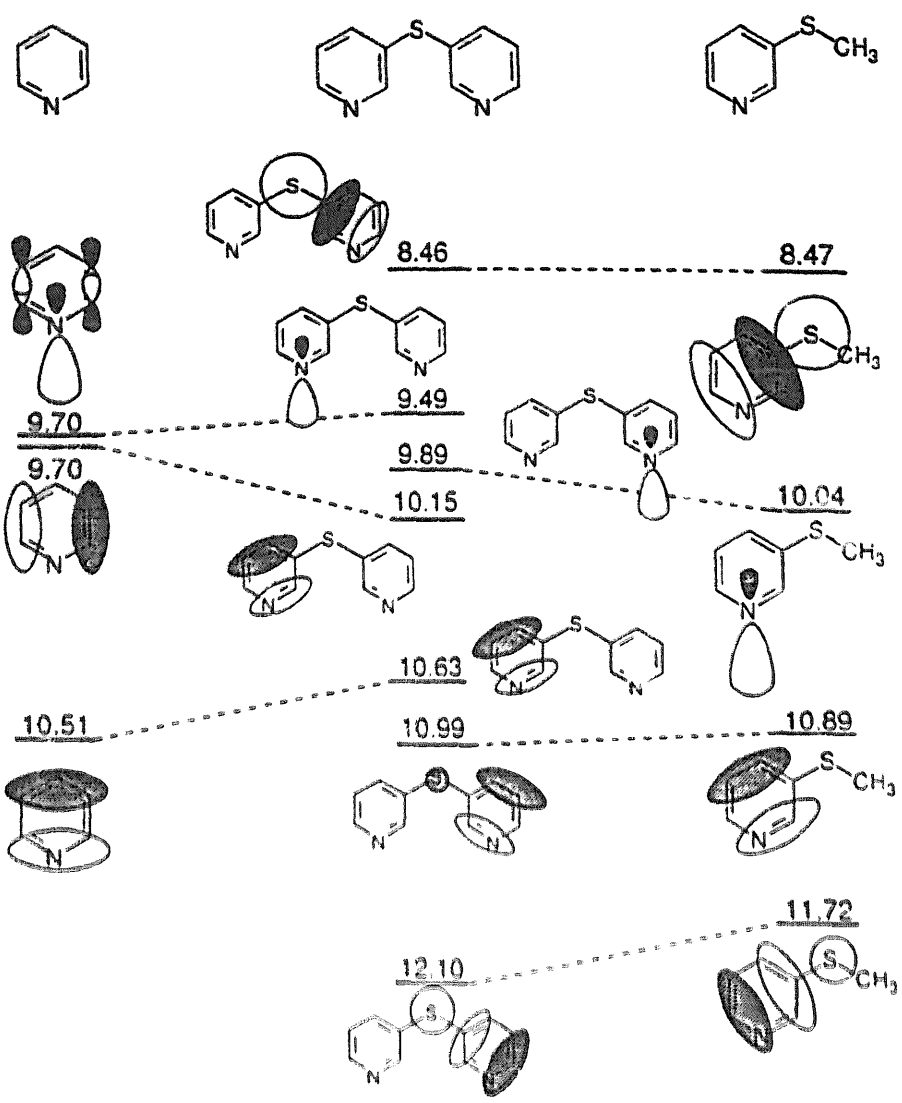

Fig. 10. Correlation diagram of the experimental IEs of 3,3'-thiobispyridine with those of pyridine and 3-methylthiopyridine. Only significant contributions to the MOs are shown. Reproduced with permission from reference [23].

tion diagram of the 2- and 3-methylthiopyridines with 2,3'-thiobispyridine (in which the sulphur interaction with only the dominant methylthiopyridine is shown). Similar correlations can be made for the 2,4'- and 3,4'-thiobispyridines.

3.5. *Selenobispyridines*

Poirer and Csizmadia [110] have documented the very few tractable basis sets available for Se. Apart from the STO-3G* minimal basis set of Pople and coworkers [111], the two most commonly used basis sets are the minimal basis set of Huzinaga and coworkers (denoted by MINI-1) [112] and the split valence (12s8p5d)/[5s4p2d] set (denoted by LWD) [84]. The first two of these basis sets are available for hydrogen, carbon and nitrogen, whereas the third basis set is only available for Se.

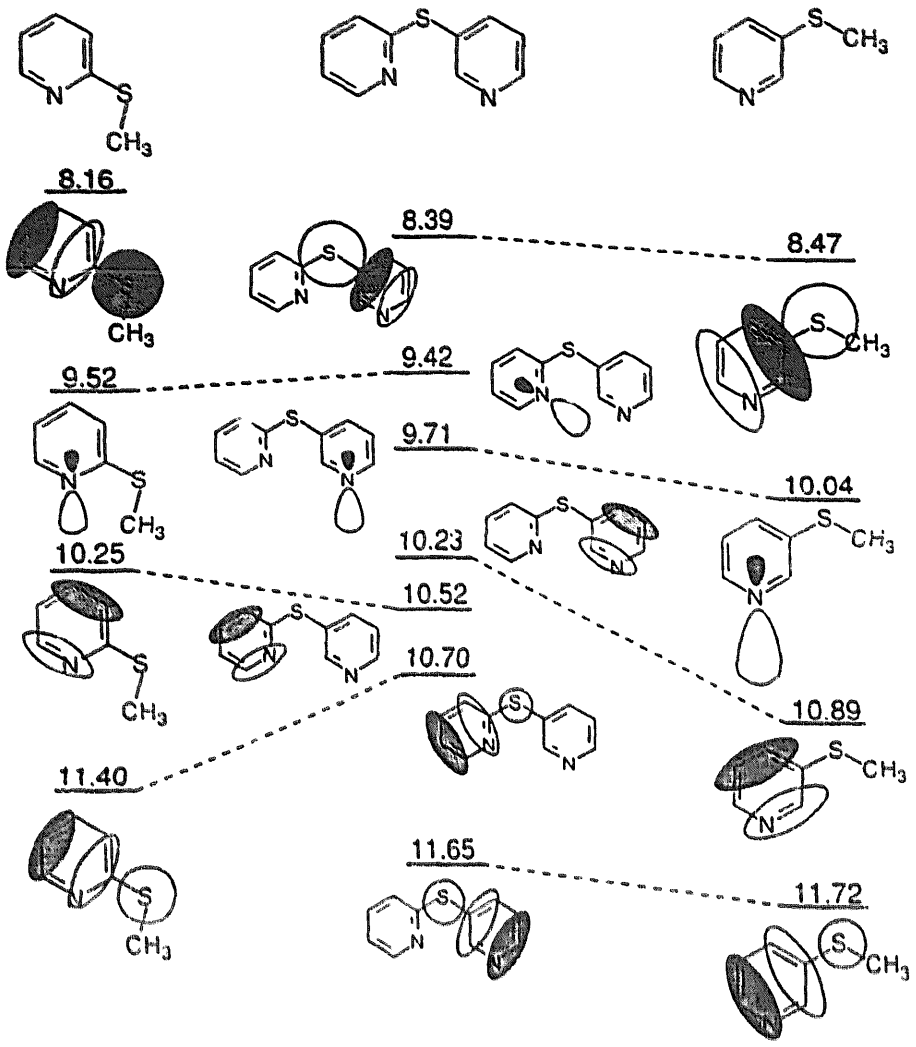

Fig. 11. Correlation diagram of the experimental IEs of 2,3'-thiobispyridine with those of 2- and 3-methylthiopyridine. Only significant contributions to the MOs are shown. Reproduced with permission from reference [23].

Therefore, to use the LWD basis set in the selenobispyridine calculations, basis sets of a similar size have to be found for H, C and N, because comparative studies have shown [113] that, as a result of a superposition error, unbalanced basis sets often give poorer results than do balanced sets. The internal 6-31G** is a split valence basis set [114] of comparable size with the LWD basis set for H, C and N, so was used in the MO calculations of the selenobispyridines [25]. It is denoted as the (6-31G**//LWD) basis set.

The ab initio energies were computed by Dunne et al. [25] using the restricted HF method within the GAUSSIAN suite of programs [42] and employing the internal STO-3G* (C, H, N, Se), 6-31G** (C, H, N) sets, and the MINI-1 and LWD basis sets (Se). The importance of the optimization of the critical structural parameters has been highlighted above (see Sections 3.1–3.4). To further the study of the barrier heights to free rotation in the bispyridine family, a series of optimiza-

tions were carried out for inter-ring angles and bond lengths at the STO-3G*, level for all rotational-distinct **A**–**D** conformers of the selenobispyridines [25].

The STO-3G(*) basis set has been largely untested for organic molecules that contain Se atoms, although Poirier and Csizmadia [110] have detailed that, on the basis of comparisons with experimental findings for six molecules, the mean absolute deviations given by the STO-3G*//STO-3G* model for the bond lengths and bond angles are 0.01 Å and 1.1° respectively. For the same molecules, the mean absolute deviation of the dipole moment when compared with the experimental findings is 0.51 D. The barrier heights for the seleno-bispyridines (calculated using the STO-3G*//STO-3G* model), along with the optimized R_{C-Se} and A_{C-Se-C} values and corresponding dipole moments, are presented in Table 13.

In general, the barrier heights of the **A**–**D** conformers of the selenobispyridines have been reduced in comparison with their thiobispyridine analogues (see Section 3.4). The number of conformers accessible at ambient temperature has not changed markedly for these congeners. The predicted minimum energy structures (**C**) are very similar to those of the thiobispyridines, i.e. either propeller-type or pseudo-**B**-type geometries. The similarity between the barrier heights of the thio- and selenobispyridines is not unexpected and reflects the delicate balance between the inter-ring bond angles and bond lengths. Because the optimized R_{C-Se} values are approximately 0.12 Å longer than the corresponding R_{C-S} parameters, it would be anticipated that a reduction in the barrier heights would result. However, the A_{C-Se-C} angles are reduced by 1°–3° in comparison with their thiobispyridine equivalents, so increasing steric hindrance and reducing the effect of the longer R_{C-Se} bonds [25].

The trends in the optimized structural parameters also mirror the results of the thiobispyridines. The **D** conformers possess the most acute inter-ring angles, because, in this conformation, steric hindrance in the C–Se–C plane is at a minimum. The shortest R_{C-Se} bond lengths are exhibited by the **C** conformers, while the **A** conformers continue to exhibit both the longest R_{C-Se} bonds and the widest A_{C-Se-C} angles to alleviate steric interactions within the molecular plane. The variation in the bond lengths between all the conformers is only 0.027 Å, while the inter-ring bond angles vary by up to 25°, again highlighting the importance of the optimization of the inter-ring angle.

For the oxybispyridines and thiobispyridines, three possible rotational mechanisms for conformer interconversion about the inter-ring bond were outlined (see Sections 3.3 and 3.4). For the selenobispyridines, the STO-3G*//STO-3G* model predicts that the barrier heights of the **B** and **D** structures are within the same order of magnitude as that of the **C** structures. While this model was unable to distinguish between the second and third mechanisms, the relatively large barrier heights to the **A**(0, 0) structure make the first mechanism highly unlikely for the selenobispyridines.

The dipole moments calculated using the STO-3G*//STO-3G* model are also presented in Table 13. A variation of up to 5 D exists between some of the conformers, and the general trend follows that of the thiobispyridines. The dipole moment is again not a diagnostic for the minimum energy structure, because the **C** structures

Table 13
Optimized parameters, barrier heights and dipole moments for the A–D conformers of the selenobispyridines[a]

Conformer	R_{C-Se} (Å)	A_{C-Se-C} (deg)	ΔE (kJ mol^{-1})	Dipole moment (D)
(a) *2,2'-Selenobispyridine*				
A(0, 0)	1.894	111.09	37.69	0.205
A(180, 180)	1.908	121.01	84.43	5.434
A(0, 180)	1.895	111.92	22.54	3.720
B(0, 90)	1.887	98.12	0.80	2.514
B(180, 90)	1.889	101.14	10.19	4.845
C(16, 66)	1.890	98.48	0.00	1.721
D(90, 270)	1.893	96.32	17.80	4.596
D(90, 90)	1.892	96.29	10.80	3.299
(b) *2,3'-Selenobispyridine*				
A(0, 0)	1.890	112.38	28.82	2.602
A(180, 180)	1.903	121.26	89.91	5.019
A(0, 180)	1.891	112.20	28.66	4.729
A(180, 0)	1.902	121.27	84.78	1.424
B(0, 90)	1.882	98.88	0.02	2.950
B(180, 90)	1.884	101.44	8.68	3.442
B(90, 0)	1.884	101.35	13.04	2.067
B(90, 180)	1.884	101.19	14.87	4.917
C(2, 89)	1.882	98.88	0.00	2.880
D(90, 270)	1.887	97.13	12.91	4.248
D(90, 90)	1.887	96.94	11.38	2.585
(c) *3,3'-Selenobispyridine*				
A(0, 0)	1.897	121.52	78.63	2.577
A(180, 180)	1.898	121.53	86.62	3.703
A(0, 180)	1.898	121.50	81.74	1.880
B(0, 90)	1.879	101.88	2.87	2.147
B(180, 90)	1.879	101.65	4.16	3.060
C(50, 50)	1.878	99.39	0.00	1.321
D(90, 270)	1.882	97.66	3.32	3.623
D(90, 90)	1.882	97.59	2.52	0.645
(d) *2,4'-Selenobispyridine*				
A(0, 0)	1.891	112.10	23.74	4.308
A(0, 180)	1.902	121.03	81.89	3.262
B(0, 90)	1.884	98.64	0.00	3.181
B(180, 90)	1.886	101.35	8.73	2.540
B(90, 0)	1.885	101.28	9.10	3.716
C(359, 92)	1.884	98.56	0.00	3.171
D(90, 90)	1.889	96.65	11.69	3.251
(e) *3,4'-Selenobispyridine*				
A(0, 0)	1.897	121.25	76.71	2.408
A(180, 0)	1.897	121.29	81.00	1.693
B(0, 90)	1.881	101.68	5.40	2.232
B(180, 90)	1.882	101.40	6.62	1.399
B(90, 0)	1.879	101.62	0.84	2.337

Table 13 (*continued*)

Conformer	$R_{C\text{-}Se}$ (Å)	$A_{C\text{-}Se\text{-}C}$ (deg)	ΔE (kJ mol^{-1})	Dipole moment (D)
C(300, 146)	1.879	99.88	0.00	2.480
D(90, 90)	1.884	97.30	4.96	1.993
(f) *4,4'-Selenobispyridine*				
A(0, 0)	1.897	121.07	74.94	0.574
B(0, 90)	1.883	101.40	2.56	1.102
C(45, 45)	1.881	99.74	0.00	1.022
D(90, 90)	1.886	97.02	6.31	0.805

[a] Reproduced with permission from reference [25].

share similar dipole moments with conformers supposedly restricted on barrier height concerns.

The basis set employed had a significant effect on the charge densities on the atoms surrounding the selenium functionality. Both atomic selenium and carbon possess Allred electronegativities of 2.55 [88], so it would be anticipated that there would not be a large disparity in the electronic distribution around the C–Se bonds. The minimal STO-3G* set, which includes d polarization functions on the heavy atoms, predicts that the selenium atom in the selenobispyridines is electron rich. (See Table 14 for the charge distributions of 2,2'- and 3,3'-selenobispyridine calculated using the STO-3G*//STO-3G*, 6-31G**–MINI-1//STO-3G* and 6-31G**–LWD//STO-3G* models [25].)

The MINI-1 set [112] predicts the selenium atom to be electropositive (about 0.1*e*), while the extended LWD basis set [84] (similar to the STO-3G* set) predicts it to be electron rich by 0.1*e*. The MINI-1 set is a minimal [4s3p1d] basis set, so it does not possess polarization functions. Using it in conjunction with 6-31G** functions on the C, H and N atoms results in a withdrawal of electrons by the polarization functions on those atoms from the selenium centre, as a result of basis set imbalance. Similar to the 6-31G** basis set, the LWD basis set is also a split valence basis set. Thus, commensurate with the STO-3G* model, the more extensive but balanced 6-31G**–LWD model predicts that the selenium atom is electron rich by 0.1*e*.

It was found in 6-31G** calculations on the thiobispyridines that the sulfur atom in these molecules became electropositive (about 0.2*e*), despite the greater electronegativity of the sulfur atom (Allred value of 2.58 [88]). Favourable overlap within the composite–molecule model results in a net transfer of electrons from sulfur 3p orbitals into the delocalized π-type MOs of the thiobispyridines. The first IE of selenium's functionality reduces the contribution of selenium electrons to the bonding MOs of the selenobispyridines, so that the selenium atom retains its electron-rich nature, despite having a similar electronegativity to that of carbon. Based on these considerations, Dunne et al. [25] believed that the LWD basis was the most reliable, so used it for the MO analysis of the selenobispyridines.

Cauletti and Distefano [115] have reviewed the literature on UPS studies on

Table 14
Comparison of charge densities for 2,2'- and 3,3'-selenobispyridine[a]

Atom	Charge density (*e*)		
	STO-3G*	6-31G**–MINI-1	6-31G**–LWD
(a) *2,2'-Selenobispyridine*			
N_1	−0.245	−0.520	−0.579
C_2	0.122	0.059	0.288
C_3	−0.073	−0.121	−0.177
C_4	−0.043	−0.074	−0.074
C_5	−0.077	−0.220	−0.221
C_6	0.040	0.145	0.144
Se	−0.112	0.111	−0.099
N_1'	−0.220	−0.448	−0.511
C_2'	0.123	−0.040	0.211
C_3'	−0.054	−0.041	−0.124
C_4'	−0.049	−0.092	−0.091
C_5'	−0.066	−0.196	−0.197
C_6'	0.036	0.119	0.120
(b) *3,3'-Selenobispyridine*			
N_1	−0.231	−0.531	−0.533
C_2	0.030	0.194	0.126
C_3	0.011	−0.300	−0.062
C_4	−0.050	−0.018	−0.075
C_5	−0.067	−0.192	−0.193
C_6	0.030	0.113	0.113
Se	−0.117	0.124	−0.097
N_1'	−0.235	−0.535	−0.536
C_2'	0.047	0.256	0.179
C_3'	−0.003	−0.464	−0.190
C_4'	−0.036	0.054	−0.025
C_5'	−0.073	−0.206	−0.206
C_6'	0.043	0.134	0.134

[a] Hydrogens are not included. Reproduced from permission from reference [25].

organo-selenium compounds. While few studies have been reported on systems that contain selenylpyridine groups, there have been several studies on the related alkyl phenyl selenides and diphenyl selenides [116–119]. The conformations of the diphenylchalcogenides (PhXPh) and some chalcanthrenes have been investigated by means of UPS, as well as theoretical computations by Traven and coworkers [120,121].

The HeI and HeII spectra of the six isomers of selenobispyridine were recorded under similar conditions to those of the thiobispyridines [25]. The spectra were calibrated using butadiene–argon mixtures. The HeI and HeII spectra were digitized for use in the density-of-states analysis [56,61] and the determination of the HeI/HeII cross-section ratios. These are given in Table 15.

The interpretation of the UPS spectra of the selenobispyridines, similar to that of their lighter congeners, is complicated by the overlapping of cationic states and the

Table 15
Relative HeI and HeII band intensities and percentage change of the selenobispyridines[a]

Band	IE range (eV)	Band intensity		Percentage change[b] (%)
		HeI	HeII	
(a) *2,2'-Selenobispyridine*				
1	7.00–8.60	1.326	0.711	−46.35
2	8.60–9.84	2.883	2.986	3.55
3	9.84–10.88	2.712	2.899	6.92
4	10.88–11.65	1.191	0.970	−18.51
5	11.65–12.34	1.242	1.014	−18.34
6	12.34–18.00	11.646	12.419	6.63
(b) *2,3'-Selenobispyridine*				
1	7.00–8.63	1.220	0.892	−26.89
2	8.63–9.80	2.701	3.411	26.27
3	9.80–10.90	2.806	2.865	2.08
4	10.90–11.74	1.131	1.048	−7.38
5	11.74–12.38	1.113	0.849	−23.70
6	12.38–18.00	12.028	11.935	−0.77
(c) *3,3'-Selenobispyridine*				
1	7.00–8.95	1.235	0.688	−44.26
2	8.93–10.32	3.641	4.715	29.47
3	10.32–11.27	1.943	2.185	12.45
4	11.27–11.96	1.015	0.973	−4.18
5	11.96–12.53	1.044	0.876	−16.05
6	12.53–18.00	12.123	11.564	−4.61
(d) *2,4'-Selenobispyridine*				
1	7.00–8.87	1.080	0.708	−34.50
2	8.87–9.94	2.302	2.756	19.72
3	9.94–10.38	1.106	1.542	39.41
4	10.38–11.20	1.424	2.124	49.10
5	11.20–11.90	0.929	0.663	−28.59
6	11.90–18.00	14.159	13.208	−6.72
(e) *3,4'-Selenobispyridine*				
1	7.00–9.03	1.189	0.749	−37.02
2	9.03–10.32	3.100	4.146	33.72
3	10.32–10.78	0.896	1.074	19.86
4	10.78–11.36	0.844	0.781	−7.47
5	11.36–12.08	1.019	0.893	−12.31
6	12.08–18.00	13.953	13.358	−4.26
(f) *4,4'-Selenobispyridine*				
1	7.00–9.12	1.183	0.754	−36.28
2	9.12–10.34	3.176	4.598	44.80
3	10.34–10.79	0.884	1.159	31.14
4	10.79–11.50	0.893	0.883	−1.21
5	11.50–12.14	0.770	0.769	−0.13
6	12.14–18.00	14.093	12.836	−8.92

[a] Reproduced with permission from reference [25].
[b] [(HeII/HeI) − 1] × 100.

possible presence of a range of conformers. It has been shown previously that the distribution of rotamers would not change by more than 4% within the thermal regime of the UPS experiments. The preceding conformational analysis on the selenobispyridines showed that the barrier heights to the Morino structure are small with respect to the minimum energy structure. It is reasonable, therefore, to use the **B** structure for the interpretation of the UPS spectra of the selenobispyridines, because the orthogonal nature of the pyridyl rings greatly simplifies the analysis.

The STO-3G* IE distribution (given in Table 16) overestimates the number of valence orbitals when compared with the experimental density-of-states analysis (as shown in Table 15 under the HeI band intensity), because it shifts most MOs approximately 1 eV below their experimental values. The 6-31G**–LWD and 6-31G**–MINI-1 models do not reproduce the experimental results well either, typically predicting 4–5 bands in the outer valence region, where experimentally 6–7 bands are expected. As has been shown above, the poor positioning of the n_N MOs by the KA–HF models causes the theoretical IE distribution to be deficient in the region around 10 eV. For example, the 6-31G**–LWD model set the n_N MOs in the range 11.1–11.8 eV.

As shown in Table 16, the KA/(6-31G**–LWD) model reproduces the experimental IEs better than do the other models. The LWD model predicts seven ionic states between 8.00 and 12.50 eV, corresponding to ionizations from an anti-bonding orbital with considerable electron density on the Se atom; a group of three π orbitals with little Se character; a bonding Se π orbital; and two delocalized n_N orbitals. The ordering of these last three orbitals was found to be isomer specific. The ordering of these orbitals mirrors that displayed by the thiobispyridines, as would be expected on electronegativity grounds. Compared with the sulphur atom, selenium has a considerably lower first ionization energy, so its degree of interaction with the pyridine MOs and the shift of those Se-containing MOs will differ from the behaviour of their thio- analogues.

The order of MOs in the 6-31G** calculations on the thiobispyridines is similar to that displayed by the 6-31G**–LWD model for the selenobispyridines. The differences result from the low energy shifts of the bonding Se π orbitals either below or between the n_N MOs. The anti-bonding Se π orbitals also shift to a similar degree but, because they are the HOMOs, there is no effect on their relative positions. A comparison between the sulfur-based anti-bonding and bonding MOs IEs (as calculated using the 6-31G**–STO-3G* model) and their selenium equivalents revealed that a shift of 0.15–0.30 eV to a lower energy level had occurred in the molecules with selenium, whereas the 'pure' ring-based orbitals showed shifts of only about 0.05 eV. The effect on the n_N MOs was less predictable in magnitude but, in all cases, a shift to lower IEs was observed.

Table 15 gives the relative HeI and HeII band intensities, and the percentage change. Bands that arise from ionizations from Se-based MOs should exhibit a reduction on changing from HeI to HeII radiation. Extensive mixing of lone pairs with the pyridine π or σ system reduces the overall percentage change. All the isomers of selenobispyridine exhibit a single IE in the region 7.9–8.7 eV, which exhibits a reduction of 27%–47% on changing from HeI to HeII radiation. If we

Table 16
Experimental and calculated IEs of the selenobispyridines[a]

Band	Experimental IE (eV)	Calculated IE (eV)			MO character
		STO-3G*	MINI-1	LWD	
(a) *2,2'-Selenobispyridine*					
1	7.95	6.81	8.22	8.18	π_6–n_{Se}
2	9.35	8.14	9.36	9.31	$\pi_{5'}$
3	9.55	8.72	10.21	10.17	π_4
4	9.74	8.79	10.34	10.29	$\pi_3 + \delta n_{Se}$
5	10.06	9.19	10.87	10.81	$\pi_2 + n_{Se}$
6	10.39	9.26	11.06	11.13	$n_N + n_{N'} + n_{Se}$
7	11.23	9.52	11.30	11.28	$n_N + n_{N'}$
(b) *2,3'-Selenobispyridine*					
1	8.09	6.99	8.42	8.38	π_6–n_{Se}
2	9.25	8.15	9.37	9.33	$\pi_{5'}$
3	9.51	8.71	10.23	10.20	$\pi_{4'}$
4	9.77	8.90	10.44	10.39	$\pi_3 + \delta n_{Se}$
5	9.99	9.18	10.99	10.94	$\pi_2 + n_{Se}$
6	10.38	9.40	11.23	11.27	$n_N + n_{N'} + n_{Se}$
7	11.35	9.76	11.43	11.41	$n_N + n_{N'} + n_{Se}$
(c) *3,3'-Selenobispyridine*					
1	8.36	7.05	8.41	8.36	π_6–n_{Se}
2	9.56	8.45	9.75	9.72	$\pi_{5'}$
3	9.91	8.80	10.20	10.15	π_4
4	10.10	9.04	10.62	10.60	$\pi_{4'}$
5	10.54	9.47	11.38	11.32	$\pi_2 + n_{Se}$
6	10.79	9.55	11.51	11.48	n_N
7	11.70	10.03	11.74	11.73	$n_{N'}$
(d) *2,4'-Selenobispyridine*					
1	8.36	7.05	8.50	8.46	π_6–n_{Se}
2	9.41	8.20	9.35	9.32	$\pi_{5'}$
3	9.72	8.60	10.14	10.11	$\pi_{4'}$
4	10.04	8.94	10.50	10.44	π_3
5	10.57	9.22	11.11	11.05	$\pi_2 + n_{Se}$
6	10.82	9.45	11.20	11.22	$n_{N'}$
7	11.61	9.73	11.44	11.44	n_N
(e) *3,4'-Selenobispyridine*					
1	8.47	7.29	8.85	8.81	π_6–n_{Se}
2	9.45	8.43	9.62	9.56	$\pi_{5'}$
3	9.77	8.61	9.92	9.88	π_4
4	10.03	9.16	10.77	10.75	$\pi_3 + \delta n_{Se}$
5	10.58	9.35	11.37	11.34	$n_{N'} + \delta n_{Se}$
6	10.94	9.60	11.60	11.54	$\pi_{2'} + n_{Se}$
7	11.75	10.20	11.84	11.82	$n_N + \delta n_{Se}$

Table 16 (*continued*)

Band	Experimental IE (eV)	Calculated IE (eV)			MO character
		STO-3G*	MINI-1	LWD	
(f) *4,4'-Selenobispyridine*					
1	8.61	7.36	8.93	8.89	π_6–n_{Se}
2	9.54	8.47	9.66	9.60	π_5
3	9.80	8.68	9.94	9.90	π_4,
4	10.05	9.03	10.64	10.63	π_3, + δn_{Se}
5	10.50	9.40	11.45	11.41	n_N
6	10.89	9.64	11.71	11.68	$\pi_2 + n_{Se}$
7	11.89	10.17	11.76	11.71	n_N, + δn_{Se}

[a] Reproduced with permission from reference [25].

express this change relative to that exhibited by the 'pure' π bands, then the reduction in intensity becomes of the order of 50%–80%. This results from the greater reduction in the photo-ionization cross-section of the Se 4p atomic orbital under HeII conditions, and the greater contribution of the Se electron density into this anti-bonding orbital, caused by the lower first IE of Se. The band assigned to the bonding Se π orbital exhibits a 1%–29% reduction in absolute terms and a 25%–78% decrease in relative terms, which suggests either a lower Se content or a greater degree of delocalization. The size of these reductions is consistent with the MO analysis of the (6-31G**–LWD)//STO-3G* model for the non-planar **B** geometry [25].

The region between 9 and 10.6 eV contains several bands that exhibit marked intensity enhancement under HeII conditions, which typifies ionization from delocalized n_N and π-based MOs. The 6-31G**–LWD model predicts that the n_N orbitals are quite delocalized, so that they will undergo only a very moderate change under HeII conditions, making unambiguous detection difficult, especially considering the degree of overlapping in this region. It was shown previously that CI methods were necessary to obtain reasonable IEs for these n_N MOs. KA–HF models provide good assignments for benzene-based aromatics, but their success has been shown to be limited with pyridine systems. This stems from the difference in the character of the n_N MO: a σ-type MO for which both correlation and relaxation processes differ from those of the π MOs.

The ΔSCF–CI method allowed only the calculation of the IE of the lowest MO in each symmetry species. However, this did allow the accurate determination of the first π IE and the IE of the n_N MO. While such calculations are not feasible on molecules as large as the selenobispyridines, the localized nature of the selenobispyridine MOs should allow a 'good' correlation between the selenobispyridine n_N MOs and those calculated for pyridine and the methylselenylpyridines at the ΔSCF–CI level. The first IEs for 2-, 3- and 4-methylselenylpyridine were calculated to be 8.55, 8.66 and 8.98 eV respectively (see Section 3.2). In comparison with the first IEs of the appropriate selenobispyridines, these values are in 'poorer' agreement than those predicted by the KA/(6-31G**–LWD) model. This may be as a result of the disparity between the basis sets utilized in the ΔSCF–CI calculations (3-21G* for C, H and

N, and LWD for Se). The usefulness of Koopmans' approximation for the determination of IEs for π-type MOs is again shown, provided that basis sets of sufficient quality are used.

The IEs for the n_N MOs of pyridine and 2-, 3- and 4-methylselenylpyridine were found to be 9.78, 9.71, 9.75 and 9.37 eV, respectively, by the ΔSCF-CI model, which is in much better agreement with the experimental findings than the values predicted by the KA–HF models (11.2–11.7 eV). The differences between the experimental IEs for the n_N MOs and those predicted by the ΔSCF–CI model are less than 0.4 eV, and are more commonly of the order of 0.2 eV. It is anticipated that, with the use of larger basis sets for the C, H and N atoms, this difference would contract. Thus, in the assignment of the UPS spectra of the selenobispyridines, these ΔSCF n_N MO IEs were used by Dunne et al. [25], in place of the KA–HF assignments. A series of three π orbitals with little Se character are also expected to lie in the region 9.0–11.0 eV, making the preferred IE sequence for the selenobispyridines in this region

$$n_N \sim n_{N'} < \pi_5 - \delta n_{Se} < \pi_4 - \delta n_{Se} < \pi_3 - \delta n_{Se}$$

This assignment is consistent with that of the oxy- and thiobispyridines (see Sections 3.3 and 3.4), but it should be stressed that an unambiguous assignment in this region is difficult, because of the mixing exhibited by these composite orbitals.

In the region 11.0–12.0 eV, there is a band that exhibits a significant intensity reduction on changing from HeI to HeII radiation, suggesting a greater n_{Se} contribution than that of IE_{2-6}. This band is assigned to the bonding Se π orbital IE_7. Hence, the preferred valence IE sequence for all the isomers of selenobispyridine is

$$\pi_6 - n_{Se} < n_N \sim n_{N'} < \pi_5 - \delta n_{Se} < \pi_4 - \delta n_{Se} < \pi_3 - \delta n_{Se} < \pi_2 + n_{Se} \quad (17)$$

which is identical to the assignment for the thiobispyridines.

Fig. 12 shows a correlation diagram of the experimental vertical IEs of 2,2'-selenobispyridine (using the above assignment) with the assignments for pyridine and 2-methylselenylpyridine. The MOs are extracted from the 6-31G**–LWD model of 2,2'-selenobispyridine. The observed correlation is good and suggests that extensive delocalization does not occur in these molecules. Similar correlation diagrams can be drawn for 3,3'- and 4,4'-selenobispyridine, giving added weight to the composite-molecule model and the IE sequence given above.

The correlation of the UPS spectra of the asymmetrical isomers of selenobispyridines with the methylselenylpyridines is more complex. The 6-31G**–LWD model indicates that conjugation with the selenium atom is dominated by only one of the rings, so that the MOs of that bispyridine have their origins with those of the dominant methylselenylpyridine. Fig. 13 shows a correlation diagram of the 2- and 3-methylselenylpyridines with 2,3'-selenobispyridine and shows that the anti-bonding and bonding Se π orbitals of 2-methylselenylpyridine correlate better with the corresponding MOs in 2,3'-selenobispyridine. A model that incorporates mesomeric interactions between Se and both pyridine rings is inappropriate. Similar correlations can also be made for 2,4'- and 3,4'-selenobispyridine.

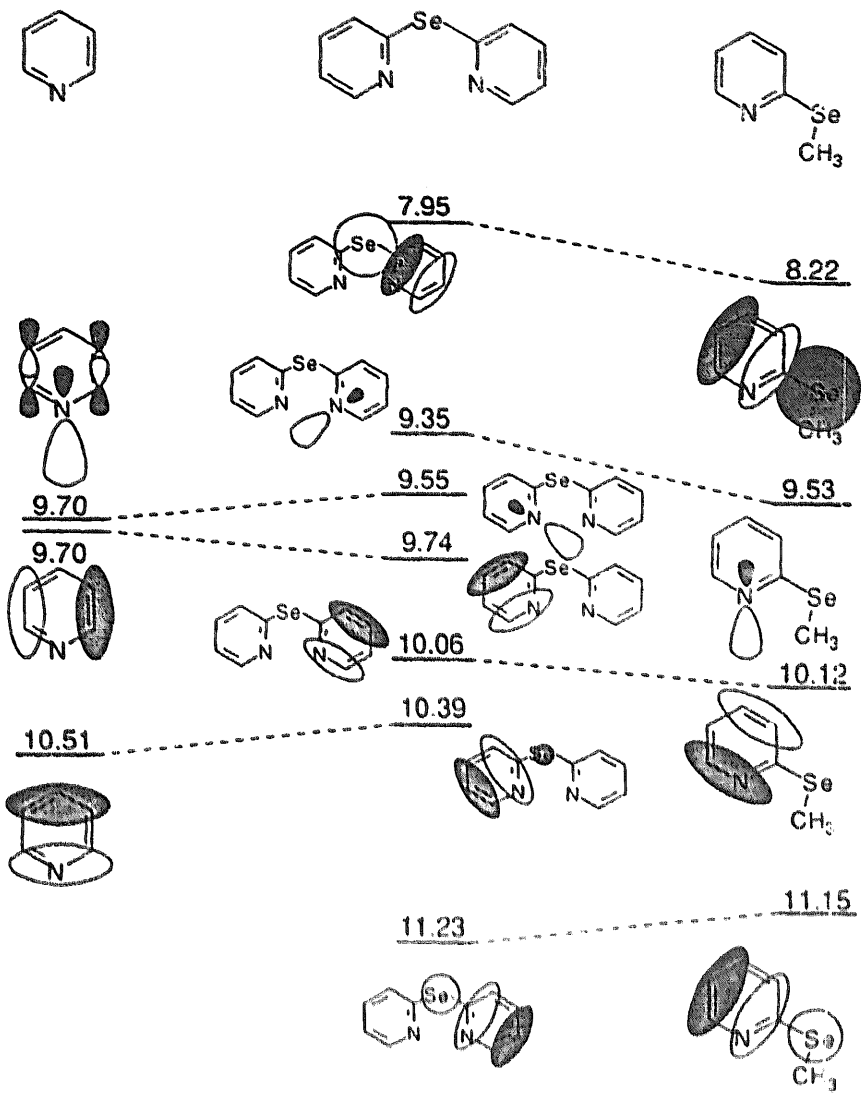

Fig. 12. Correlation diagram of the experimental IEs of 2,2'-selenobispyridine with those of pyridine and 2-methylselenylpyridine. Reproduced with permission from reference [25].

3.6. *Tellurobispyridines*

The electron-dense nature of tellurium has restricted theoretical studies on tellurium-containing systems. Apart from the STO-3G* minimal basis set of Pople and coworkers [111], very few basis sets have been applied to systems that contain tellurium. Poirier and Csizmadia [110] have detailed that, on the basis of comparisons with experimental findings for six molecules that contain the lighter chalcogens, the mean absolute deviations given by the STO-3G*//STO-3G* model for optimized bond lengths and bond angles are 0.01 Å and 1.1° respectively. No such comparison is currently available for organic molecules that contain fourth-row atoms, so the STO-3G(*) basis set remains largely untested for tellurium compounds. To complete the study of the barrier heights to free rotation in the chalcogenobispyridine family, a series of optimizations of inter-ring angles and bond lengths were performed at

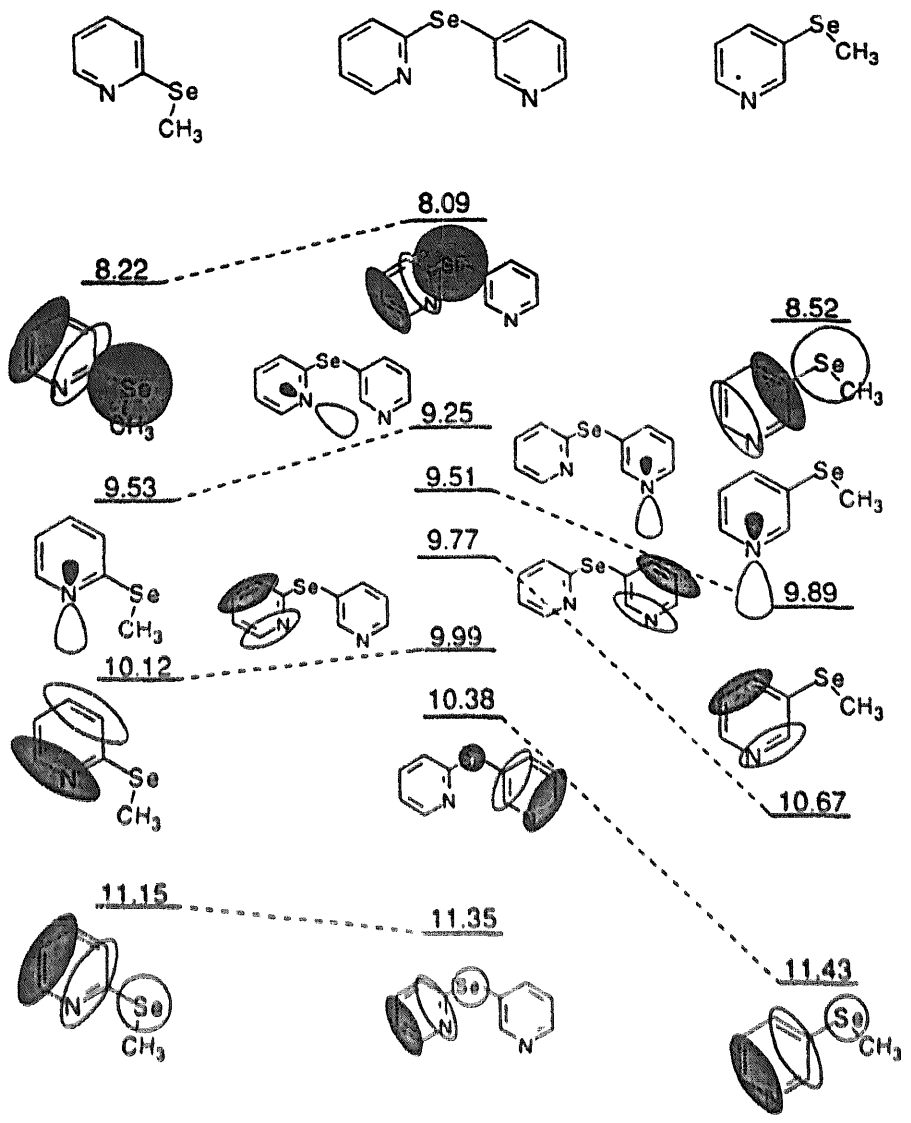

Fig. 13. Correlation diagram of the experimental IEs of 2,3'-selenobispyridine with those of 2- and 3-methylselenylpyridine. Reproduced with permission from reference [25].

the STO-3G* level for all the rotational-distinct A–D conformers of the tellurobispyridines [26].

For tellurobispyridines, Dunne et al. [26] calculated ab initio energies using the restricted HF method within the GAUSSIAN suite of program [42] and using the internal STO-3G* (C, H, N, Te) basis set. The barrier heights for the tellurobispyridines (calculated using the STO-3G*//STO-3G* model), along with the optimized $R_{C\text{-}Te}$ and $A_{C\text{-}Te\text{-}C}$ values and corresponding dipole moments, are presented in Table 17.

While the barrier heights of the A–D conformers of the tellurobispyridines have generally been reduced in comparison with their selenobispyridine analogues, the range of conformers accessible at ambient temperature has not changed markedly for these congeners. The predicted minimum energy structures (C) of the telluro-

Table 17
Optimized parameters, barrier heights and dipole moments for the A–D conformers of the tellurobispyridines[a]

Conformer	R_{C-Te} (Å)	A_{C-Te-C} (deg)	ΔE (kJ mol^{-1})	Dipole moment (D)
(a) *2,2'-Tellurobispyridine*				
A(0, 0)	2.106	106.99	22.09	0.471
A(180, 180)	2.122	115.58	55.46	5.588
A(0, 180)	2.108	106.76	6.23	3.801
B(0, 90)	2.103	96.25	1.85	2.545
B(180, 90)	2.106	97.97	7.16	4.752
C(37, 39)	2.101	96.75	0.00	1.100
D(90, 270)	2.111	95.77	16.74	4.571
D(90, 90)	2.110	95.23	11.49	3.267
(b) *2,3'-Tellurobispyridine*				
A(0, 0)	2.103	107.33	11.66	2.331
A(180, 180)	2.117	115.84	59.31	5.124
A(0, 180)	2.104	107.00	10.92	4.726
A(180, 0)	2.116	115.86	54.85	1.652
B(0, 90)	2.096	96.88	0.00	2.999
B(180, 90)	2.099	98.30	4.84	3.407
B(90, 0)	2.100	98.52	9.26	1.975
B(90, 180)	2.101	98.19	10.54	4.823
C(1, 88)	2.096	96.88	0.00	2.926
D(90, 270)	2.103	95.86	11.91	4.206
D(90, 90)	2.102	95.78	10.57	2.560
(c) *3,3'-Tellurobispyridine*				
A(0, 0)	2.111	116.20	49.92	2.318
A(180, 180)	2.112	116.12	56.53	3.690
A(0, 180)	2.111	116.15	52.32	2.053
B(0, 90)	2.094	98.79	0.44	2.189
B(180, 90)	2.095	98.37	1.19	2.963
C(53, 49)	2.092	96.76	0.00	1.350
D(90, 270)	2.097	96.33	3.14	3.593
D(90, 90)	2.097	96.25	2.41	0.537
(d) *2,4'-Tellurobispyridine*				
A(0, 0)	2.105	107.02	7.14	4.215
A(180, 0)	2.117	115.67	52.78	3.308
B(0, 90)	2.099	96.64	0.00	3.233
B(180, 90)	2.102	98.06	4.91	2.450
B(90, 0)	2.100	98.26	6.01	3.600
C(0, 92)	2.099	96.64	0.00	3.233
D(90, 90)	2.105	95.58	10.99	3.229
(e) *3,4'-Tellurobispyridine*				
A(0, 0)	2.111	115.96	49.66	2.440
A(180, 0)	2.112	115.93	53.30	1.559
B(0, 90)	2.097	98.63	3.87	2.324
B(180, 90)	2.097	98.25	4.55	1.253
B(90, 0)	2.095	98.48	0.02	2.277

Table 17 (*continued*)

Conformer	R_{C-Te} (Å)	A_{C-Te-C} (deg)	ΔE (kJ mol^{-1})	Dipole moment (D)
C(95, 352)	2.094	98.35	0.00	2.204
D(90, 90)	2.100	96.08	5.90	1.992
(f) *4,4'-Tellurobispyridine*				
A(0, 0)	2.111	115.85	48.17	0.477
B(0, 90)	2.097	98.33	1.21	1.170
C(40, 40)	2.096	97.73	0.00	1.175
D(90, 90)	2.102	95.84	6.91	0.926

[a] Reproduced with permission from reference [26].

bispyridines are also similar to those of their thio- and seleno- analogues, i.e. either propeller-type or pseudo-**B**-type geometries. Only for the 2,3'- and 2,4'- isomers are the Morino structures also the minimum energy structures [26].

The optimized R_{C-Te} values are approximately 0.2 Å longer than the corresponding R_{C-Se} variables (minimizing steric hindrance), while the A_{C-Te-C} angles are reduced by 1°–5° in comparison with their selenobispyridine equivalents (so increasing steric hindrance in the plane of the inter-ring bridge). The variation in the optimized bond lengths between all conformers was only 0.028 Å, while the inter-ring bond angles were found to vary by up to 11°. This again highlights the importance of the optimization of the inter-ring angle. The longer R_{C-Te} bonds reduce the degree to which the inter-ring angle must open to allow for the planar conformation.

Three possible rotational mechanisms for conformer interconversion about the inter-ring bond have been outlined (see Sections 3.3–3.5). For the thio- and selenobispyridines, the second and third mechanisms are possible, because the 6-31G**–STO-3G* model predicts that the barrier heights of the **B** and **D** structures are of the same order of magnitude as the **C** structures. It was shown in Sections 3.3–3.5 that the use of extensive basis sets (such as the 6-31G** set) with the STO-3G(*) optimized geometries resulted in a reduction of the relative barrier heights to the **B** and **D** conformers. Therefore, it was anticipated that this would hold true for the telluro- analogues [26]. In the case of the tellurobispyridines, the STO-3G*//STO-3G* model yields similar conclusions to those given for the thio- and selenobispyridines, slightly favouring the second mechanism over the third mechanism. The relatively large barrier heights to the **A** structures make the first mechanism unlikely for the entire family of chalcogenobispyridines; however, for the 2,2'-, 2,3'- and 2,4'-tellurobispyridines, the barrier heights to the A(0, 0) and A(0, 180) conformers are not prohibitive.

Therefore, a range of almost isoelectronic conformers (that possess a similar electronic structure) are expected to surround the minimum energy structures. The calculations suggest that low energy pathways exist between the 'propeller' and Morino forms, permitting concerted disrotatory motion through a range of **C** and **B** forms without any need to adopt **A** or **D** structures [25]. This large-scale motion

was supported by NMR data in which magnetic equivalence was noted for all chemically equivalent atoms [49].

The dipole moments calculated using the STO-3G*//STO-3G* model are presented in Table 17. The calculated dipole moments cannot be considered as predictive, because Green [107] has demonstrated that a double-zeta basis set with polarization functions is required for quantitative agreement with the experimental findings. It can be seen that the **C** structures share similar dipole moments to those of the high energy conformers, so limiting the use of dipole moment measurements for the determination of minimum energy structures.

The conformational properties of the chalcogenobispyridines are seen to vary only slightly down the group. As anticipated, there is a contraction of the inter-ring angle and an elongation of R_{C-X} bond lengths for congeners down the group. In all cases, the minimum energy structures are predicted by the STO-3G(*)//STO-3G(*) models to be of the 'propeller' (**C**) or 'Morino' (**B**) forms, with an almost perpendicular attitude being maintained between the ring planes. The predicted angles are shown in Table 18, along with the corresponding values for their diphenyl analogues [90,96,120].

In their review on the photoelectron spectroscopy of organic derivatives of selenium and tellurium, Cauletti and Distefano [28] report the UPS spectra of several dialkyl and cyclic tellurides [86,122,123], telluroanisole [119], diphenyl telluride [120,121], the telluro- derivative of phthalic anhydride [124], and some homo- and hetero-nuclear chalcanthrenes [125,126]. The HeI and HeII UPS spectra of the tellurobispyridines are interpreted in terms of the models discussed above and are correlated with the UPS spectra of the other chalcogenobispyridines. Their spectra were digitized for use in the density-of-states analysis [56,61] and in the determination of the HeI/HeII cross-section ratios, both of which are given in Table 19.

While minimal basis sets fortuitously predict geometrical parameters in good agreement with the experimental findings, predicted Koopmans' approximation IEs are often poorly distributed. The 6-31G** basis set yields results close to the HF limit and is available for H, C and N atoms, but not for Te. For large-scale conformational analysis, the 6-31G** basis set is uneconomical but it is tractable

Table 18
Predicted angles between the ring planes for the chalcogenobispyridines using the STO-3G(*)//STO-3G(*) model[a]

X	Ring plane attitude (deg)							
	2,2'-X	2,3'-X	3,3'-X	2,4'-X	3,4'-X	4,4'-X	Ph_2-X	Ph_2-X
O	84	88	94	86	90	90	74	104
S	74	92	92	78	86	94	92	76
Se	82	92	100	92	94	90	96	76
Te	76	90	102	92	102	80	—	—

[a] Reproduced with permission from reference [26].

Table 19
Relative HeI and HeII band intensities and percentage change of the tellurobispyridines[a]

Band	IE range (eV)	Band intensity		Percentage change[b] (%)
		HeI	HeII	
(a) *2,2'-Tellurobispyridine*				
1	7.0–8.3	1.201	0.612	−49.04
2	8.3–10.0	3.898	4.102	5.23
3	10.0–11.0	2.638	2.799	6.10
4	11.0–12.0	1.630	1.219	−25.21
5	12.0–18.0	11.633	12.268	5.46
(b) *2,3'-Tellurobispyridine*				
1	7.0–8.2	1.144	0.754	−34.10
2	8.2–10.0	4.106	4.621	12.55
3	10.0–10.5	1.400	1.510	7.87
4	10.5–11.2	1.130	1.037	−8.24
5	11.2–18.0	13.221	13.078	−1.08
(c) *3,3'-Tellurobispyridine*				
1	7.5–8.5	1.084	0.660	−39.11
2	8.5–10.0	3.573	4.256	19.12
3	10.0–10.7	1.953	2.038	4.35
4	10.7–11.4	0.975	0.996	2.15
5	11.4–18.0	13.415	13.050	−2.72
(d) *2,4'-Tellurobispyridine*				
1	7.5–8.5	1.187	0.732	−38.33
2	8.5–10.3	4.079	4.952	21.40
3	10.3–10.9	1.578	1.523	−3.49
4	10.9–11.6	1.056	0.883	−16.38
5	11.6–18.0	13.099	12.909	−1.45
(e) *3,4'-Tellurobispyridine*				
1	7.5–8.7	1.244	0.825	−33.68
2	8.7–10.1	3.544	4.626	30.53
3	10.1–10.9	1.897	2.174	14.60
4	10.9–11.6	1.137	1.147	0.88
5	11.6–18.0	13.177	12.229	−7.19
(f) *4,4'-Tellurobispyridine*				
1	7.5–8.7	1.580	0.917	−41.96
2	8.7–10.2	4.563	4.569	0.13
3	10.2–11.0	1.773	1.629	−8.12
4	11.0–11.7	1.133	1.082	−4.50
5	11.7–18.0	11.950	12.804	7.15

[a] Reproduced with permission from reference [26].
[b] [(HeII/HeI) − 1] × 100.

for single-point calculations, making it preferable to the minimal basis set calculations for the assignment of the UPS spectra of the tellurobispyridines.

Comparative studies have shown [113] that, as a result of a superposition error, unbalanced basis sets often give poorer results when compared with balanced sets. Therefore, it was necessary to choose a basis set for tellurium that was of comparable size with the internal split-valence 6-31G** set used for the C, H and N atoms. Few tractable basis sets have been published for Te. Poirier et al. [127] (PKC) list a number of basis sets for tellurium with various contraction schemes, from which the (15s, 11p, 6d)/[10s, 8p, 4d] set was chosen as a best fit to that criterion. The combination of this Te basis set and the 6-31G** sets for C, H and N yields the 6-31G**–PKC model. The interpretation of the UPS spectra of the tellurobispyridines, similar to that of their lighter congeners, is complicated by the overlapping of cationic states and the possible presence of a range of conformers. Bands that arise from distinct conformers could be resolved in the UPS spectra of the methylchalcogenopyridines (see Section 3.2). This was not the case for the chalcogenobispyridines. Although overlapping peaks in the more bispyridine complex spectra may have masked their presence, it is thought that the fully conjugated **A** forms were not present in detectable amounts (based on calculated barrier heights). Bands that arise from ionization from the HOMO were well resolved for most of the chalcogenobispyridines and show no splitting (unlike the corresponding bands of the methylchalcogenopyridines).

The presence of rotamers may be demonstrated by a comparison of the FWHM values of the HOMO bands of the methylchalcogeno- and chalcogenobispyridines. The average FWHM values of the HOMOs for the methylthio- and methylselenyl-compounds were both 0.35 eV, while those of the thio- and selenobispyridines were 0.45 and 0.43 eV respectively. This broadening of the HOMO bands suggests the presence of near-isoenergetic conformers, although the difference in broadening is of the order of the operating resolution of the instrument. Because no splitting of the valence bands was observed, the presence of a range of near-isoenergetic conformers does not further complicate the spectra. This is further substantiated by the HF models that predicted only small differences (an average of about 40 meV) between the valence Koopmans' approximation IEs of **B** and **C** rotamers. Hence, interpretation of the UPS spectra of the tellurobispyridines based on single-point calculations for the **B** structure is acceptable, because the preceding conformational analysis on the tellurobispyridines showed that the barrier heights are again small for the Morino structure.

Table 20 shows that the STO-3G* model yields the number of valence orbitals in the region 7–11 eV in good agreement when compared with the experimental density-of-states analysis, except for the 2,4′- and 3,4′- isomers. The more extensive 6-31G** models, however, give a more balanced view. The poor positioning of the n_N MOs by the HF models, as evidenced in the assignments of pyridine (Section 3.1), the methylchalcogenopyridines (Section 3.2) and the lighter chalcogenobispyridines (Sections 3.3 and 3.4), generally causes the theoretical distribution to be deficient in the region around 10 eV.

CI methods were necessary to predict accurate IEs for the n_N MOs of pyridine

Table 20
Experimental and calculated vertical IEs of the tellurobispyridines[a]

Band	Experimental IE (eV)	Calculated IE (eV)			MO character
		STO-3G*	6-31G**–PKC	6-31G**–PKC[b]	
(a) *2,2'-Tellurobispyridine*					
1	7.52	6.12	7.64	7.64	π_6–n_{Te}
2	9.04	7.97	9.31	9.31	$\pi_{5'}$–δn_{Te}
3	9.43	8.60	9.93	9.65	$n_N + \delta n_{Te}$
4	9.77	8.65	10.17	9.78	$n_N + n_{N'} + \delta n_{Te}$
5	10.19	8.86	10.45	9.93	π_4–δn_{Te}
6	10.66	9.03	10.49	10.17	$\pi_{3'}$–δn_{Te}
7	10.89	9.07	11.01	10.49	$\pi_2 + \delta n_{Te}$
(b) *2,3'-Tellurobispyridine*					
1	7.69	6.35	7.90	7.90	π_6–n_{Te}
2	9.15	8.01	9.32	9.32	$\pi_{5'}$–δn_{Te}
3	9.40	8.62	10.09	9.65	$n_N + n_{N'} + \delta n_{Te}$
4	9.77	8.79	10.17	9.78	$n_N + n_{N'} + \delta n_{Te}$
5	9.90	8.99	10.62	10.09	π_4–δn_{Te}
6	10.36	9.15	10.68	10.17	$\pi_{3'}$–δn_{Te}
7	10.95	9.26	11.17	10.62	$\pi_2 + \delta n_{Te}$
(c) *3,3'-Tellurobispyridine*					
1	8.06	6.49	7.94	7.94	π_6–n_{Te}
2	9.34	8.26	9.66	9.66	$\pi_{5'}$–δn_{Te}
3	9.59	8.71	9.97	9.78	$n_N + n_{N'} + \delta n_{Te}$
4	9.86	8.92	10.48	9.79	$n_N + n_{N'} + \delta n_{Te}$
5	10.47	9.27	10.84	9.97	π_4–δn_{Te}
6	10.47	9.39	11.15	10.48	$\pi_{3'}$–δn_{Te}
7	11.11	9.48	11.46	10.84	$\pi_2 + \delta n_{Te}$
(d) *2,4'-Tellurobispyridine*					
1	7.82	6.40	7.97	7.97	π_6–n_{Te}
2	9.18	8.20	9.30	9.30	$\pi_{5'}$
3	9.50	8.33	10.05	9.65	$n_N + n_{N'} + \delta n_{Te}$
4	9.75	8.83	10.16	9.78	$n_N + n_{N'} + \delta n_{Te}$
5	10.01	9.02	10.69	10.05	π_4–δn_{Te}
6	10.50	9.21	10.75	10.16	$\pi_{3'}$–δn_{Te}
7	10.81	9.26	11.15	10.69	$\pi_2 + \delta n_{Te}$
(e) *3,4'-Tellurobispyridine*					
1	8.09	6.53	8.26	8.26	π_6–n_{Te}
2	9.27	8.52	9.51	9.41	$n_N + n_{N'} + \delta n_{Te}$
3	9.58	8.53	9.81	9.51	$\pi_{5'}$
4	9.58	8.77	10.61	9.78	$n_N + n_{N'} + \delta n_{Te}$
5	9.91	9.34	11.06	9.81	π_4–δn_{Te}
6	10.32	9.40	11.12	10.61	$\pi_{3'}$–δn_{Te}
7	10.82	9.53	11.41	11.06	$\pi_2 + \delta n_{Te}$

Table 20 (*continued*)

Band	Experimental IE (eV)	Calculated IE (eV)			MO character
		STO-3G*	6-31G**–PKC	6-31G**–PKC[b]	
(f) *4,4'-Tellurobispyridine*					
1	8.03	6.69	8.32	8.32	π_6–n_{Te}
2	9.37	8.46	9.56	9.41	$n_N + n_{N'} + \pi n_{Te}$
3	9.69	8.62	9.82	9.56	π_5
4	9.81	8.67	10.46	9.78	$n_N + n_{N'} + \delta n_{Te}$
5	9.94	9.33	11.14	9.82	$\pi_{4'}$
6	10.35	9.44	11.22	10.46	$\pi_{3'}$–δn_{Te}
7	10.86	9.60	11.40	11.14	$\pi_2 + \delta n_{Te}$

[a] Reproduced with permission from reference [26].
[b] IEs of the n_N and $n_{N'}$ MOs adjusted to the extrapolated values of the ΔSCF–CI model.

and the methylchalcogenopyridines (see Sections 3.1 and 3.2). The n_N IEs of the chalcogenobispyridines are poorly predicted by the HF models. A more useful predictor of the position of the n_N IEs of the chalcogenobispyridines is given by the correlation with the corresponding IEs of the methylchalcogenopyridines. This can be rationalized on the grounds that the n_N MOs are localized on only one ring. The assigned n_N IEs in the symmetrical isomers of oxy-, thio- and selenobispyridines were within about 0.18 eV (on average) from the n_N IEs assigned in the corresponding isomers of the methylchalcogenopyridines. While the UPS spectra of the methyltellurylpyridines have not been studied, extrapolations can be made from the results on the lighter congeners to predict more accurately the IEs of the n_N MOs of the telluro-analogues.

Assuming a linear relationship between the n_N MO IEs and the electronegativities of the substituents, one can plot the ΔSCF–CI n_N IEs (calculated for the O, S and Se analogues) against the Allred values [88] to obtain estimates of the n_N(Te) IEs. Fig. 14 shows the plots of n_N(ΔSCF–CI) IEs for the methylchalcogenopyridines (O, S, Se) vs. the Allred electronegativities, along with the equations for the lines of best fit obtained from the regression analyses. On substituting the Allred value of 2.1 for tellurium into these equations, the predicted n_N IEs were 9.65, 9.79 and 9.41 eV for 2-, 3- and 4-methyltellurylpyridine respectively. These values are in far better agreement with the experimental assignments than are those predicted by the 6-31G**–PKC model. These projected n_N IEs will be used in place of the 6-31G**–Te assignments for the interpretation of the UPS spectra of the telluro-bispyridines, yielding the 6-31G**–PKC(adj) model.

Table 20 presents the experimental IEs, along with the IEs calculated for the **B** geometry using the STO-3G*, 6-31G**–PKC and 6-31G**–PKC(adj) models. The MOs for the third of these models (based on a composite-molecule model) are also listed in Table 20. The 6-31G**–PKC(adj) model predicts seven ionic states between 7.00 and about 11.0 eV, corresponding to ionizations from an anti-bonding orbital with considerable electron density on the Te atom; two delocalized n_N orbitals, a

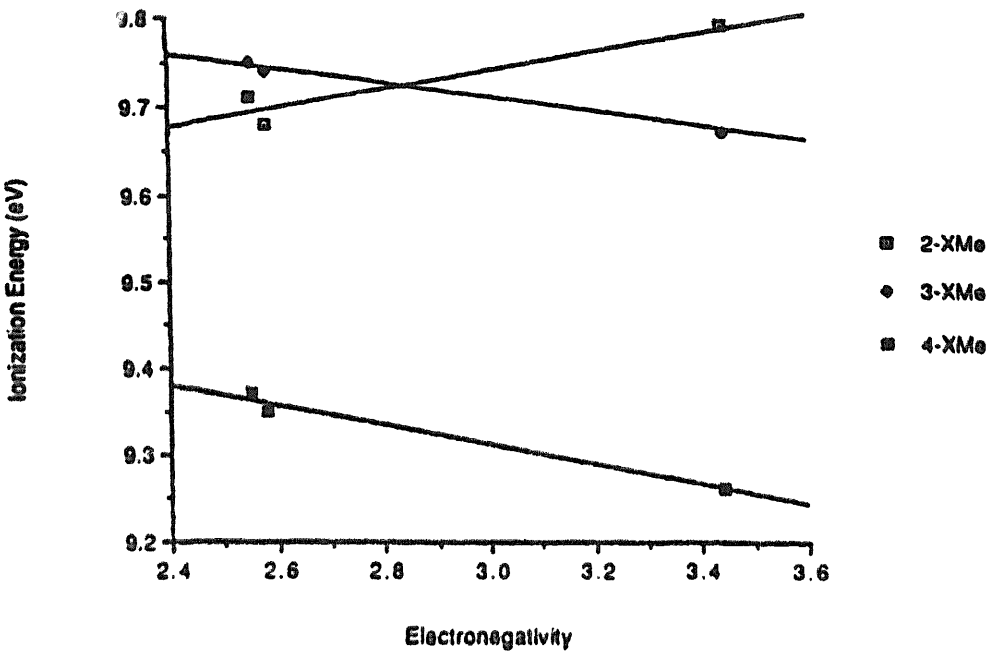

Fig. 14. Plot of the calculated ΔSCF–CI n_N IEs vs. Allred electronegativities for the methylchalcogenopyridines, along with the lines of best fit from the regression analyses: □, 2-methylchalcogenopyridines, with $IE(n_N) = 9.419 + 0.108$ and electronegativity $R^2 = 0.915$; ◆, 3-methylchalcogenopyridines, with $IE(n_N) = 9.966 - 0.086$ and electronegativity $R^2 = 0.993$; ■, 4-methylchalcogenopyridines, with $IE(n_N) = 9.955 - 0.115$ and electronegativity $R^2 = 0.980$.

group of three π orbitals; and a bonding Te π orbital (although with little Te character).

The first IE of pyridine is 9.70 eV, whereas the IEs of the chalcogen lone pairs are expected to span this value. For example, the IEs of the chalcogen lone pairs in dimethyl ether, dimethyl sulphide, dimethyl selenide and dimethyl telluride [119] are 10.04, 8.67, 8.40 and 7.89 eV respectively. Assuming that the first IEs of the dimethyl chalcogenides are representative of the chalcogen lone pairs in an environment devoid of mesomeric interactions, a composite-molecule model would therefore suggest that the degree of resonance interaction with the pyridine HOMOs is significantly reduced (on energy grounds) when compared with the sulfur and selenium lone pairs. This results in the first MO of the tellurobispyridines being of greater tellurium character than the comparable MOs of the thio- and seleno- analogues.

Thus, the first IEs of the tellurobispyridines are shifted to IEs that are lower by up to 0.6 eV from their seleno- analogues. The bonding Te π MOs are shifted closer to the IE of the pyridine π MO (from which they are derived), as a result of the decreased contribution of Te electron density to this MO.

Ionizations from Te-based MOs should exhibit a significant intensity reduction on changing from HeI to HeII radiation. Table 19 presents the relative HeI and HeII band areas, along with the percentage change in those bands on changing the radiation source. All the isomers of tellurobispyridine exhibit a single IE in the range 7.5–8.1 eV, which undergoes a reduction of 33%–50% on changing from HeI to

HeII radiation, as a result of the smaller photo-ionization cross-section of the Te 5p atomic orbital under HeII conditions. By expressing this change relative to that exhibited by the 'pure' π bands, the reduction becomes of the order of 42%–66%. The size of these reductions is similar to the size of the reductions displayed by the corresponding bands in the selenobispyridines and are supported by the cross-section data of Manson [54]. In fact, the Te π anti-bonding MOs display a slightly smaller reduction in intensity than do their seleno- analogues, in line with their lower first IEs. The photo-ionization cross-section curves for selenium and tellurium are almost identical for photoelectron energies in the range 5–40 eV, with the cross-section decreasing at higher energies. The lower IEs of the tellurobispyridines result in greater photoelectron kinetic energies and, hence, in an expected smaller reduction. Thus, an almost 'pure' n_{Te} orbital may exhibit a lesser reduction under HeII conditions than would a π–n_{Se} MO with considerable ring character. The band assigned to the bonding Te π orbital shows a 1%–15% reduction in absolute terms and a 1%–25% decrease in relative terms, suggesting a lower contribution of the Te electron density. The magnitudes of these reductions are consistent with the MO analysis of the (6-31G**–Te)//STO-3G* calculations.

The studies by Tschmutova and Bock [119] and Rodin et al. [120] show that the Te electrons are delocalized to a greater extent in diphenyl telluride (7.64 eV) than in dimethyl telluride (7.89 eV), as evidenced by the first IE. As expected, methyl phenyl telluride exhibited a split first band: the first component (7.6 eV) corresponds to the HOMO of the planar conformer in which Te π overlap is maximized, and the second component (7.83 eV) corresponds to the n_{Te} MO of the non-planar conformer. The non-planar conformer was shown to dominate in a ratio of 2:1. The first IEs of the tellurobispyridines suggest that the Te 5p electrons are localized on the Te centre. 2,2'-, 2,3'- and 2,4'-Tellurobispyridine possess a lower first IE than that of dimethyl telluride. The presence of the ortho ring-nitrogen (a strong π acceptor) may draw electron density from the Te centre, extending the delocalization. However, the first IEs of 3,3'-, 3,4'- and 4,4'-tellurobispyridine suggest that the HOMO is almost n_{Te} in character, which is consistent with the HeI/HeII cross-section analysis.

A series of three π orbitals with little Te character are also expected to lie in the region 9.0–10.6 eV, making the preferred IE sequence for the tellurobispyridines in this region

$$n_N \sim n_{N'} \sim \pi_5 - \delta n_{Te} < \pi_4 - \delta n_{Te} < \pi_3 - \delta n_{Te}$$

This assignment is consistent with that of the entire family of chalcogenobispyridines, but it should be stressed that an unambiguous assignment is difficult, as a result of the overlapping of bands in this region.

In the region 10.8–11.5 eV, there is a band that shows a variable intensity on changing from HeI to HeII radiation. This band is assigned to the bonding Te π orbital (IE_7), although the Te content of this MO is very much reduced (as evidenced by its behaviour under HeII conditions).

Based on the preferred assignments given by the 6-31G**–PKC(adj) model,

correlations can be made with the UPS assignments of the lighter congeners. Figs. 15–17 show correlation diagrams of the valence ionic states for the 2,2′-, 2,3′-, 3,3′-, 2,4′-, 3,4′- and 4,4′-chalcogenobispyridines (X=O, S, Se, Te) respectively. These correlations show that, except for the anti-bonding X–π MOs, the valence MOs are not shifted uniformly with the electronegativity of the bridging atom, reflecting the complexity of the interactions between the σ and π systems. As highlighted earlier, the effect of substitution on the MOs of pyridine is a rotation of the electron density in the 2- and 3-pyridyl systems. If the π electron density on the nitrogen atom is increased, then the resultant MO is stabilized relative to its pyridine parent (increased IE), while a decrease in the π density on the nitrogen results in a lowering of the IE.

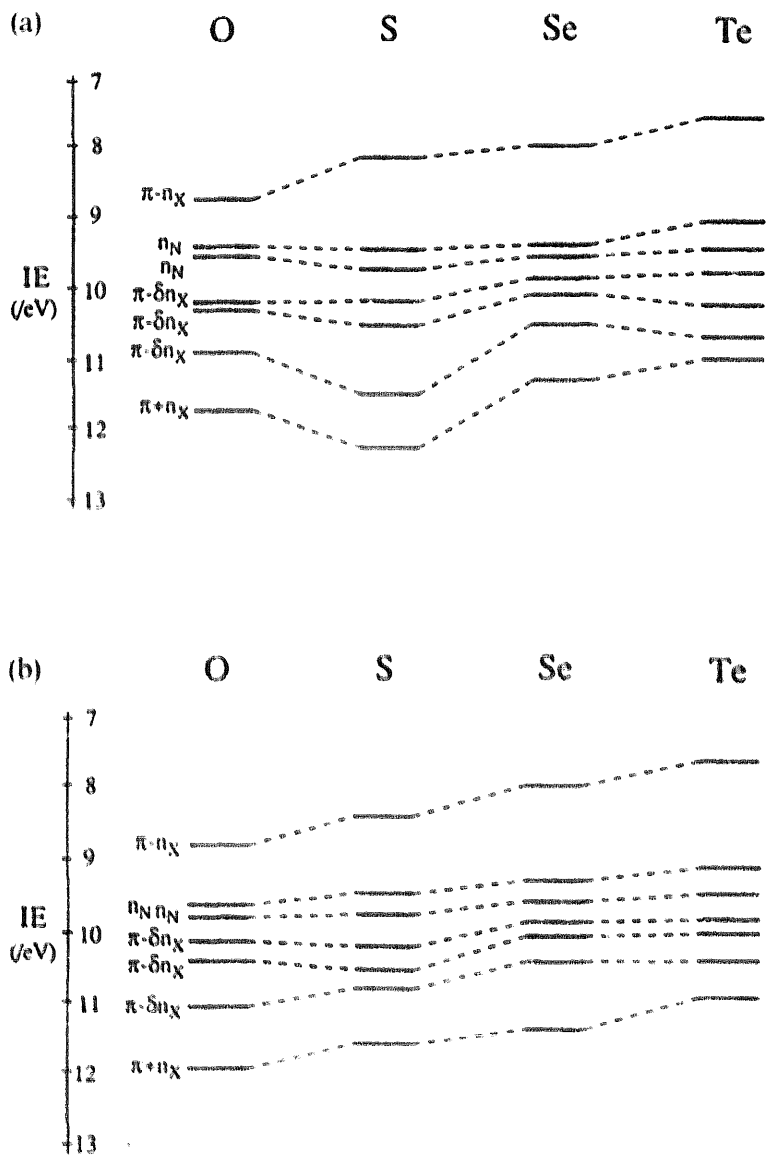

Fig. 15. (a) Correlation diagram for the valence IEs of the 2,2′-chalcogenobispyridines and (b) correlation diagram for the valence IEs of the 2,3′-chalcogenobispyridines.

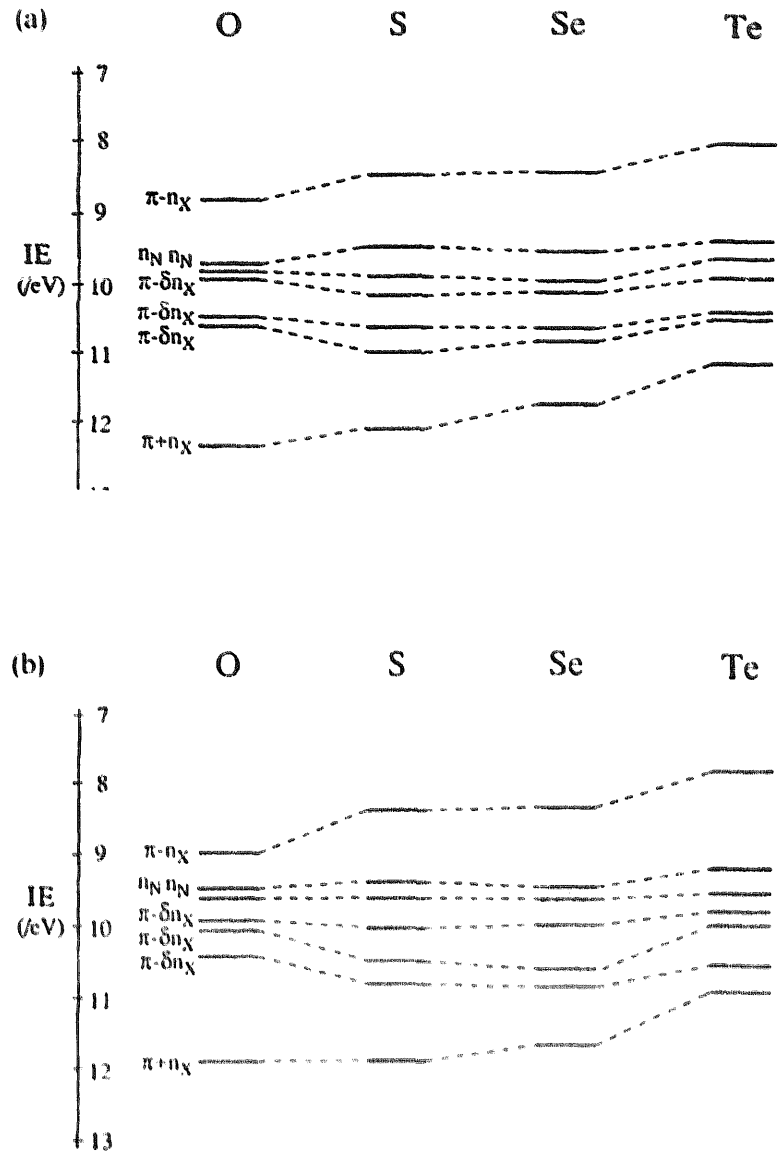

Fig. 16. (a) Correlation diagram for the valence IEs of 3,3′-chalcogenobispyridines and (b) correlation diagram for the valence IEs of the 2,4′-chalcogenobispyridines.

The in-plane n_N MO cannot undergo this shift, so is only affected by the electronegativity and position of the substituent. The greater the electron donation is from the chalcogen atom into the σ framework of the pyridyl ring, the greater will be the shift of the n_N MO to lower IE values. The proximity of the substituent has a marked effect on the magnitude of the inductive shift of the n_N IE.

The IEs of the chalcogenobispyridines are a complex function of conformation, of the first IE of the bridging atom (which determines the degree of overlap with the pyridine π system) and of positional isomerism. Conformational analyses have shown that the ring planes in the chalcogenobispyridines will occupy an almost orthogonal attitude and that these compounds are capable of concerted torsional motion. How then are the X np electrons able to conjugate with the π systems of

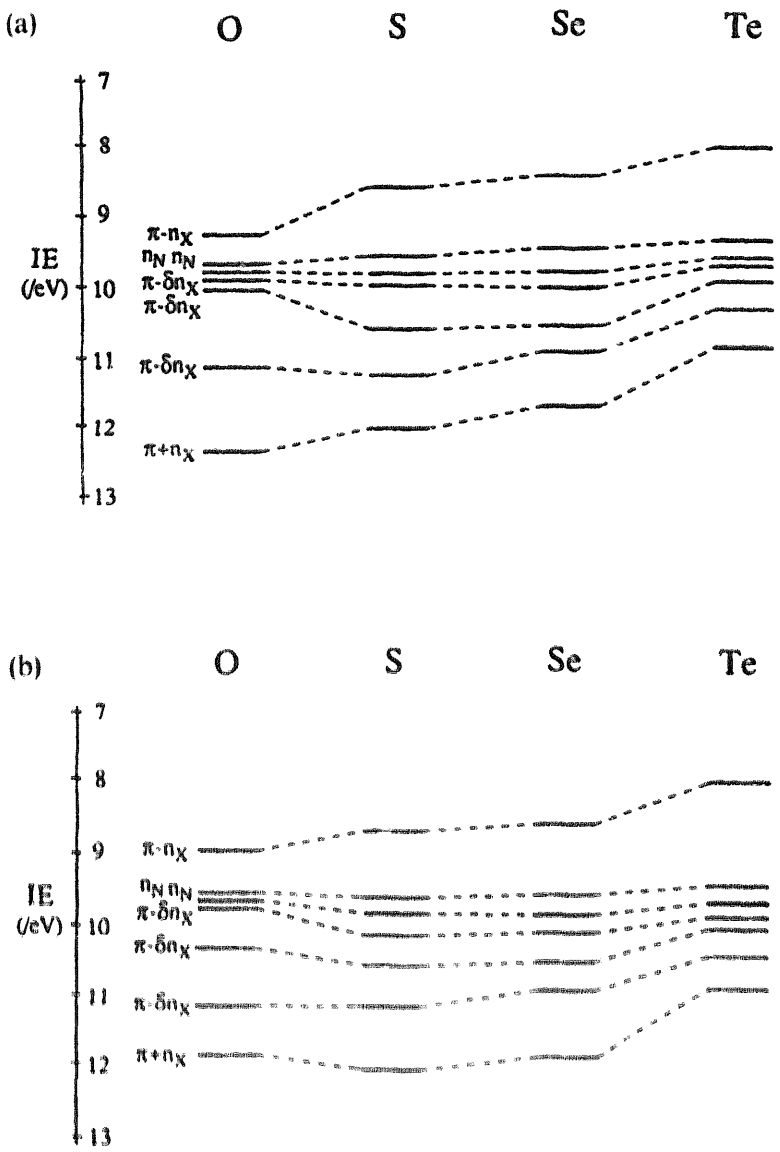

Fig. 17. (a) Correlation diagram for the valence IEs of 3,4'-chalcogenobispyridines and (b) correlation diagram for the valence IEs of 4,4'-chalcogenobispyridines.

the pyridine rings? HeI/HeII studies by Dunne et al. [25–27] have provided strong evidence for the formation of X–π bonding and anti-bonding MOs. The intensity variations displayed by these bands are in line with these assignments and the changing chalcogen content to these MOs down the group.

HF models predict that the π MOs are localized on only one ring system. The conjugation will be maximized when one of the ring planes is coplanar with the C–X–C bridge plane. As one ring rotates out of the plane and the other rotates into it, the maximum degree of conjugation with the X np electrons changes from one ring to the other ring. For the symmetrical isomers, this shift can be easily understood, because this change does not alter the nature of the resultant MOs.

However, for the asymmetrical isomers, the situation is less clear. For example,

up to 0.65 eV separates the HOMO vertical IEs of the 2,2'- and 4,4'- congeners. Hence, if the IEs of the HOMOs of the 2,4'- congeners oscillate in character between that of the respective symmetrical isomers, then significant broadening of the bands should result. The first bands of the asymmetrical isomers are no broader (as measured by their FWHMs) than the corresponding bands of the symmetrical congeners. Concerted rotation in these molecules may result in a smooth shifting of the IE about a central maximum, because the first IEs of the asymmetrical isomers are generally intermediate between those of the corresponding symmetrical isomers. In several cases, they lie closer to the first IE of one isomer than to that of the other isomer, implying that the rotational potential energy surface may not be symmetrical—as supported by the conformational analyses presented in this work.

Based on IE distributions, HeI/HeII cross-section ratios and correlations with the assignment of the lighter congeners, the preferred valence IE sequence for all the isomers of tellurobispyridine is [26]

$$\pi_6 - n_{Te} < n_N \sim n_{N'} \sim \pi_5 - \delta n_{Te} < \pi_4 - \delta n_{Te} < \pi_3 - \delta n_{Te} < \pi_2 + \delta n_{Te} \quad (18)$$

which differs from the ab initio calculations, but is consistent with experimental analysis.

4. Conclusions

The UPS spectra of the chalcogenobispyridines and related compounds revealed the changing nature of the interaction between the chalcogen valence p orbitals and the pyridine π MOs. Favourable overlap results in the resonance interaction between these two fragments, leading to the formation of anti-bonding and bonding $\pi - n_X$ combinations. The character of these combinations was shown to be dependent on the IEs of the fragments from which they were derived. Thus, the b_1 MO in pyridine was resonately shifted on interaction with a chalcogen substituent, while the former a_1 and a_2 MOs were subject only to inductive effects. The decrease in the electronegativity of the chalcogens down the group resulted in a greater donation of electron density from these centres into the ring system. This increase in electron density had the effect of destabilizing the anti-bonding MOs. For those pyridine rings substituted in the 2 or 3 position, the rotation of the a_2 MO increased the electron density on the ring-nitrogen, so stabilizing that MO (as a result of the strong π acceptor nature of nitrogen).

The alignment between the chalcogen and the ring system greatly affected the MO characters of these systems. In the UPS spectra of the methylchalcogenopyridines, peaks for distinct conformers could be resolved in some cases. In particular, the population of a non-planar conformer was predicted by HF models to increase down the group, in line with spectral findings. The reduction in overlap of the heavy chalcogen np atomic orbitals with the ring π system and the decrease in steric hindrance caused by the longer C–X bonds make the non-planar forms accessible.

The interpretation of the UPS spectra of these systems was further complicated by the presence of non-equivalent planar conformers.

Bands that arose from other rotamers could not be resolved in the UPS spectra of the chalcogenobispyridines. Conformational analyses performed using a number of ab initio models revealed the presence of low energy pathways between near-isoenergetic conformers. Free rotation of the pyridine rings in these systems was discounted, on the basis of the inaccessibility of the fully conjugated planar form of these compounds. The calculated barrier height to this form was found to decrease down the group, although its presence would still be difficult to detect in the UPS spectra.

Within a composite–molecule model, the UPS spectra of the chalcogenobispyridines were interpreted using IEs calculated for a Morino structure, in which the ring planes were orthogonal and one ring lay in the plane formed by the C–X–C angle. Geometry optimizations supported the use of this structure, because, for all the congeners, a near-perpendicular attitude was predicted between the rings (although only for the 2,3′- and 2,4′- isomers was the predicted minimum energy structures actually of the Morino form). The use of this structure facilitated correlations of the valence IEs of the chalcogenobispyridines with those of pyridine and the corresponding methylchalcogenopyridines. Good correlations were achieved, highlighting the lack of interaction between the two ring systems. The X π MOs in the chalcogenobispyridines shared similar IEs to those in the methylchalcogenopyridines, demonstrating the similar degree of delocalization in these systems and further supporting the composite–molecule model.

KA–HF models were shown to predict incorrectly the IE distributions in pyridine-based systems. While they produced satisfactory assignments for the π-type MOs, their success was limited for the in-plane n_N MOs. A ΔSCF–MP2 method was found to take better account of the correlation and relaxation processes of these MOs. The ΔSCF method is limited by symmetry constraints, because it restricts the calculation of IEs to only the uppermost MO of each symmetry species. However, this did allow the accurate calculation of the n_N IEs for pyridine and the methylchalcogenopyridines. The localized nature of the n_N MO permitted 'good' correlations of the n_N IEs of these systems with those of the chalcogenobispyridines.

The importance of relaxation and correlation processes for the correct assignment of the UPS spectra of pyridine-based systems necessitates the use of configuration interaction or multiconfigurational SCF techniques. Such calculations on molecules as electron dense as the chalcogenobispyridines would be very computer intensive.

Acknowledgements

One of us (S.J.D) acknowledges the Australian Postgraduate Research Award. E.v.N-F acknowledges the generous support of the Australian Research Council and the Research Management Committee, University of Newcastle.

References

[1] L.A. Summers, J. Heterocyclic Chem., 24 (1987) 533.
[2] S.J. Dunne, L.A. Summers and E.I. von Nagy-Felsobuki, J. Heterocyclic Chem., 29 (1992) 117.
[3] S.J. Dunne, L.A. Summers and E.I. von Nagy-Felsobuki, J. Heterocyclic Chem., 30 (1993) 409.
[4] S.J. Dunne, L.A. Summers and E.I. von Nagy-Felsobuki, J. Heterocyclic Chem., 32 (1995) 1671.
[5] A. Matsuda, Jpn. Pat., 16 (1978) 385; Chem. Abstr., 89 (1978) 118478.
[6] A. Matsuda, Jpn. Pat., 18 (1978) 579; Chem. Abstr., 89 (1978) 43121.
[7] K. Hamamoto and T. Kajiwara, Jpn. Pat., 13 (1966) 985; Chem. Abstr., 65 (1966) 20108.
[8] D.E. Butler, B.P.H. Poschel and J.G. Marriott, J. Med. Chem., 24 (1981) 346.
[9] J.A. Kolmer, H. Brown and G.W. Raiziss, J. Pharm. Exp. Ther., 61 (1937) 253.
[10] J. Cheymol, P. Chabrier, J. Renault and M. Pazin, Therapie, 7 (1952) 514.
[11] J. Delarge, L. Thunus, C. Beckers, A. Ghys, J. Denef and J.C. Jamoulle, Euro. J. Med. Chem. Chim. Ther., 19 (1984) 559.
[12] B. Boduszek, J.S. Wieczorek, M. Mordarski and J. Wieczorek, Arch. Immunol. Ther. Exp., 33 (1985) 331.
[13] B. Boduszek and J.S. Wieczorek, Pol. Pat., 106 (1980) 957; Chem. Abstr., 95 (1981) 80745.
[14] I. Taniguchi, K. Toyosawa, H. Yamaguchi and K. Yasukouchi, J. Electroanal. Chem. Interfacial Electrochem., 140 (1982) 187.
[15] I. Taniguchi, K. Toyosawa, H. Yamaguchi and K. Yasukouchi, J. Chem. Soc., Chem. Commun. (1982) 1032.
[16] J. Haladjian, P. Bianco and R. Pilard, Electrochim. Acta, 28 (1983) 1823.
[17] M. Nakagawa, F. Sumino, M. Hiro, N. Kashimura and S. Nagahara, Jpn. Pat., JP 02 66 (1990) 556; Chem. Abstr., 113 (1990) 181410.
[18] L.A. Summers, Adv. Heterocyclic Chem., 35 (1984) 281.
[19] I. Hargittai and B. Rozsondai, in S. Patai and Z. Rappoport (Eds.), The Chemistry of Organic Selenium and Tellurium Compounds, Vol. 1, Wiley, New York, 1986.
[20] S.J. Dunne, L.A. Summers and E.I. von Nagy-Felsobuki, J. Heterocyclic Chem., 27 (1990) 1787.
[21] S.J. Dunne, L.A. Summers and E.I. von Nagy-Felsobuki, J. Heterocyclic Chem., 29 (1992) 851.
[22] S.J. Dunne, L.A. Summers and E.I. von Nagy-Felsobuki, J. Molec. Struct., 230 (1991) 219.
[23] S.J. Dunne, L.A. Summers and E.I. von Nagy-Felsobuki, J. Molec. Struct., 268 (1992) 373.
[24] S.J. Dunne, L.A. Summers and E.I. von Nagy-Felsobuki, Phosph. Sulf. Silicon Rel. Elements, 72 (1992) 103.
[25] S.J. Dunne, L.A. Summers and E.I. von Nagy-Felsobuki, J. Molec. Struct., 273 (1992) 373.
[26] S.J. Dunne, L.A. Summers and E.I. von Nagy-Felsobuki, J. Molec. Struct., 291 (1993) 287.
[27] S. J. Dunne, L.A. Summers and E.I. von Nagy-Felsobuki, Org. Mass Spectrom., 28 (1993) 316.
[28] C. Cauletti and G. Distefano, in S. Patai (Ed.), The Chemistry of Organic Selenium and Tellurium Compounds, Vol. 2, Wiley, New York, 1987.
[29] F.P. Colonna, G. Distefano, V. Galasso, G.C. Pappalardo and G. Scarlata, J. Chem. Soc., Farad. Trans. II, 73 (1977) 822.
[30] F.P. Colonna, G. Distefano, V. Galasso, K.J. Irgolic and G.C. Pappalardo, J. Chem. Soc., Perkin Trans. II (1981) 281.
[31] R.O. Loutfy, J. Chem. Phys., 66 (1977) 4781.
[32] C.L. Bird and A.T. Kuhn, Chem. Soc. Rev., 10 (1981) 49.
[33] J. W. Rabalais, Principles of Ultraviolet Photoelectron Spectroscopy, Wiley, New York, 1976.
[34] T.A. Carlson, Photoelectron and Auger Spectroscopy, Plenum, New York, 1975.
[35] J.D.H. Eland, Photoelectron Spectroscopy: An Introduction to Ultraviolet Photoelectron Spectroscopy in the Gas Phase, Halstead, New York, 1974.
[36] R.E. Ballard, Photoelectron Spectroscopy and Molecular Orbital Theory, Adam Hilger, Bristol, 1978.
[37] J. Berkowitz, Photoionization, Photoabsorption and Photoelectron Spectroscopy, Academic Press, New York, 1979.
[38] P.S. Dewar, F. Ernstbrunner, J.R. Gilmour, M. Godfrey and J.M. Mellor, Tetrahedron, 30 (1974) 2455.

[39] A.D. Baker, G. Horozoglu Armen, Y. Guang-di, D. Liotta, N. Flannagan, C. Barnum, M. Saindane, G.C. Zima and J. Grossman, J. Org. Chem., 46 (1981) 4127.
[40] J. Berkowitz and P.M. Guyon, Int. J. Mass Spectrom. Ion. Phys., 6 (1971) 302.
[41] T. Koopmans, Physica, 1 (1934) 104.
[42] M.J. Frisch, J.S. Binkley, H.B. Schlegel, K. Ragavachari, C.F. Melius, R. Martin, J.J.P. Stewart, F.W. Dohrowicz, C.M. Rohlfing, L.R. Kahn, D.J. DeFrees, R. Seeger, R.A. Whiteside, D.J. Fox, E.M. Fluder and J.A. Pople, GAUSSIAN 86, Carnegie-Mellon Quantum Chemistry Publishing Unit, Pittsburgh, PA, 1984.
[43] R. McWeeny and G. Dierksen, J. Chem. Phys., 49 (1968) 4852.
[44] J.A. Pople and R.K. Nesbet, J. Chem. Phys., 22 (1959) 571.
[45] C. Møller and M.S. Plesset, Phys. Rev., 46 (1934) 618.
[46] R. Krishman and J.A. Pople, Int. J. Quant. Chem., 14 (1978) 91.
[47] W.J. Hehre, R.F. Stewart and J.A. Pople, J. Chem. Phys., 51 (1969) 2657.
[48] J.A. Pople, in H.F. Schaefer III (Ed.), Modern Theoretical Chemistry, Vol. 4, Plenum, New York, 1976.
[49] S.J. Dunne, A synthetic and ultraviolet photoelectron spectroscopic study of the chalcogenobispyridines and related compounds, Ph.D. Thesis, The University of Newcastle, Newcastle, 1992.
[50] R. Fletcher and M.J.D. Powell, Comput. J., 6 (1963) 163.
[51] J.E. Del Bene, J. Am. Chem. Soc., 97 (1975) 5330; Chem. Phys., 51 (1969) 2657.
[52] G. O. Sorensen, L. Mahler and N. Rastrup-Andersen, J. Molec. Struct., 20 (1974) 119.
[53] C.N. Yang, Phys. Rev., 74 (1948) 764.
[54] S.T. Manson, J. Electron Spectrosc. Rel. Phenom., 2 (1973) 482.
[55] S.T. Manson and A. Msezane, Phys. Rev. A, 20 (1979) 1005.
[56] E.I. von Nagy-Felsobuki, J. Chem. Educ., 66 (1989) 821.
[57] J.J. Huang and F.O. Ellison, J. Electron Spectrosc. Rel. Phenom., 4 (1974) 233.
[58] I.G. Kaplan and A.P. Markin, Opt. Spectrosc., 24 (1968) 475; 25 (1968) 275.
[59] A. Schweig and W. Theil, J. Electron Spectrosc. Rel. Phenom., 3 (1974) 27; J. Chem. Phys., 60 (1974) 951.
[60] J.W. Rabalais, in C.R. Brundle and A.D. Baker (Eds.), Electron Spectroscopy: Theory, Techniques and Applications, Vol. 2, Elsevier, New York, 1978.
[61] M.K. Livett, E.I. von Nagy-Felsobuki, J.B. Peel and G.D. Willett, Inorg. Chem., 17 (1978) 1608.
[62] W. von Niessen, W.P. Kraemer and G.H.F. Diercksen, Chem. Phys., 41 (1979) 113.
[63] B. Dobson, I.H. Hillier, J.A. Connor, D. Moncrieff, M.J. Scanlan and C.D. Garner, J. Chem. Soc., Farad. Trans. II, 79 (1983) 295.
[64] K. Kimura, S. Katsumata, Y. Achiba, T. Yamazaki and S. Iwata, Handbook of Hel Photoelectron Spectra of Fundamental Organic Molecules, Halsted Press, New York, 1981.
[65] C.R. Brundle, M.B. Robin and N.A. Kuebler, J. Am. Chem. Soc., 94 (1972) 1466.
[66] H. Daamen and A. Oskam, Inorg. Chim. Acta, 27 (1978) 209.
[67] S.J. Dunne, L.A. Summers and E.I. von Nagy-Felsobuki, unpublished results, 1995.
[68] R.C. Bingham, M.J.S. Dewar and D.H. Lo, J. Am. Chem. Soc., 97 (1975) 1285, 1294, 1302, 1311.
[69] L. Åsbrink, C. Fridh and E. Lindholm, Chem. Phys. Lett., 52 (1977) 69.
[70] L. Åsbrink, C. Fridh, E. Lindholm, S. de Bruijn and D.P. Chong, Phys. Scr., 22 (1980) 475.
[71] Program 393, Quantum Chemistry Program Exchange, Indiana University, Bloomington, IN, 1985.
[72] L. Åsbrink, C. Fridh, E. Lindholm and S. De Bruijn, Chem. Phys. Lett., 66 (1979) 411.
[73] G.H. King, J.N. Murrell and R.J. Suffolk, J. Chem. Soc., Dalton Trans. (1972) 564.
[74] E. Heilbronner, V. Hornung, F.M. Pinkerton and S.F. Thames, Helv. Chim. Acta, 55 (1972) 289.
[75] M.J. Cook, S. El-Abbady, A.R. Katritzky, C. Guimon and G. Pfister-Guillouzo, J. Chem. Soc., Perkins Trans I. (1977) 1652.
[76] L. Adamowicz, Chem. Phys. Lett., 161 (1989) 73.
[77] M.J. Nowak, L. Lapinski, H. Rostkowska, A. Les and L. Adamowicz, J. Phys. Chem., 94 (1990) 7406.
[78] H. Preut, F. Huber and K.H. Hengstmann, Acta Crystall., C44 (1988) 468.
[79] A.P. Bozopoulos, S.C. Kokkou, P.J. Rentzeperis and P. Karagiannidis, Acta Crystall., C40 (1984) 944.

[80] W.J. Hehre, R.F. Stewart, and J.A. Pople, J. Chem. Phys., 51 (1969) 2657.
[81] A. Schweig and N.Thon, Chem. Phys. Lett., 38 (1976) 482.
[82] P.S.Dewar, E. Ernstbrunner, J.R. Gilmore, M. Godfrey and J.M. Mellor, Tetrahedron, 30 (1974) 2455.
[83] J. P. LaFemina, Int. J. Quant. Chem., 36 (1989) 563.
[84] J.M. Lehn, G. Wipff and J. Demuynck, Helv. Chim. Acta, 60 (1977) 1239.
[85] E.I. von Nagy-Felsobuki and K. Kimura, J. Phys. Chem., 94 (1990) 8041.
[86] S. Cradock and R.A.Whiteford, J. Chem. Soc., Farad. Trans. II (1972) 281.
[87] R.J. Boyd and S.L. Boyd, J. Am. Chem. Soc., 114 (1992) 1652.
[88] A.L. Allred, J. Inorg. Nucl. Chem., 17 (1961) 215.
[89] A. Albert and G.B. Barlin, J. Chem. Soc. (1959) 2384.
[90] V. Galasso, G. De Alti and A. Bigotto, Tetrahedron, 27 (1971) 6151.
[91] K. Higasi, S. Ueyo and S. Yamaguchi, Bull. Instrum. Phys. Chem. Res. (Tokyo), 23 (1967) 788.
[92] F.K. Fong, J. Chem. Phys., 40 (1964) 132.
[93] J.E. Katon, W.R. Feairheller and E.R. Lipponcott, J. Molec. Spectrosc., 13 (1964) 72.
[94] J.H.S. Green, Spectrochim. Acta, A24 (1968) 1627.
[95] R.J.W. Le Ferve, A. Sundaram and K.M.S. Sundaram, Bull. Chem. Soc. Jpn., 35 (1962) 690.
[96] R.J.W. Le Ferve and J.D. Saxby, J. Chem. Soc. (1966) 1064.
[97] I.A. Bogdanov and M.F. Vuks, Vestn. Leningr. Univ., Ser. Fiz. Khim., 20 (1965) 3; 46.
[98] K. Higasi, Dipole, Molecule and Chemistry, Monograph Series of the Research Institute of Applied Electricity, Vol. 13, Hokkaido University, Sapporo, 1965.
[99] C. Garrigou-Lagrange, M. Horak, R.K.K. Khanna and E.R. Lipponcott., Coll. Cz. Chem. Commun., 35 (1970) 3230.
[100] D. Gust and K. Mislow, J. Am. Chem. Soc., 95 (1973) 1535.
[101] O.G. Rodin, V.F. Traven, V.V. Redchenko, M. Yu. Eismont and B.I. Stepanov, ZH. Obschch. Khim., 49 (1979) 192.
[102] B. Rozsondai, I. Hargittai and G.C. Pappalardo, Z. Naturforsch., 34A (1979) 752.
[103] B. Rozsondai and I. Hargittai, Kem. Kozl., 54 (1980) 268.
[104] C. Chachaty, G.C. Pappalardo and G. Scarlata, J. Chem. Soc., Perkin Trans. II (1976) 1234.
[105] V. Galasso, G.C. Pappalardo and G. Scarlata, J. Molec. Struct., 34 (1976) 123.
[106] A.M. Porto, L. Altieri, A.J. Castro and J.A. Brieux, J. Chem. Soc. (1971) 1360.
[107] S. Green, Adv. Chem. Phys., 25 (1974) 179.
[108] R.S. Glass, J.L. Broeker and M.E. Jatcko, Tetrahedron, 45 (1989) 1263.
[109] R. Gleiter, E. Heilbronner and V. Hornung, Helv. Chim. Acta, 55 (1972) 255.
[110] R. Poirer and I.G. Csizmadia, in S. Patai (Ed.), The Chemistry of Organic Selenium and Tellurium Compounds, Vol.1, Wiley, New York, 1986.
[111] J.B. Collins, P. v.R. Schleyer, J.S. Binkley and J.A. Pople, J. Chem. Phys., 64 (1976) 5142.
[112] Y. Sakai, H. Tatewaki and S. Huzinaga, J. Comp. Chem., 3 (1982) 6.
[113] R.A. Poirer, R. Daudel, R.E. Kari and I.G. Cszimadia, Int. Quant. Chem., 21 (1982) 799.
[114] M.M. Franci, W.J. Pietro, W.J. Hehre, J.S. Binkley, M.S. Gordon, D.J. DeFrees and J.A. Pople, J. Chem. Phys., 77 (1982) 3654.
[115] C. Cauletti and G. Distefano, in S. Patai (Ed.), The Chemistry of Organic Selenium and Tellurium Compounds, Vol. 2, Wiley, New York, 1987.
[116] P.S. Dewar, E. Ernstbrunner, J.R. Gilmor, M. Godfrey and J.M. Mellor, Tetrahedron, 30 (1974) 2455.
[117] A. Schweig and N. Thon, Chem. Phys. Lett., 38 (1976) 482.
[118] A.D. Baker, G. Horozoglu Armen, Y. Guang-di, D. Liotta, N. Flannagan, C. Barnum, M. Saindaine, G.C. Zima and J. Grossman, J. Org. Chem., 46 (1981) 4127.
[119] G. Tschmutova and H. Bock, Z. Naturforsch., B31 (1976) 1611.
[120] O.G. Rodin, V.F. Traven, V.V. Redchenko, M. Yu Eismont and B.I. Stepanov, Zh. Obshch. Khim., 53 (1983) 2537.
[121] V.F. Traven, O.G. Rodin, M. Yu Eismont and B.I. Stepanov, Proc. Euro. Workshop on UV Molecular Photoelectron Spectroscopy, Rimini, Italy, 1983.
[122] A.W. Potts and W.C. Price, Proc. R. Soc. London, Ser. A, 326 (1972) 181.

[123] S. Pignataro and G. Distefano, Chem. Phys. Lett., 26 (1974) 356.
[124] A. Bigotto, V. Galasso, G. Pellizer, G. Distefano, G.C. Pappalardo, J. Bergman and L. Engman, Spectrochim. Acta, A38 (1982) 185.
[125] F.P. Colonna, G. Distefano, V. Galasso, K.J. Irgolic, C.E. King and G.C. Pappalardo, J. Organomet. Chem., 146 (1978) 235.
[126] G. Distefano, V. Galasso, K.J. Irgolic and G.C. Pappalardo, J. Chem. Soc., Perkin Trans. II (1983) 1109.
[127] R. Poirier, R. Kari and I.G. Csizmadia, Handbook of Gaussian Basis Sets: A Compendium for Ab-initio Molecular Orbital Calculations, Physical Sciences Data 24, Elsevier, Amsterdam, 1985.